MATHEMATICAL MODELLING OF FUEL MELTING AND RELOCATION DURING A SEVERE ACCIDENT IN A FBR

By

A. JASMIN SUDHA
(Enrollment No: ENGG02200704002)

Indira Gandhi Centre for Atomic Research
Kalpakkam – 603102
Tamil Nadu, India

A thesis submitted to the
Board of Studies in Engineering Sciences
In partial fulfillment of requirements
For the Degree of

DOCTOR OF PHILOSOPHY

of

HOMI BHABHA NATIONAL INSTITUTE

Mumbai

August 2013

Homi Bhabha National Institute

Recommendations of the Viva Voce Board

As members of the Viva Voce Board, we certify that we have read the dissertation prepared by **Mrs. A. Jasmin Sudha** entitled **"Mathematical Modelling of Fuel Melting and Relocation During a Severe Accident in a FBR"** and recommend that it may be accepted as fulfilling the dissertation requirement for the Degree of Doctor of Philosophy.

________________________ Date: 24-01-2014

Chairman – Dr. B.K. Panigrahi

________________________ Date: 24.01.2014

Convener/Guide – Dr. K. Velusamy

________________________ Date: 24-1-14

Member – Dr. M. Sai Baba

________________________ Date: 24/1/2014

Member – Dr. B.P.C. Rao

________________________ Date: 24/01/2014

External Examiner – Dr.A.W.Patwardhan

Final approval and acceptance of this dissertation is contingent upon the candidate's submission of the final copies of the dissertation to HBNI.

Date: 24-01-2014

Place: Kalpakkam

CERTIFICATE

I hereby certify that I have read this dissertation prepared under my direction and recommend that it may be accepted as fulfilling the dissertation requirement.

Date: **(K. Velusamy)**

Place: **Guide**

STATEMENT BY AUTHOR

This dissertation has been submitted in partial fulfillment of requirements for an advanced degree at Homi Bhabha National Institute (HBNI) and is deposited in the Library to be made available to borrowers under rules of the HBNI.

Kalpakkam

August 2013

(A. Jasmin Sudha)

DECLARATION

I hereby declare that the investigation presented in the thesis has been carried out by me. The work is original and has not been submitted earlier as a whole or in part for a degree / diploma at this or any other Institution / University.

(A. Jasmin Sudha)

Many, O LORD my God, are thy wonderful works which thou hast done, and thy thoughts which are to us-ward: they cannot be reckoned up in order unto thee: if I would declare and speak of them, they are more than can be numbered.

–Psalms 40:5

Dedicated to my Lord and Saviour

Jesus Christ

என் தேவனாகிய கர்த்தாவே, நீர் எங்கள் நிமித்தஞ்செய்த உம்முடைய அதிசயங்களும் உம்முடைய யோசனைகளும் அநேகமாயிருக்கிறது; ஒருவரும் அவைகளை உமக்கு விவரித்துச் சொல்லி முடியாது; நான் அவைகளைச் சொல்லி அறிவிக்க வேண்டுமானால் அவைகள் எண்ணிக்கைக்கு மேலானவைகள்.

–சங்கீதம் 40:5

Acknowledgement

I thank God Almighty for preserving and sustaining me all through my life and for the wonderful people He has given to adorn my life. I owe a lot to my parents Mr.S.Asir Dhanaraj & Mrs. Gethsy Sornavally Asir and also to my paternal grandma Mrs. Noorji Pushpam Soundararaj, because of whom I have grown to what I am today. I am greatly indebted to all my teachers, right from my first standard teacher to HBNI professors. I have been a very good student all along and it is because of the fact that I have had very good teachers. Friends have always made my life cheerful and worthwhile. It is their admiration and affinity towards me that helped me build self esteem overcoming an inherent shy and timid nature.

I am thankful to Dr. P.R.Vasudeva Rao Director, IGCAR and to Dr.P.Chellapandi, Director, RDG for their kind approval to my studies. I am also thankful to my erstwhile superiors, Mr.S.E.Kannan and Mr.M.Rajan who have contributed much to my growth. I express my sincere thanks to Shri.P.Selvaraj, AD, RDG, Shri.B.K.Nashine, Head, SED and Smt. Lydia Gnanadhas, friend turned section head for their support.

I am thankful to Dr. T.Jayakumar (Dean, HBNI, Kalpakkam) and Dr. M.Saibaba (Convener, Engineering Sciences Committee & DC member) for their constant support and encouraging words. I am grateful to Dr.B.K.Panigrahi (Chairman, DC) and Dr. B.P.C.Rao (Member, DC), for their continuous monitoring of my research work. Their views and comments have meant a lot to my growth and progress. I also remember with gratitude Dr.C.Anand Babu and Dr.P.V.Sivaprasad who were in my DC for sometime.

I owe my profound thanks to Dr. K.Velusamy, my mentor. He has been a great source of inspiration and support to me. I have high regard and a lot of admiration for his unmatched intellectual capacity, cool temperament, excellent engineering aptitude and unassuming nature. I learnt the basics of Reactor Engineering and CFD from him. But for his presence and support as guide, I would not have enrolled for a doctoral degree in the field of heat transfer. It is a great privilege to be called the student of such a great researcher. I am immensely thankful to his wife, Mrs. Gunadevi Velusamy for the cordial welcome accorded to me and my family at their residence at all times. She is such a warm, friendly person that she is always one step ahead in reciprocating good will towards us.

I would like to thank my husband, Mr.S.Johnson Samuel wholeheartedly for his unwavering support and encouragement. Despite my frail physique, if I had the courage to register for a higher degree in HBNI which demanded very strenuous course work – it is solely because of his motivation. He stood by me like a solid pillar through thick and thin times. He became a man of unshakable faith in God and his earnest prayers for me have always kept me going with a smiling face amidst difficulties.

My heartfelt thanks are due to Punitha, my best friend and great supporter. When I was getting acquainted with basic concepts of engineering, she introduced me to good books. I benefitted a lot from her positive approach to life. I am also thankful to my friends Deivanayagi, Malarvizhi, Shyamala and Malathi and friends from SED and RSD. My RPD friends Sheela, Sunil and Shanthi (I call them 'the triple S') always have a kind and encouraging word for me and I enjoyed the liberty to walk into their rooms anytime, to dump my heavy bag and rest my feet for a few minutes, whenever I walked past their division.

I am thankful to my relatives and family friends, particularly to Joe annan, Vijaya akka, Shanthi akka, Ruby aththai, Ramola anni, Josila aunty, Cynthia and her mom, Jemimah, Johnson annan, Vasumathy akka, EU fellowship and women's fellowship of our church for their comforting words and prayer support in times of need. Words fail me when I try to express my gratitude to Mrs. L.Prabha, our family friend for her unflinching physical and moral support to us during both good and bad times. I thank my son Joshua Praveen who brought a lot of joy and happiness into my life. His wide eyed appreciation of my academic accomplishments always gives me a great feeling. The gentleness and maturity that he displayed in times of my ill health are remarkable.

Finally, I thank the many researchers whose scientific contributions have enriched my knowledge indirectly.

(A.JASMIN SUDHA)

CONTENTS

ABSTRACT

Fast Breeder Reactors (FBRs) are provided with redundant and diverse plant protection systems with a very low failure probability ($<10^{-6}$/reactor year), thus making Core Disruptive Accident (CDA), a Beyond Design Basis Event (BDBE). Nevertheless, safety analysis is carried out even for such events in order to mitigate their consequences by providing engineered safeguards such as the in-vessel core catcher. During a CDA, a significant fraction of the hot molten fuel moves downwards and gets relocated to the core catcher. The core catcher design requires prior knowledge of core-melt relocation time which is the time taken for the molten fuel to reach the lower plenum from the active core region. This is because of the fact that the decay heat contained in the fission products of the core-melt is a strong function of time. Therefore the initial thermal load on the core catcher is primarily dictated by the core melt relocation time.

This research work aims at determining the upper and lower bounds for core-melt relocation time for postulated accident conditions of Protected Loss of Heat Sink (PLOHS) accident and Unprotected Loss of Flow Accident (ULOFA) respectively. The natural convection setting in the cold sodium plenum which can influence this time estimate is also studied with a view to prescribe proper boundary condition for the grid plate bottom following a ULOFA. Finally, a new multi layer core catcher capable of handling the debris generated from a whole core melt down accident is proposed.

In the first part of the research, natural convection of liquid sodium contained in the cold plenum below the grid plate has been investigated in detail employing a low Reynolds number k-ε turbulence model. The two dimensional axisymmetric study considers heat conduction in the thick grid plate and natural convection in liquid metal simultaneously, both in laminar and turbulent regime. Based on this study, suitable

correlations for Nusselt number in terms of Boussinesq number and other influencing parameters has been developed for various specifications of boundary conditions.

The second part of the research focuses on estimating the time taken for grid plate melt-through in case of ULOFA. Towards this, a computer code HEATRAN-1 has been developed which solves transient nonlinear heat conduction equation including phase change using a finite difference method. It is based on enthalpy formulation incorporating Voller's improved algorithm for tracking the melt-front. To account for displacement of lighter molten steel by the heavier core-melt, a dynamic displacement procedure has been adopted. The code has been validated against standard benchmark solutions for Stefan problem. In case of PLOHS accident, molten material relocation is analyzed starting from the active core region, sequentially moving through the lower axial blanket region, lower fission gas plenum, tail piece of subassembly with flow entry nozzles and honeycomb structures for flow zoning, discriminator at the foot of the subassembly and the grid plate. Each region is approximated as a porous body with effective thermophysical properties and heat conduction analysis is performed to estimate the core-melt relocation time.

In the final part of research work, a new multi layer core catcher is conceptualized which essentially consists of a top refractory layer, a middle delay bed layer and a base load bearing structural member. The thickness of the intermediate delay bed has been optimized by analyzing the transient response of the composite structure, taking into account time varying decay heat of core debris. The purpose of this transient two dimensional heat transfer study is to limit the temperature at the base layer within design safety limits following a whole core accident.

LIST OF TABLES

LIST OF FIGURES

NOMENCLATURE

A	Aspect Ratio (Height / Diameter of the cavity)
Bi	Biot number, $Bi = h\,L / \kappa_{SS}$
Bo	Boussinesq number, $Bo = g\,\beta\,\Delta T\,L^3 / \alpha^2$
$Bo*$	Modified Boussinesq number based on heat flux $Bo* = Gr \times \Pr^2 = \dfrac{g\beta \dot{q}''\,L^4}{\kappa_{Na}\,\alpha^2}$
C	Specific heat capacity
D	Diameter of the plate
Fo	Fourier number, $Fo = \alpha\,t / L^2$
g	Acceleration due to gravity
Gr	Grashof number, $Gr = g\,\beta \Delta T L^3 / \upsilon^2$
$Gr*$	Modified Grashof Number, $Gr* = \dfrac{g\,\beta L^4 q''}{\kappa_{Na}\,\upsilon^2}$
H	Enthalpy
h	Heat transfer coefficient
k	Turbulent kinetic energy
L	Characteristic length / Latent heat of fusion
l	Thickness of the plate
$l*$	Height ratio / Non dimensional plate thickness
Nu	Nusselt number $Nu = h\,L / \kappa_{Na}$

Pr	Prandtl number, $\Pr = C_P \mu / \kappa$
q''	Heat flux
q'''	Volumetric heat generation rate
r	Radial coordinate
Ra	Rayleigh number Ra = Gr×Pr
t	Time
T	Temperature
z	Axial coordinate

Greek symbols

α	Thermal diffusivity
β	Coefficient of thermal expansion of sodium
ΔT	Temperature difference between bottom surface of the plate and bulk sodium
Δt	Time step
Δz	Axial mesh size
ε	Dissipation rate of turbulent kinetic energy
κ	Thermal conductivity
κ^*	Conductivity ratio between metal and sodium
μ	Dynamic viscosity of sodium
ν	Kinematic viscosity of sodium
ρ	Density
τ	Time constant

Subscripts

0	initial condition at t = 0
amb	ambient
ave	average
eff	effective
f	fuel
eq	equivalent
i	i th region
m	Melting point
Na	sodium
p	plate / at constant pressure
SS	stainless steel
t	turbulent

Abbreviations

ALWR	Advanced Light Water Reactor
APR	Advanced Pressurized Reactor
BDBE	Beyond Design Basis Event
BEM	Boundary Element Method
CDA	Core Disruptive Accident
CDFR	Commercial Demonstration Fast Reactor
CFD	Computational Fluid Dynamics

CSR	Control Safety Rod
DFR	Dounreay Fast Reactor
DHRS	Decay Heat Removal System
DSR	Diverse Safety Rod
EFR	European Fast Reactor
EVCC	Ex-Vessel Core Catcher
FBR	Fast Breeder Reactor
FCI	Fuel Coolant Interaction
FDM	Finite Difference Method
FEM	Finite Element Method
FFTF	Fast Flux Test Facility
FVM	Finite Volume Method
GP	Grid Plate
HBIM	Heat Balance Integral Method
JSFR	Japanese Sodium cooled Fast Reactor
OGDHRS	Operation Grade Decay Heat Removal System
PFBR	Prototype Fast Breeder Reactor
PFR	Prototype Fast Reactor
PLOHS	Protected Loss of Heat Sink
SCRAM	Safety Control Rod Accelerated Movement
SDS	Shut Down System

SFR	Sodium Fast Reactor
SGDHRS	Safety Grade Decay Heat Removal System
SPX	Super PheniX
ULOFA	Unprotected Loss of Flow Accident
UTOPA	Unprotected Transient Overpower Accident

CHAPTER 1

INTRODUCTION

1.1 FOREWORD

Nuclear power is one of the promising and environmentally sustainable options to cater to the ever increasing energy demand. Among the various types of nuclear reactors, the fast reactors have a strong potential to use a large fraction (about 75%) of uranium resource and burn the waste generated in thermal reactors. Considering these factors many developed as well as developing countries pursue active research in the area of science and technology of Fast Breeder Reactors (FBRs). In the wake of untoward sequence of events at Fukushima Daiichi nuclear accident, more emphasis has been placed on safety perspective of nuclear reactors all over the globe. With the advancement of numerical methods and computing technology in the recent past, Computational Fluid Dynamics (CFD) has been harnessed to address and solve many of the thermal hydraulic challenges in the design and safety of FBRs. This is evident from the published work of Tenchine for French FBRs and Velusamy et al. for Indian FBRs (Tenchine, 2010 and Velusamy et al., 2010).

In the design and safety analysis of FBR, post accident core material relocation and post accident heat removal assume primary importance, demanding systematic heat transfer analysis towards devising strategies to mitigate the consequences of extremely low probability beyond design basis events (Velusamy, 2008). The present research work aims at quantifying molten fuel relocation time to the main vessel lower plenum for a few postulated accident scenes and proposes a new conceptual core catcher - marking a few baby steps in this mammoth field full of interesting challenges and complexities.

All the studies performed as part of this research work belong to the less explored grey areas that lie interwoven within the core melt down accident sequences. Full fledged experimental simulation of a severe nuclear accident is very difficult due to the small time scales and large quantum of heat generation involved, combined with significant spatial and temporal variations. An ideal approach would be to conduct small scale model experiments, complemented by computational modelling. However, in the present work, recourse to numerical simulation has been taken and validation has been achieved with benchmark data and empirical correlations.

Physical processes accompanying nuclear reactor accidents are rather complicated and computational capacities for the comprehensive analysis of the whole accident are limited. It is usual practice to evaluate the progression of these accidents in several stages, using separate computational modules which are robust for each of the particular processes and then integrating the findings of the separate effect studies. In the present research work, natural convection in cold sodium plenum, time for core-melt relocation to core catcher and heat transfer studies of a multi layer core catcher are investigated in succession, making use of the results obtained from one study as the input for the subsequent study as shown below.

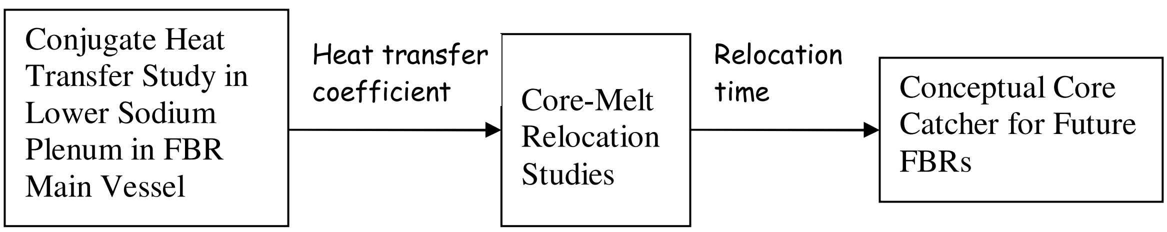

Attempt has been made to state the envisaged sequence of events in unambiguous terms and carry out the mathematical modelling with appropriate physical justification for the adopted model. It is a tough task to define any nuclear accident progression precisely, in clear cut terms. Considering the example of core debris settling on the core catcher, this challenge is best described by Kayser who has illustrated different possible configurations of the fuel and stainless steel debris on the core catcher (Muller and

Gunther, 1982). His comical portrayal of the phenomenon is given in Appendix – 1. Though he has depicted it as a cartoon, it is serious enough to stir the thought of researchers, drawing their attention to the level of uncertainty that can exist in the definition of accident scenario. Therefore it is worth highlighting here that the usefulness and credibility of any accident analysis hinges on the initial axioms that are postulated at the beginning of the study and this particular study is no exception.

All the analyses have been performed for a whole core accident, in line with the targeted objective of conceptualizing a core catcher to handle debris generated from a whole core-melt. Heat generating mass consists of molten fuel component only, devoid of stainless steel and sodium. Relocation of the whole core material in the downward direction is improbable because a fraction of the molten core may be dispersed in the upward direction with reference to active core region and can settle on available flat surfaces on the upper part of the hot sodium pool. Another possibility of a part of the core to be left behind in its original location cannot be ruled out either. Nonetheless, whole core is considered to arrive at conservative estimates for the analysed output parameters such as core-melt relocation time to the core catcher and the thickness of the delay bed in the multi layer core catcher.

1.2 OVERVIEW OF CDA

The vertical section of a typical medium sized pool type fast reactor is depicted in Fig 1.1. The main components immersed in the large inventory of liquid sodium (~1100 t) inside the main vessel of a pool type FBR are the primary sodium pumps, intermediate heat exchangers, the entire lot of core subassemblies (SAs) which includes fuel, blanket, control rod, reflector and shielding SAs, grid plate supporting the SAs, inner vessel separating the cold and hot sodium pools, core support structure and the core catcher assembly. The core catcher is provided to protect the reactor main vessel from thermal and mechanical loads produced by the relocated core-melt / debris following an accident.

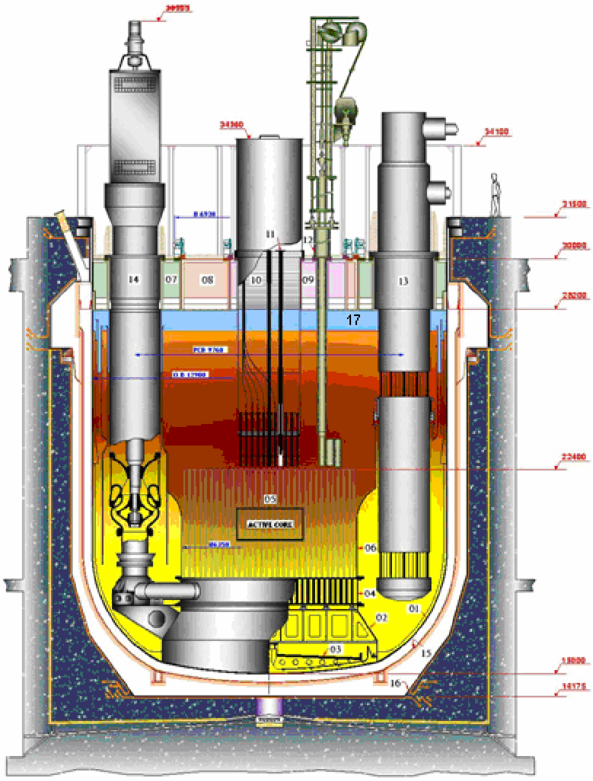

1 - main vessel
2 - core support structure
3 - core catcher
4 -grid plate
5 – Active core region
6 - inner vessel
7 - roof slab
8 - large rotatable plug
9 - small rotatable plug
10 - control plug
11 - control & safety rod drive mechanism
12 - invessel transfer machine
13 - intermediate heat exchanger
14 - primary sodium pump
15 - safety vessel
16 - reactor vault
17- Argon cover gas

Fig. 1.1 Vertical section of reactor main vessel

Argon acts as cover gas above the free surface of sodium. The roof slab which forms the thermal and biological shield accommodates the control plug, small rotatable plug and large rotatable plug facilitating fuel handling. Grid Plate (GP) consists of two stainless steel plates each of thickness 5 cm, separated by a sodium volume of 1 m axial gap in which the two primary sodium pumps, feed cold sodium through four sodium pipes to all the subassemblies.

The overall description of a core disruptive accident is given in the next few sections. An Unprotected Loss Of Flow Accident (ULOFA) or a Loss of Heat Sink Accident (LOHS) in a fast reactor can lead to whole core melt down depending upon the severity of the accident. The accident is termed unprotected if the shut down systems (control rods) of the reactor fail to trip / shut down the reactor by SCRAM (Safety Control Rod Accelerated Movement) on demand. Unprotected Transient Overpower Accident (UTOPA) can be arrested and terminated early due to the fuel squirting behaviour (Sathiyasheela, 2008). Fast reactors are provided with two diverse and fast acting shut down systems, viz., Shut Down System – 1 (SDS -1) and Shut down System – 2 (SDS – 2), which are capable of bringing the reactor to a safe shutdown state independently, in case of an initiator of an accident.

Traditionally, SDS-1, the first group of control rods is used for power and reactivity control as well as for shutting down the reactor by SCRAM whereas SDS-2 which comprises of another group of control rods is used only for tripping the reactor by way of SCRAM. Each system is capable of shutting down the reactor independently with adequate safety margin. Also, single failure criterion is applied such that effective reactor shut down is ensured even when one control rod in a group does not act. Diverse concepts are employed in the design of the two systems. The reactor parameters that are continuously monitored to trigger SCRAM are divided into two different groups each activating one shut down system on demand. An optical link is provided between the two systems to ensure that both systems act even when one is actuated by a SCRAM parameter crossing the threshold. The probability of simultaneous failure of these two devices is kept below 10^{-6}/reactor year because of the extreme care taken in their design. Therefore, Core Disruptive Accident (CDA) has been categorized as Beyond Design Basis Events (BDBE) in fast reactor design.

Nevertheless, analysis of the severity of these events becomes necessary in order to assess the damage they can cause. Such assessment helps in the design of certain engineered safeguard features which can be incorporated in the reactor to mitigate the consequences of the BDBE. This philosophy is called the defense in depth philosophy which aims at minimising the hazard and risk associated with nuclear reactors. The chain of events describing a CDA in a fast breeder reactor is pictorially represented in Fig. 1.2.

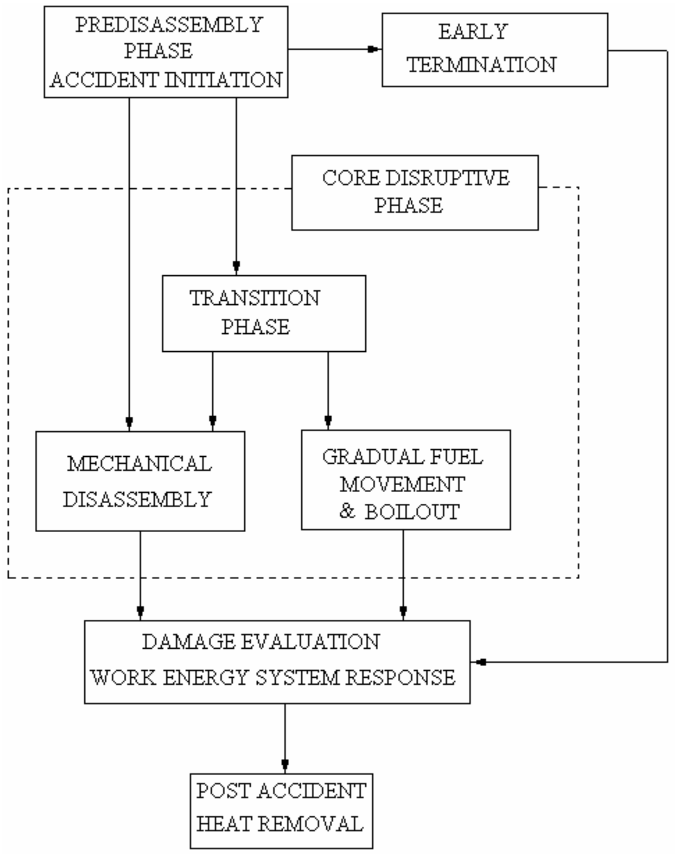

Fig. 1.2 CDA Scenario in FBR

The progression of CDA is generally analysed step by step using the cause and effect relationship under different phases namely, predisassembly phase, transition phase, disassembly phase, system response phase and post accident heat removal phase (Walter and Reynolds, 1981). A brief description of these phases is given below.

1.2.1 Predisassembly Phase

This phase of LOFA / TOPA analysis involves the calculations of core neutronics, reactivity feedbacks, thermal hydraulics, sodium boiling, fuel pin mechanics leading to failure, cladding and fuel slumping and their relocation and fuel coolant interaction. Predisassembly phase lasts till the fuel reaches the boiling point and starts dispersing the core material. Beyond this point, fuel displacement reactivity feedback dominates with short time scales and this phase is known as disassembly phase. Predisassembly phase provides the initial conditions for the disassembly phase.

1.2.2 Transition Phase

The predisaasembly phase can lead to early termination of the accident if there are sufficient negative feedbacks. On the other hand if reactivity addition rates are large, it leads to energetic dispersal of the core which is called the disassembly phase. A third possibility comes into picture when there are insufficient negative feedbacks to terminate the accident and insufficient reactivity addition for core explosion. In such a case, large segments of core could slowly melt and proceed to involve the whole core. This slowly developing boiling process has been termed the Transition Phase, since it is sandwitched between predisassembly and disassembly phases. In this phase, the multichannel model of predisassembly phase breaks down and one cannot use the disassembly idealization of treating the entire core as fluid. The end of the neutronic event may come either by energetic disassembly or due to gradual boiling or melting of the core.

1.2.3 Disassembly Phase

In this phase, one calculates mainly the fuel displacement feedback coupled with the core neutronics and core hydrodynamics. This phase lasts till the reactor attains subcriticality due to core dispersal. The timescale of disassembly phase is very small, of the order of milliseconds.

1.2.4 System Response Phase

At the end of the disassembly phase, though neutronically the reactor is in its shutdown state, core is still in its expanding state and thermal energy release is capable of performing significant mechanical work on the system. This mechanical work is augmented by the Fuel Coolant Interaction (FCI) and consequent vapourisation and expansion of coolant. Once the source pressure term is established from FCI or normal reactor material expansion, the response of the reactor system is analysed.

1.2.5 Post Accident Heat Removal (PAHR)

The final phase in the analysis is the evaluation of PAHR. That is one wants to know how the fuel comes to rest in various parts of the system ultimately, where it can be permanently cooled. This present research work addresses a few issues related to this phase of CDA.

1.3 ANALYSIS OF LOFA

Since UTOPA gets terminated early due to the fuel squirting behaviour, only ULOFA exemplifies the generic behavior over the whole range of CDA spectrum of circumstances. Hence it can be used to adequately characterize the spectra of energetic consequences. One of the initiators for ULOFA is loss of electrical power supply to the primary pumps. In this type of accident, coolant boiling in coolant channels takes place first. Due to positive void coefficient, power shoots up which then leads to fuel pin failure and fuel slumping.

Four characteristics of LMFBR cores – positive sodium void worth, core geometry not in its most reactive configuration, high fuel reactivity worth and an extensive background of experience in accident analysis, led to choice of ULOFA as the principal scenario for study, in the international community. In the safety analysis of both SUPER PHENIX (Rigoleur, 1982) and EFR (Dufour, 2007), only ULOFA was considered as whole core accident for safety analysis. A possible scenario that leads to ULOFA in a FBR is shown schematically in Fig. 1.3.

The transient is initiated due to loss of primary coolant flow resulting from power supply failure to the primary pumps. The pump speed reduces gradually due to the large inertia of the flywheel. Flow reduction leads to coolant temperature rise in core that gives

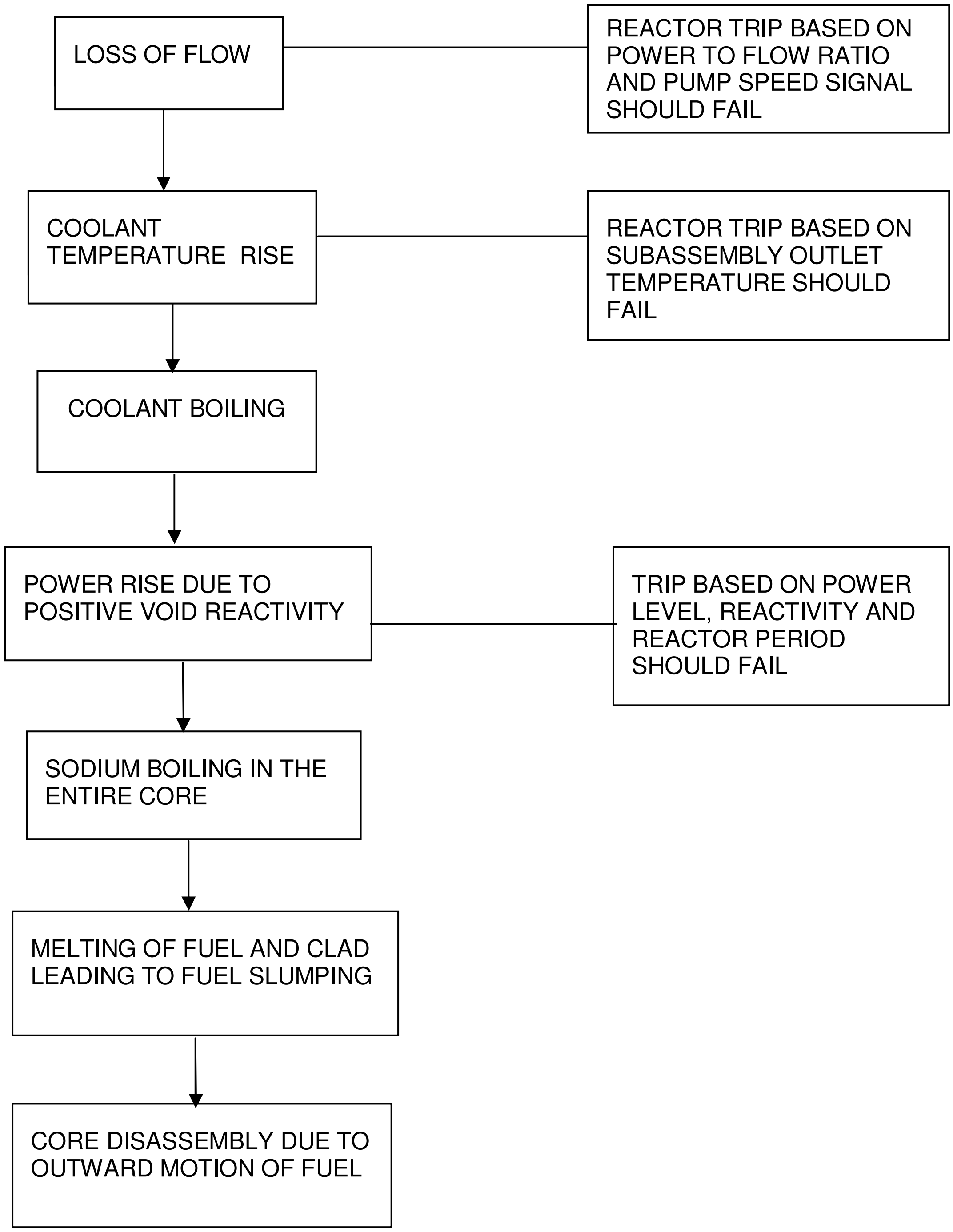

Fig. 1.3 Unprotected LOFA

positive reactivity. The heating of the spacer pads results in negative reactivity. These negative reactivity components dominate over the positive reactivity components from clad and coolant heating and hence the net reactivity is negative. This results in decrease in power. However, the power to flow ratio is high which leads to coolant temperature rise and ultimately coolant boiling (voiding) in the upper part of the core. Subsequently, sodium voiding spreads radially outward and axially downward. Due to the positive reactivity introduced when the sodium voiding propagates into the central part of the core, the net reactivity begins to increase and becomes positive. It leads to power excursion and finally to rapid increase in clad and fuel temperatures that result in clad and fuel melting. At this stage, molten fuel may be swept out of the core by shearing force of fission gas pressure in irradiated fuel. This will lead to large negative reactivity addition and reactor shutdown. A part of the fuel propagates downwards, melting the underlying materials. To model this transition phase, detailed evaluation of the fuel and clad movement and the consequent reactivity effects are required (Srinivasan, 2008).

1.4 ANALYSIS OF PROTECTED LOSS OF HEAT SINK (PLOHS) ACCIDENT

A fast breeder reactor can enter into an extremely low probability event of core melt down called PLOHS when there is no means of decay heat removal generated within the nuclear fuel even after the reactor is shut down. Normally, FBRs are provided with two decay heat removal systems. The probability of combined failure of both these systems is below 10^{-7}/reactor year. Nevertheless, their integrity could be jeopardized due to an earthquake of very large magnitude or a combination of natural calamities for which they are not designed. This can culminate in a PLOHS accident.

1.5 MOTIVATION FOR THE CURRENT RESEARCH

As stated in the foreword, this research aims at addressing a few thermal hydraulic issues that fall under the scope of severe accident analysis following a core disruptive / melt down accident in a FBR. The molten nuclear fuel which is flowing out of the disrupted core is called 'core-melt'. Eventually it becomes 'core debris' after being quenched by liquid sodium. Core-melt is a heat source not only by virtue of its initial high temperature but mainly because of the decay heat of contained fission products. The fission products decay into stable isotopes with course of time. Therefore decay heat is a rapidly decreasing function of time.

In the first part of the research work, natural convection of liquid sodium in lower plenum of reactor main vessel is investigated. Empirical correlations for convective heat transfer in liquid metals are rather limited because of inherent difficulties in conducting experiments with them. Internal natural convection in an enclosure heated from above and cooled at the cylindrical side wall is of paramount importance in the post accident scenario of a FBR. In the present study, the vertical cylindrical enclosure containing liquid sodium is heated from above and cooled along the side wall. Heat transfer correlations for such a geometry and low Prandtl number (0.004) are not reported in open literature. A few correlations are available for a hot plate facing upward / downward in an infinite liquid metal pool or a differentially heated cavity where one of the side walls is maintained at a higher temperature than the other side wall which is cold. Yadav and Kant (2008) have experimentally studied conjugate heat transfer from a vertical flat plate of finite thickness under natural convective cooling and concluded that conductivity ratio and aspect ratio greatly influence the heat transfer behaviour. Gazit (1998) in his study with mercury bath has quoted a very early work by Stewart and Weinberg stating that natural convection in enclosures depends strongly on geometry and quantitative results for one geometry cannot be derived from another. Jabbar (2001) has reviewed natural convective heat transfer coefficients for high Prandtl number liquids in two and three dimensional enclosures and summarized the discrepancies between various correlations. The discrepancies are found to be upto a factor of 5 for vertical surfaces, a factor of 4 for horizontal surfaces facing upward and upto a factor of 8 for horizontal surfaces facing downward for high prandtl number liquids. This large uncertainty associated with heat transfer from downward facing hot surfaces in enclosures has further motivated the present study of developing natural convective heat transfer correlations. These correlations are essential for prescribing realistic boundary condition for the numerical investigation related to grid plate melting which is the next part of the study.

In the second part of the study, a mathematical model is formulated using the explicit enthalpy method and a finite difference code HEATRAN-1 is developed for solving heat conduction heat transfer in the grid plate with phase change. Heat transfer problems involving phase change are nonlinear and are not amenable to analytical solutions except in very simple cases. In the problem at hand, non linear heat source and boundary conditions add further to the complexity of the problem which has necessitated the development of a computer code for a reasonably good prediction of grid plate melting. The melting models available in many commercial codes do not offer scope for prescribing separate properties for solid and liquid phases. Moreover tracking of the melt-front with respect to time and displacement of the melting substance which is in contact with a denser hot source are very difficult to be implemented in these codes. To overcome these difficulties, HEATRAN-1 code has been developed to analyse grid plate melting problem.

As we know, core-melt relocation time is one of the crucial input parameters for the design of core catcher. Therefore, having obtained the time estimate for grid plate melt-through, a conceptual core catcher is hypothesized to withstand a whole core meltdown and this forms the final part of the research. For generation IV sodium fast reactors, in-vessel accommodation of a whole core accident is desired for enhancing the safety of the reactor. The need for such an improved core catcher for future FBRS has given the impetus for this part of the study. Sharma et al. (2009), in their study have proposed a triple tray core catcher for Indian FBRs. But distribution of core debris equally on all the trays is a challenge. In the upcoming Japanese reactor JSFR, multiple tray approach is adopted with special guide tubes to effect tray to tray debris transfer (Sato, 2009). After considering various design options for FBR core catchers, particular emphasis has been placed on multi layer core catcher, in the present work. A multi layer core catcher comprising of a top sacrificial layer, a middle delay bed and a base layer of high mechanical strength is proposed and its adequacy is substantiated by detailed heat transfer analysis.

1.6 SPECIFIC PROBLEMS ADDRESSED

1.6.1 Natural Convection in Cold Sodium Plenum

During natural convection in enclosures, the fluid is driven by density variations in a body-force field, and natural convection heat transfer is highly sensitive to the heating or cooling conditions at the boundaries (Akins, 1986). Flow and temperature fields in these systems are governed by the continuity equation, Navier-Stokes equations and energy equation. Turbulence is modelled by solving two additional transport equations, one for turbulent kinetic energy and the other for its dissipation rate. Due to the non linearity of the equations and a strong coupling between momentum and energy equations, general analytical solutions are still not possible except for a few simple cases. Most research efforts have been based on experimental work and, more recently, on numerical approaches particularly for liquid metals (Wenxian, 2004).

In this research work, CFD analysis is carried out to estimate heat transfer coefficient for prescribing proper convective boundary condition at the bottom of the grid plate for its melting studies. Based on detailed parametric studies, Nusselt number correlations are obtained as a function of Boussinesq number for both isothermal and isoflux boundary conditions for the top heated and side wall cooled sodium filled cylindrical cavity. In the next case, the lower sodium plenum is approximated as a cylindrical enclosure. Here, both transient and steady state heat transfer correlations are developed for natural convection setting in liquid sodium in the enclosure heated from above and cooled at the side wall. The effect of the finite thickness of top plate on heat transfer is also investigated by imposing constant temperature boundary on the top surface of the plate. A correlation is developed which shows the dependence of Nusselt number on Boussinesq number, conductivity ratio and height ratio for a thick plate.

1.6.2 Core-melt Relocation Studies

The second part of the research deals with core-melt relocation time to the core catcher. Heat transfer studies have been carried out to obtain the time taken for core-melt relocation by penetration through the underlying steel structures before settling on the core catcher. This time estimate is essential in defining initial thermal load on the core catcher (Roychowdhury, 2003). ULOFA and PLOHS are taken to be bounding events which would give an estimate of minimum and maximum time for core-melt relocation to the core catcher. In the case of ULOFA it is envisaged that the core-melt is swept out of the core due to the combined effect of core bubble and fission gas pressures and it gets deposited on the grid plate. The disrupted core and the core-melt lying above the bottom plate of grid plate are depicted in Fig. 1.4. The starting point of the present calculation is that the core-melt has reached the lower plate of the grid plate and rests on it, thereby melting it. Hence, grid plate is the only structure considered to undergo melting to determine core-melt relocation time. The case of PLOHS event is perceived to lead to the slowest of core-melt progression, where it is assumed that the active core is molten and subassemblies remain intact with melting starting from the bottom axial blanket region and progressing through successive underlying regions. Here, the molten material movement is idealistically taken to resemble that of a candle burning slowly and melting away. In the case of ULOFA, core-melt reaches the grid plate within a few seconds after the accident and the lower plate of the grid plate is a solid obstacle for the molten corium to melt through, before settling on the in-vessel core catcher.

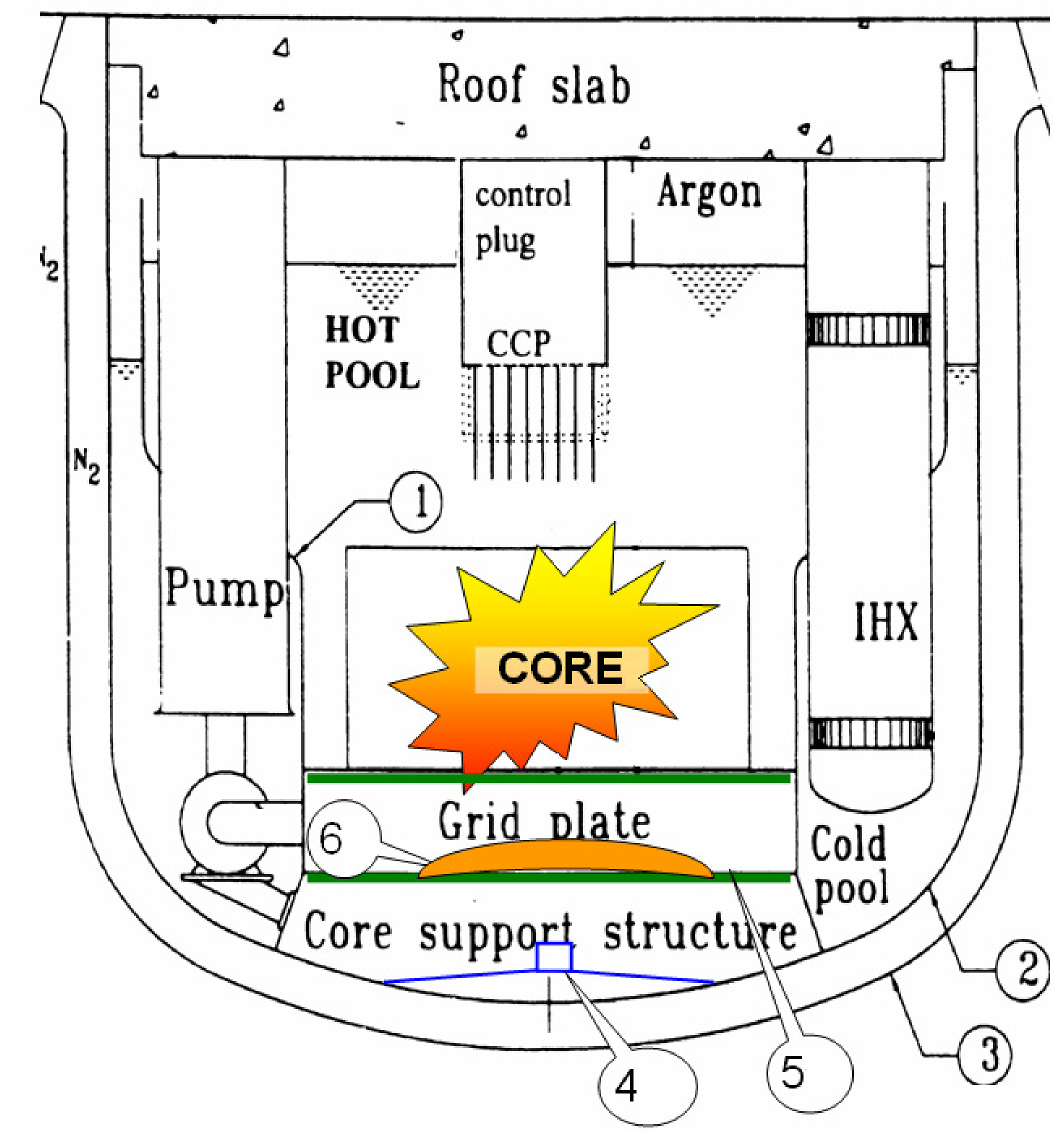

1- Inner vessel	2-Main Vessel	3-Safety Vessel
4- Core catcher	5- Grid plate	6- Core-melt

Fig. 1.4 Vertical section of a FBR with degraded core after a CDA

This problem of 'grid plate melt-through' for some possible core-melt configurations and boundary conditions is addressed as part of the investigation of ULOFA scenario using HEATRAN-1 code. Heat transfer analysis has been carried out using the code for a medium sized mixed oxide fuelled reactor. Decay heat as a function of time is the volumetric heat source in the core-melt. The code is validated with both semi analytical solution and available benchmark data for BN 800 reactor problem. A salient feature of the code is that it employs dynamic adaptation of the computational mesh, giving way for the molten grid plate material to be displaced as the heavier molten fuel sinks into it. The thickness of the thin molten film underneath the core-melt is calculated by the analytical solution obtained from the work of Moallemi and Viskanta who have extensively worked in the field of migrating / moving heat sources on melting substrates. The code can capture the evolution of phase change front with time and also can handle separate properties for the solid and liquid phases.

In the next case, PLOHS event is analysed to determine melt relocation time. The vertical section of a fuel subassembly and the computational domain for this PLOHS event are illustrated in Fig. 1.5.

Core-melt progression takes place slowly starting from the bottom axial blanket region, moving through the fission gas plenum, tail piece, discriminator and grid plate top plate. Porous body formulation is adopted and effective thermophysical properties are defined for each region which are made up of different components such as uranium oxide, sodium, stainless steel cladding etc. For this analysis, it is assumed that boiling fuel is in constant touch with the underlying composite regions.

1.6.3 Multi Layer Core Catcher

Finally, the heat bearing ability of the new proposed core catcher is analysed using the core-melt relocation time obtained from the previous study to define the initial decay heat load on it. In general, for nuclear reactors, there are two approaches for permanent retention of core debris. The retention may be achieved either, in-vessel, within the primary system or, ex-vessel, external to the primary system but within the containment building.

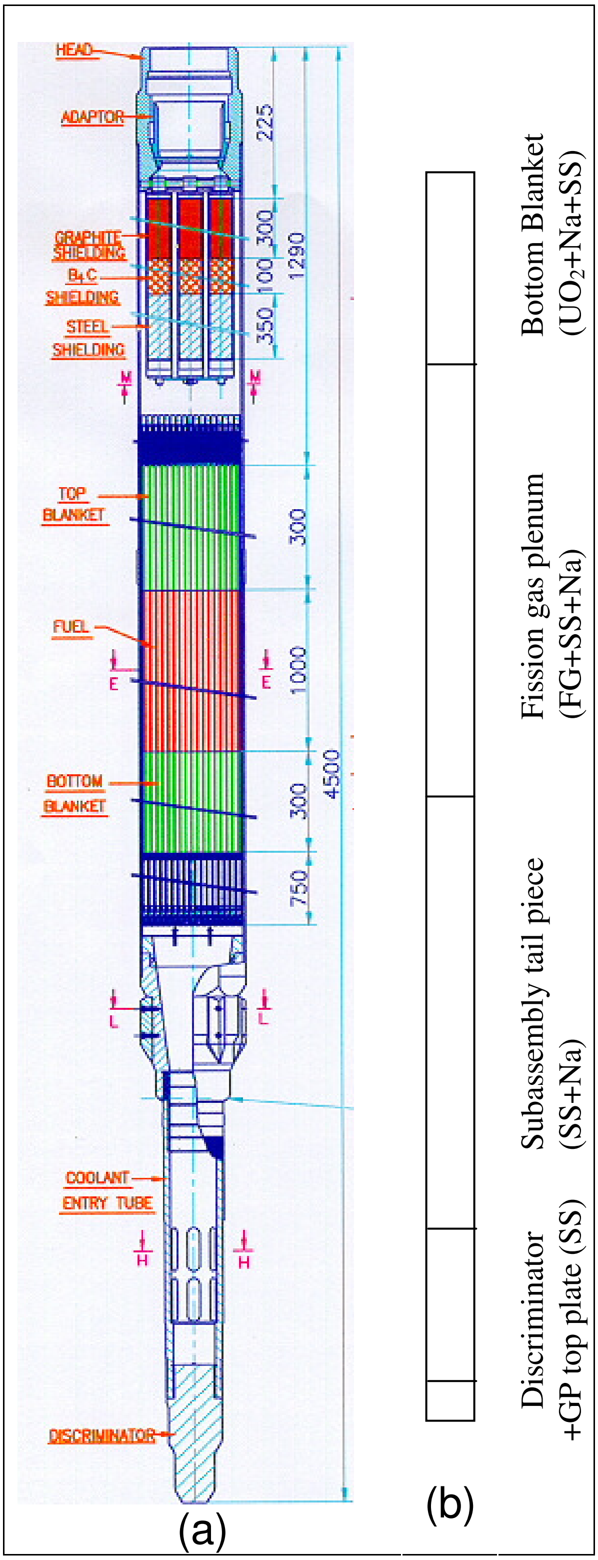

Fig. 1.5 Schematic of (a) FBR fuel subassembly and (b) mathematical model for PLOHS

The invessel core catchers are generally single or multiple plates with inclusion of sacrificial layers. Ex-vessel core catchers adopt large spreading compartment type catchers as in EPR or multiple crucible catchers as in VVER. But in the case of sodium cooled fast breeders, because of hazardous reaction of sodium with air and water, main vessel has to be intact and invessel core catcher is the best option. Therefore, the core catcher is provided at the bottom of the main vessel to protect it from intense thermal and mechanical loads following an accident. Nevertheless, there are many possible design options which might enhance core debris retention capacity. The choice of core catcher material and its configuration leading to its optimization is an important scientific task which needs to be addressed for future fast breeders. Several design options of core catchers for fast breeders are discussed in the present work with particular emphasis on the multi layer core catcher. A multi layer core catcher comprising of a sacrificial layer of Molybdenum, delay bed of thoria or magnesia and the bottom most base layer made of stainless steel is proposed and its adequacy is substantiated by heat transfer analysis.

1.7 ORGANIZATION OF THE THESIS

Chapter 1 gives introduction to the research problem and outlines the scope of the work. Chapter 2 provides the review of literature in the relevant research areas. Mathematical formulation of the problems and solution procedures are elucidated in Chapter 3. Chapter 4 deals with natural convection studies in top heated and side wall cooled sodium filled cylindrical enclosures in general followed by analysis of the lower cold sodium plenum of the reactor vessel in particular. The development of HEATRAN-1, the transient heat conduction code which includes melting phenomenon is detailed and its application to the grid melting problem following ULOFA is presented in Chapter 5. Core-melt relocation following PLOHS accident is also presented in the same chapter. The concept of multi layer core catcher is put forth along with relevant heat transfer analysis and the results are highlighted in Chapter 6. The major conclusions drawn from the studies are summarized in Chapter 7.

CHAPTER 2

REVIEW OF LITERATURE

2.1 INTRODUCTION

The works reported in open literature in relevant areas, namely (i) natural convection in enclosures, (ii) numerical methods for phase change problems and close contact melting process and (iii) various available options for invessel retention of core debris, are reviewed in detail to lay the foundation for the present research objectives.

2.2 NATURAL CONVECTION IN ENCLOSURES

Natural convection in a top heated and side wall cooled liquid sodium enclosure which simulates the lower sodium plenum of reactor vessel is one of the problems to be solved. It is a well known fact that heat transfer characteristics of liquid sodium are quite different from that of normal liquids because of its very low Prandtl number. Empirical correlations for convective heat transfer in sodium are rather limited because of inherent difficulties in performing sodium experiments. Wolff et al. (1988) have presented a combined experimental and numerical study of natural convection heat transfer in vertical cavities filled with liquid metals. Experiments are performed in two different test cells with two opposing side walls held at constant but different temperatures and the remaining walls insulated. Kek and Muller (1993) have conducted experiments in liquid sodium filled horizontal layers heated from below with cavity aspect ratio close to 0.1. They proposed the following two correlations for Nusselt number (Nu) in terms of Rayleigh number (Ra)

$$Nu \propto Ra^{0.31} \quad \text{for } 1\times10^{4} < Ra < 5\times10^{4} \tag{2.1}$$

$$Nu \propto Ra^{0.2} \quad \text{for } 5\times10^{4} < Ra < 2.55\times10^{5} \tag{2.2}$$

But, when the aspect ratio of the cylinder is close to one with Pr = 0.004, they have indicated that Nusselt number correlation prposed by Kudryavtsev gives reasonably accurate results.

$$Nu = 0.38\,(Ra \times \mathrm{Pr})^{0.33} \quad \text{for} \quad Ra{\times}Pr = 2000 \text{ to } 8000 \tag{2.3}$$

On comparing with various available correlations they have noted that the correlations follow the 1/3 power law though the proportionality constants vary significantly. Sheriff and Davies (1979) have made experimental measurements for natural convection from plane surfaces in liquid sodium. On comparing their results with those of Cliffton and Chapman (1969) and Fujii et al. (1974) they found that their results were 15% higher. For isothermal horizontal downward facing hot surfaces in sodium, they suggest the following correlation for Nusselt number

$$Nu = 0.5212(Gr \times \mathrm{Pr}^2)^{\frac{1}{5}} \tag{2.4}$$

For uniform heat flux conditions, average Nusselt number is given by

$$Nu = 0.620(Gr^* \times \mathrm{Pr}^2)^{\frac{1}{6}} \tag{2.5}$$

Rigoleur (1982) conducted experimental studies and obtained the following correlation for isothermal downward facing surfaces as

$$Nu = 0.6(Gr \times \mathrm{Pr}^2)^{\frac{1}{5}} \tag{2.6}$$

The study by Uotani (1987) also endorses the same correlation. For constant flux condition, he has developed an empirical correlation using modified Boussinesq number Bo^* as

$$Nu = 0.59(Gr^* \times \mathrm{Pr}^2)^{\frac{1}{6}} \quad for \quad 8.6\times10^5 < Gr^* \times \mathrm{Pr}^2 < 3\times10^6 \tag{2.7}$$

Mohamed and Viskanta (1993) have modeled turbulent buoyant flow and heat transfer in liquid metals. The cavity is either heated differentially or heated from below. The flow becomes turbulent for Bo > 4800. For a differentially heated cavity, Nusselt number correlation is derived as

$$Nu = 0.386\,Bo^{0.286} A^{0.213} \tag{2.8}$$

Rossby (referred by Kek and Muller, 1993) has carried out heat transfer experiments with $Pr = 0.025$ in the range $10^3 < \mathrm{Ra} < 5\times10^5$ and developed an empirical correlation

$$Nu = 0.147\,Ra^{0.257} \tag{2.9}$$

Rossby also claims that he could not observe truly laminar convection in his test apparatus above the critical Rayleigh number required for convection to set in (Kek and Muller, 1993).

In all of the above cited works, the effect of the finite thickness of the wall on convective heat transfer has not been addressed. Generally, heated or cooled walls are treated as thin plates of negligible thickness and of uniform temperature distribution. The temperature drop across the wall or plate is not accounted for. In the present case of reactor application, liquid metal contained in the enclosure has high thermal conductivity compared to the surrounding walls. Since the heat source is applied upon the top plate having significant conductive resistance, the plate is subjected to large temperature gradient and hence the effect of finite thickness of the plate on heat transfer cannot be neglected. Therefore in the present study, a conjugate heat transfer analysis is carried out and the influence of conductivity ratio of the solid plate to that of enclosed liquid and the height ratio, on Nusselt number is investigated. The conductivity ratio between the plate and that of the liquid (κ^*) has a role to play in conjugate heat transfer even for $Pr > 1$ as inferred from the literature. The works of a few researchers in different geometries are summarized below.

Shaarawi and Negm (1999) have studied steady conjugate heat transfer in open ended vertical annulus and stressed the influence of conductivity ratio on the induced flow behaviour under laminar natural convection. Trevino et al. (1997) have studied forced convective heat transfer, in laminar flow parallel to a thin finite thickness plate with uniform temperature at the lower surface. They found that only for Brun numbers larger than 0.1, the thermal resistance of the wall can be neglected. Brun number is defined as the ratio of longitudinal heat transfer parameter to the aspect ratio of the plate. The longitudinal parameter discussed by Trevino et al. (1997) is a function of conductivity ratio, Reynolds number and Prandtl number. Chida (2000) also has investigated a similar external flow problem and indicated the influence of conductivity ratio on heat transfer is significant.

Yadav and Kant (2008) have experimentally studied conjugate heat transfer from a vertical flat plate of finite thickness under natural convective cooling and also obtained analytical solutions for the same. They have concluded that Rayleigh number and heat conduction parameter which is a function of conductivity ratio and aspect ratio greatly influence the heat transfer behaviour. Mamun et al. (2008) have carried out a numerical study of conjugate heat transfer for a vertical flat plate with heat generation effect and have inferred that the temperature of the fluid increases with increasing heat generation parameter and decreasing conduction parameter and Prandtl number. Furthermore they found that the rate of heat transfer decreases with increasing heat generation parameter, conduction parameter and decreasing Prandtl number.

Makinde (2011) has adopted a computational approach to study mixed convection from a convectively heated vertical plate to a fluid with internal heat generation. The effects of local Grashof number, Prandtl number, Biot number and internal heat generation parameter on the velocity and temperature profiles are interpreted in this study. Vynnycky and Kimura (1996) have studied two dimensional conjugate free convection due to a heated vertical plate of finite extent, adjacent to a semi infinite fluid region, analytically and numerically. They have elicited the dependence of heat transfer on Rayleigh number, Prandtl number, conductivity ratio and plate aspect ratio. Averaging the temperature over the plate length and solving one dimensional heat conduction and convection, they have also obtained an average Nusselt number.

Mostofa et al. (2003) have studied natural convection heat transfer in a rectangular enclosure with a single cold side wall both experimentally as well as numerically and found that $Nu \propto Ra^{0.25}$ for high *Pr* liquids. Turbulent natural convection in a transparent medium in a rectangular enclosure with differentially heated side walls has been investigated by Velusamy et al. (2001). They found that in tall enclosures, the convective Nusselt number exhibits three distinct regimes with respect to aspect ratio, namely, slow growth regime, accelerated growth regime and saturated regime. The wide range of discrepancy observed in natural convective correlations for different orientations of hot surfaces is reported in a review paper by Jabbar (2001). Gazit (1998) in his study has pointed out the strong dependence of natural convection on geometry for low Prandtl number liquids in enclosures. Hence, it is essential to establish natural convection heat transfer correlations for liquid sodium heated through the top surface in a cylindrical enclosure and cooled by the side wall , with an aspect ratio close to 0.4. This study assumes importance in severe accident analysis of nuclear reactors wherein heat generating core-melt settles upon the grid plate. The grid plate laden with core-melt, the core support structure at the side and the main vessel bottom form the cylindrical enclosure.

2.2.1 Choice of Turbulence Model

Two equation high Reynolds number k-ε turbulence models are generally employed to handle turbulence in a simplified yet efficient manner for forced convection flows. Direct Numerical Simulation (DNS) and Large Eddy Simulation (LES) are other possible options for studying turbulent convection. DNS models are computationally prohibitive. LES models too are computationally expensive because they model turbulence in 3 D and time dependence is an essential feature. Moreover, the success of LES relies on robust and accurate sub-grid scale models (Grotzbach and Worner, 1999). Natural convection which is mildly turbulent can be treated reasonably well with low Reynolds number k-ε model. Standard k-ε models which rely on wall functions to relate the quantities close to wall tend to overpredict the turbulent quantities for natural convections (Henkes, 1991). In low Reynolds number k-ε model, grids have to be placed packed close to the wall upto the laminar sub layer. This eliminates the need for wall functions and is able to predict natural convection more accurately than the other models. Therefore to study turbulent natural convection of sodium, it is proposed to use the low Re turbulence model proposed by Lam and Bremhorst (Wilcox, 1994).

2.3 CORE-MELT RELOCATION STUDIES

During melt relocation studies, heat conduction along with melting is the dominant physical process to be modelled. Therefore, a suitable mathematical model has to be formulated and a robust computer code is to be developed for solving transient heat conduction with phase change with the view to determine melt relocation time to core catcher. From the literature, it is seen that heat transfer studies related to molten material relocation have been carried out for reactors like SPX-1, CDFR and BN 800 to assess the time taken for the core debris to reach the core catcher (Dufour, 2007, Niwa, 1994 and Voronov, 1994). In these analyses, the time taken for molten material relocation to the core catcher which includes melt through of grid plate is assessed from a minimum of hundred seconds to a maximum value of 5.5 hours based on reactor design, various assumptions and initial conditions. Similar investigations for Indian FBRs are to be performed for safety analysis. In literature, both analytical and numerical methods are available for the solution of phase change problems. Hybrid of analytical methods and numerical methods are also available. Stefan's problem offers analytical solution for melting / solidification phenomenon in semi infinite media and it serves as the basic benchmark for validation of computer codes that are used to seek solution to complex phase change problems.

2.3.1 Analytical Solution for Phase Change Problems

Heat transfer problems involving phase change are nonlinear and are not amenable to analytical solutions except in very simple cases (Ozisik, 1977, Carslaw, 2005 and Croft, 1977). Exact analytical solution is available for the classical Stefan type of problems where the material under consideration is initially maintained at the melting temperature. (S.P.Venkateshan, 2004 Ozisik, 1994 and Poulikakos, 1994) The problem is schematically represented in Fig.2.1. Since the substance is initially maintained at the melting temperature T_m and is subjected to a constant temperature $T_0 > T_m$ at one face, the energy equation in the melting liquid region is given by

$$\frac{\partial T}{\partial t} = \alpha_l \frac{\partial^2 T}{\partial x^2} \qquad 0<x<s(t),\ \ t>0 \qquad (2.10)$$

where α_l is the thermal diffusivity of the liquid.

Initial condition

$$T(x>0,0)=T_m$$

Boundary condition

$$T(0,t>0)=T_0,\ T(s,t>0)=T_m$$

Energy balance at the solid - liquid interface gives the boundary condition at x=s

$$-\kappa_l \left.\frac{\partial T}{\partial x}\right|_{x=s} = \rho_s L \frac{ds}{dt} \qquad (2.11)$$

where ρ_s is the density and L is the latent heat of melting.

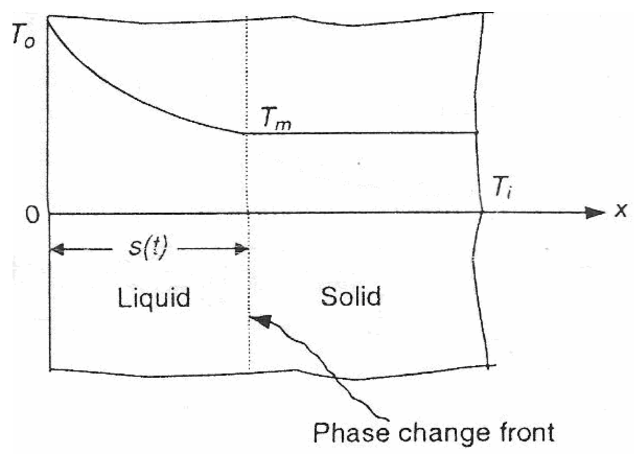

Fig. 2.1 Stefan Problem for melting in semi infinite space

The Neumann problem deals with the melting of a substance initially at a temperature below the melting temperature. The surface of the solid is brought instantaneously to a temperature above the melting point and is held constant at that value. This problem is represented in Fig. 2.2.

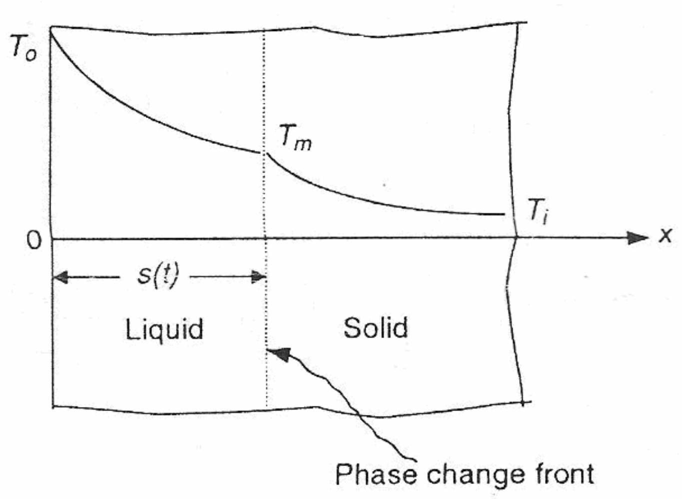

Fig. 2.2 Neumann Problem for melting in semi infinite space

The main difference between Stefan and Neumann problems is the prevalence of temperature variations in both the liquid phase and the solid phase in the latter case. Also at the phase change front, the heat conducted from the liquid side is shared between the heat used in melting and the heat conducted into solid phase. The corresponding governing equations are as follows:

Liquid phase:

$$\frac{\partial T}{\partial t} = \alpha_l \frac{\partial^2 T}{\partial x^2} \qquad 0<x<s(t), \quad t>0 \qquad (2.12)$$

Solid phase:

$$\frac{\partial T}{\partial t} = \alpha_s \frac{\partial^2 T}{\partial x^2} \qquad s(t)<x<\infty, \quad t>0 \qquad (2.13)$$

Interface condition is given by considering energy balance at x=s

$$\begin{bmatrix} \text{conduction of heat flux} \\ \text{through liquid phase} \end{bmatrix} - \begin{bmatrix} \text{conduction of heat flux} \\ \text{through solid phase} \end{bmatrix} = \begin{bmatrix} \text{rate of heat absorbed} \\ \text{during melting} \\ \text{per unit area of interface} \end{bmatrix}$$

which can be expressed mathematically as

$$-k_l \left.\frac{\partial T}{\partial x}\right|_{x=s} + k_s \left.\frac{\partial T}{\partial x}\right|_{x=s} = \rho_s L \frac{ds}{dt} \qquad (2.14)$$

The initial and boundary conditions are:

$T = T_0$	at x = 0	for t>0
$T = T_m$	at x = s	for t>0
$T \rightarrow T_i$	as $x \rightarrow \infty$	for t>0

2.3.1.1 Analytical Solution for Stefan's Problem

The Stefan problem can be solved analytically since a general solution to the heat equation is

$$T(x,t) = A + B\,erf\left[\frac{x}{2\sqrt{\alpha_l t}}\right] \qquad (2.15)$$

where $A = T_0$

$$B = \frac{T_m - T_0}{erf\left[\frac{s}{2\sqrt{\alpha_l t}}\right]}$$

The moving boundary condition can be written in the nondimensional form as

$$Ste = \sqrt{\pi}\mu e^{\mu^2} erf(\mu) \quad (2.16)$$

where $Ste = \dfrac{C_{pl}(T_0 - T_m)}{h_{sl}}$

$$\mu = \frac{s}{2\sqrt{\alpha_l t}}$$

The Stefan number (Ste) signifies the importance of sensible heat to latent heat. If the Stefan number is very small, say less than about 0.1, the heat released or absorbed by the interface during phase change is affected very little as a result of the variation of the sensible heat content of the substance during the phase change process (Ozisik, 1994, Dieter, 2006). During grid plate melting, the Stefan number is greater than 2. Therefore, analytical solution, by way of approximating to Stefan problem will not yield accurate result.

Even in Stefan problem, if the boundary condition is of Neumann (flux prescribed) or Robbin (convective boundary) type, solution of the problem becomes extremely difficult. Moreover, analytical solution is applicable to semi infinite media whereas in practical applications, the material under consideration has finite dimensions. Therefore one has to resort to numerical solution option.

2.3.2 Semi Analytical Methods

There are also semi analytical methods available for solving phase change problem, namely, the Heat Balance Integral Method (HBIM) (J.Caldwell,1994 and 1998), nodal integral methods, (Uddin, 1999) perturbation methods (Caldwell,2003 and Yigit, 2008) and Boundary Element method (BEM) (Silva,1994, Lewis and Morgan, 1981 and Zhifeng, 1988). HBIM was originally proposed by Goodman and he assumed a particular temperature profile, integrated the heat equation over an appropriate interval to obtain a set of heat balance integral equations. The equations are then solved to obtain the motion of the interface boundary. HBIM explicitly tracks the motion of isotherms by front tracking methods. However front tracking methods often result in complicated schemes that are difficult to apply in multidimensional problems (Caldwell, 1998). Uddin has used nodal integral method to solve 1D phase change with periodic Dirichlet boundary condition. He has reported that the effect of the oscillating surface temperature on the evolution of the moving boundary is most pronounced when the domain is small and diminishes as the domain grows.

BEM falls under the classification of semi analytical solutions. It requires discretisation of only the surface of the solidifying body and follows a numerical method of solving linear partial differential equations which have been formulated as integral equations. The integral equation may be regarded as an exact solution of the governing partial differential equation. The boundary element method is often more efficient than other methods in terms of computational resources for problems where there is a small surface to volume ratio. Boundary element formulations typically give rise to fully populated matrices. This means that the storage requirements and computational time will tend to grow according to the square of the problem size(Zabaras, 1987). A restriction of the boundary element method is that the fundamental solution to the original partial differential equation is required in order to obtain an equivalent boundary integral equation. Another restriction is that domain integrals are needed to account for nonhomogeneous terms arising from initial conditions and body loads. (Honnor, 2004).

2.3.3 Numerical Solution Methods

The restrictions associated with semi analytical solutions have turned the interest of the research community towards numerical methods. The availability of high end computing facilities have further fuelled this interest. Many authors have applied numerical methods for solving the freezing / melting problem and a spectrum of different methods is available in the literature. Poulikakos (1989) has investigated the solidification of a binary alloy, modeling the mixed phase mushy region. The thermal properties of the mush are assumed to be volume fraction weighted averages of the properties of the individual phases. In addition, he has identified seven dimensionless groups and the effect of these groups on the size and growth rate of the mushy zone is reported. Naterer (2000) has formulated an entropy based method using the second law of thermodynamics for accurate simulations of phase change problems with fluid flow. Heim (2005) has proposed an effective heat capacity method and additional heat source method as improvisations of enthalpy method for applications in phase change materials. Naaktgeboren (2007) has presented an isothermal moving boundary approach to model phase change process. This zero phase model can be applied as an analytical approximation for cases having small Biot numbers.

To study core degradation in LWRs, Dosanjh (1988) has developed the MELTPROG code and Ahmed (1988) has developed the APRIL code in which phase change phenomena have been modelled. Kwang (2004) has investigated numerically the heat transfer characteristics of a liquid metal pool subjected to a partial solidification process using the MPCOOL code. He solved the conservation of mass, momentum and energy equations. For the energy equation, enthalpy formulation has been used. Similarly, Farmer (1990) has developed a one dimensional multicell Eulerian finite difference computer code for freezing of molten corium on concrete or steel substrate.

The broad classification of methods available for solution of phase change problems is given below.

2.3.3.1 Classification Based on Solved Variable

The mathematical formulation of the phase change problem, depending on the variable to be solved, can be of two types, namely temperature formulation and enthalpy formulation. In the first one, the energy equation is cast in a form with temperature as the dependent variable and total enthalpy is the dependent variable in the latter formulation. Enthalpy method was initially developed for materials which are not eutectic where the melting or solidification takes place over an extended range of temperature. But rigorous mathematical analysis has proven that it could be applied with equal ease and accuracy for phase change of eutectics as well. (Shamsundar, 1975). But the temperature formulation can be applied for eutectics only. In both these formulations the differential form of the energy equation is generally used. Effective heat capacity methods and source based methods follow the temperature formulation.

2.3.3.2 Classification Based on Discretisation Procedure

Numerical solution can be sought using finite difference method, finite volume method (Patankar, 2004), finite element method or combined volumes-elements method (Naterer, 2000) which are all volume discretisation methods or by BEM which is a surface discretisation method. Finite difference method is based on differential formulation whereas all the other methods employ integral formulation. Hybrid methods and meshless methods are recent additions to this vast range of methods (Thakur, 2009). Control Volume Finite Element Method (CVFEM) combines the advantages of finite volume method and finite element method. CVFEM formulations are easily amenable to physical interpretations and their solutions satisfy local and global conservation requirements even on coarse grids which are the desirable traits inherited from finite volume methods. Besides they also provide the geometric flexibility that is traditionally associated with FEMs (Baliga, 1997). Voller in his work has presented a deforming CVFEM solution to solidification problem on a uniformly cooled pipe and has presented oscillation free temperature history that matches closely with analytical solution (Voller, 1997).

Generally, Finite Element Methods (FEM) Finite Difference Methods (FDM) and Finite volume methods are the popular ones employed for the solution of melting/ solidification problems (Seetharamu, 2001, Nithiyarasu, 2000). A comprehensive review of various methods available and their relative merits and demerits is available in the work of Henry and Argyropoulosz (1996) and also in the work of Voller(1997). They conclude that FDM is advantageous if the geometry is regular and it lends itself for easy programming. Because of these advantages, FDM is adopted in the present study.

2.3.3.3. Classification Based on Grid Generation Techniques

Based on the discretisation procedures, the numerical methods can be further classified as fixed grid method, variable grid method, front fixing method, isotherm migration method and adaptive grid generation method (Ozizik, 1994 and Lewis and Morgan, 1981). In fixed grid method, the space time domain is subdivided into a finite number of equal grids Δx, Δt for all times. The moving solid-liquid interface will in general lie somewhere between two grid points at any given time. It is tracked by means of a suitable interpolation formula. In the variable grid method, the space-time domain is subdivided into equal intervals in one direction only and the corresponding grid size in the other direction is determined so that the moving boundary always remains at a grid point. The variable time step approach has been reported by Gupta and Kumar (1981).

In front fixing method, the moving boundary is fixed for all times using a coordinate transformation. Isotherm migration method calculates how the specified temperatures move through the medium by capturing the isotherms and can be applied to problems where the phase change boundary is an isotherm. Extension of isotherm migration method is possible from regular geometries to arbitrary shaped ones and has been applied to solve two dimensional problems as well (Shyy, 1994).

Adaptive grid generation is very promising for solving multidimensional moving boundary problems in bodies having irregular shape (Brackbill,1982). In this approach, the numerical grid generation is applied to map the irregular region into a regular shaped region in the computational domain where the problem is solved with finite differences and the results are transformed back into physical domain.

2.3.4 Close Contact Melting of a Migrating Heat Source

In the core-melt relocation study, molten fuel which is denser than stainless steel grid plate is lying above the grid plate melting it. Because of the density difference, molten stainless steel gets displaced by the heavier and denser molten fuel. Therefore, apart from the phase change, displacement due to close contact melting also has to be modelled.

Close contact melting occurs when a solid melts while being in contact with a heat source. The liquid generated at the melting front is squeezed out from under the solid by the pressure maintained in the central section of the film by the weight of the free solid. It is known that contact melting is a wide and complex area of study (Moallemi, 1985). Exact study of molten material displacement requires solution of flow and energy equations and also entails the use of free surface models combined with proper viscosity definition for the molten material in Navier-Stokes equations. Moallemi in his study has obtained an expression for the film thickness of the melting object in contact with an isothermal heat source in terms of force due to apparent weight and Stefan number (Moallemi and Viskanta, 1985 and Chen, 2008).

Chen et al., (2008) have investigated the process of temperature difference driven contact melting of solid phase change material around a horizontal cylinder and they have authorized that Moallemi and Viskanta’s model is more convenient for use and is accurate especially for calculating the melting rate of the hot body, Groulx and Lacroix

(2003) quote that in most of the investigations reported in the open literature, the process by which the melt is squeezed out of the small gap separating the heat source and the solid is considered quasi steady and heat transfer through the liquid film is by conduction only. Therefore, it is proposed to use Moallemi and Viskanta's expression for film thickness to define the threshold for dynamically adapting the spatial grid in the grid plate melting problem and treat contact melting as conduction problem only.

2.3.5 Choice of Method for Phase Change Problem

Since the methods available for phase change problem are quite numerous, the choice of the method depends on the problem that is analysed. A particular method can't be labeled as superior to others in all respects. Therefore a judicious choice has been made to use fixed grid finite difference method in enthalpy formulation. Simplicity, ease of programming and ease of physical interpretation are the chief reasons for this choice. Explicit finite differencing method is used. Enthalpy method is advantageous since the location of the interface need not be tracked by solving a separate equation and there is no need to consider the solid and liquid regions separately. Adapting to non-eutectics can be easily done, if the enthalpy as a function of temperature in the melting range of temperatures i.e., in the mushy region is known. The position of the interface can be found by comparing the enthalpy between the successive nodes. Fixed grid method is employed and the interface location with resolution equal to that of spatial mesh size can be readily obtained from the solution. For exact prediction of the interface, the algorithm proposed by Voller and Cross (Voller, 1981) has been used. Moreover, enthalpy method is shown to be accurate even with coarser grids (Caldwell,1998).

Another salient feature of the study is that it employs dynamic adaptation of the computational mesh, giving way for the molten grid plate material to be displaced as the heavier molten fuel sinks into it. The essentials of contact melting problem are incorporated by defining a thin film thickness below the hot source which squeezes the molten material. Convection in the molten film and its flow around the moving heat source are not modelled.

2.3.6 Study of PLOHS

PLOHS can happen on the failure of Decay Heat Removal Systems (DHRS) namely, Operating Grade Decay Heat Removal system (OGDHRS) and Safety Grade Decay Heat Removal System (SGDHRS) whose combined failure probability is of the order of less than 10^{-7}/reactor year (Endo, 1986). The SGDHRS is a passive system which relies on natural convection of sodium for the decay heat removal from the hot pool. The only active component of the system is the air damper which can be opened either manually or pneumatically. In the SGDHRS system, the functionality of the sodium-sodium decay heat exchanger and sodium- air heat exchanger and the tall hood to aid the air draft have undergone experimental testing at test facilities and have been validated with supporting computations before being erected (Revathy et al., 2011, Sajish et al., 2009). Nevertheless, as part of the safety analysis, the consequence of this rare accident is analysed to quantify the time taken for the molten material to get relocated to the core catcher.

In general, molten material relocation to the core catcher following a severe accident in a FBR is a matter of safety concern which needs to be analysed systematically for various possible accident scenarios to define the initial thermal load on the core catcher(Niwa,1994). Such analyses are found in the literature for reactors like Superphenix and BN 800. For Superphenix the core-melt relocation time is estimated to be around 3000 s (Gluekler et al., 1982). For the BN 800 reactor, slow melting away of the structures underneath the core is postulated and the time estimate for relocation is estimated to lie between 3.5 hours to 5.5 hours depending upon the initial axioms set forth for the accident sequence (Voronov, 1994 and Vlasichev et al., 1994).

The different regions along the length of a fuel are blanket region, fission gas plenum, tail piece of subassembly, discriminator at foot of subassemblies and top of grid plate. These are the regions to be modeled to study the downward relocation of molten core-melt. Each region consists of fractions of materials like sodium, stainless steel, depleted uranium oxide and helium and other fission gases. Mathematical modeling of the exact geometry of a fuel subassembly with 217 fuel pins for thermal hydraulic analysis is very difficult primarily because of meshing requirements which would further entail huge computational resources and time (Velusamy et al., 2010 and Gajapathy et al., 2007). The finer details of clad melting, its downward motion in the coolant channel, freezing, plugging the channel, remelting etc., are furthermore complex phenomena for modelling. Such work have been modelled in comprehensive safety analysis computer codes such as SAS-4 and SIMMER by introducing specific multi phase modules like EPIC, PLUTO and LEVITATE (Garner and Abramson, 1979 and Bowers et al., 1979). In the present analysis, it is proposed to incorporate a simplified but global treatment of molten material relocation adopted for the BN 800 reactor, wherein a porous body formulation is chosen.

2.4 CORE CATCHER FOR FBRS

Core catcher design for future FBRs shall take into account the existing designs and modifying them suitably so that a whole core melt down can be accommodated on the core catcher. A brief review of the existing FBR core catchers is given below. In the French sodium cooled reactors, Rapsodie had an external gas cooled outer vessel. Super Phenix-1 (SPX-1) had in-vessel core catcher which can accommodate debris generated from melting of only seven subassemblies. Heat transfer by natural convection in sodium pool above and below the internal core catcher in SPX-1 was evaluated by Rigoleur and

Tenchine (1982). In the design of UK reactors, Dounreay Fast Reactor (DFR) had fuel dispersion cone to avoid lump formation and splash plates to direct the corium to core catcher plate to manage the thermal load, Prototype Fast Reactor (PFR) had a single layer of trays with retention capacity for entire core, with forced cooling provision underside of the plate. Commercial Demonstration Fast Reactor (CDFR) design had vertical standpipes attached to the core catcher plate to aid natural convection of sodium and avoid sodium dryout within the debris bed (Broadly et al., 1982, Waltar and Reynolds, 1980).

Ex-vessel core catcher can be considered as an additional provision only, apart from the in-vessel core catcher. It cannot be a stand alone provision for FBRs because of reactive nature of sodium. The idea of ex-vessel core catcher was tried for Fast Flux Test Facility (FFTF), in the design stage; but was later dropped due to space and other constraints (Friedland and Tilbrook, 1974). Forced cooling of the gap between main vessel and safety vessel is yet another viable additional safety option. KALIMER 150 which is a small metal fuelled Korean reactor is relying upon forced main vessel cooling for its decay heat removal. For larger reactors, forced air / nitrogen cooling may not be sufficient to cool the main vessel surface. In Phenix reactor, cooling pipes were wound around the safety vessel surface for forced convection heat removal. The disadvantage with this approach is that in-service inspection of the vessel becomes difficult.

The in-vessel core catcher in the Indian PFBR consists of a heat shield plate and a core catcher plate made of stainless steel each of thickness 20 mm and separated by a sodium gap of 20 mm. It has a central chimney of diameter 500 mm and height 180 mm along with an inverted cone structure to aid the natural convection of liquid sodium from below the plate. The design safety limit is set at 923 K for the core catcher based upon creep considerations. (Sati et al., 2010). It was originally designed to withstand the thermal and heat load from a 7 subassemblies melting accident. Subsequent analysis predicts that it can contain the consequences of accident encompassing 19 subassemblies too (Roychowdhury, 1998). For future Indian FBRs, a core catcher which is capable of retaining, dispersing and cooling core debris from a whole core event is to be designed. Towards meeting this requirement, a multi layer core catcher is proposed. It is conceptualized based on the core catcher designs existing elsewhere for ALWRs and modified to meet specific requirements of sodium cooled reactors.

2.4.1 Performance Enhancement of Core Catcher

There are several possible methods to improve the core catcher heat retaining capacity in FBRs. The performance of in-vessel core catcher can be enhanced by adopting new techniques such as

- Refractory coating on the core catcher plate
- Multi tray concept
- Multi layer concept

Multi tray concept is planned to be adopted for the upcoming Japanese reactor JSFR, which is a loop type reactor. The other two concepts are still in nascent stage for sodium cooled FBRs and need rigorous analysis and careful evaluation of the material choice, to be of practical use in the future reactors. A passive ex-vessel core catcher can be additionally housed in the reactor cavity / vault as a diverse safety measure.

2.4.2 Refractory Coating on Core Catcher

This concept has been adopted for high power APRs (Kanga et al., 2007). A joint U.S.-Korean effort to design and evaluate the feasibility of an enhanced in-vessel core catcher for APR-1000 has been reported in literature (Condie et al., 2004). The core catcher consists of two material layers with an option to add a third layer, if deemed necessary: (i) a base material, which has the capability to support and contain the mass of core materials that may relocate during a severe accident; (ii) an insulator coating material on top of the base material, which resists interactions with high temperature core materials; and (iii) an optional coating on the bottom side of the base material to prevent any potential oxidation of the base material during the lifetime of the reactor. Results from scoping thermal and structural analyses suggest that an in-vessel core catcher is feasible with stainless steel as base material, MgO or ZrO with thickness upto 1 mm as the coating material with a 100 micron of bond coating with Nickel based alloy. This concept has not been tried with sodium cooled FBRs due to vulnerability of the coating peeling off because of corrosion in sodium environment. Experimental studies in liquid sodium could throw more light on the feasibility of such a core catcher for FBRs.

2.4.3 Multi Tray Core Catcher Concept for FBRs

The option to use multiple trays stems from the fact that if the total heat load can be distributed to several trays, it is easy to maintain plate temperatures within design safety limits. Sharma et al., (2008 and 2009) have discussed the option of using a set of three trays. They have established that triple tray can dissipate a heat load of 25 MW without tray temperatures exceeding 923 K. Multi tray core catchers promise scope for invessel retention, but the height of the lower plenum may have to be increased which would entail more cost. Ensuring equal distribution of the core debris to all the plates too is a challenging task.

In JSFR which is a loop type reactor, it is proposed to use a multi tray core catcher (Sato et al., 2011). In order to facilitate tray-to-tray debris transfer, ‘‘debris guide tubes’’ are adopted. This structure consists of a hole surrounded by a vertical collar and allows pouring off of the excess debris above this collar. Preliminary analysis showed that the decay heat from the100% fuel can be transported successfully to the heat sink by natural circulation.

2.4.4 Ex-vessel Core Catcher

Several preliminary concepts for an Ex-Vessel Core catcher (EVCC) were evaluated for FFTF including a completely passive system, a passive system with natural circulation cooling and an active system with forced cooling (Friedland and Tilbrook, 1974). The EVCC system consisted of a sacrificial barrier of depleted urania or thoria brick, bounded at the sides and bottom of the lower cavity by the heat removal circuits. Due to space constraint to accommodate a forced cooling loop, the idea of EVCC was given up and eventually FFTF had a steel lined cavity (Walter and Reynolds, 1980).

2.4.5 Multi Layer Core Catcher in ALWRs

The concept of multilayer core catcher is already in use in ex-vessel core catchers in ALWRs. Szabo et al. (1995) have studied the feasibility of multi crucible ex-vessel core catcher for ALWRs. The vertical multi-crucible core catcher concept includes three main components, viz., a collector which surrounds the reactor pressure vessel, an assembly of a few tens of vertical crucibles located below the collector and a passive cooling system. The crucible consists of three layers namely, (i) the inner most sacrificial layer made of Magnesium aluminium oxide, (ii) the outer most layer is SS and (iii) ZrO_2 is sandwiched between these two layers.

Akopov (1998 and 2003) in his paper has discussed about using Titanate composites, termed synrocs as donor materials in the ex-vessel core catcher system. There is another concept for ex-vessel compartment type core catcher for VVER-1000. The main functional elements of this core catcher are the heat exchanger and the basket containing a sacrificial material. As a result of the comprehensive studies by Gusarov et al. (2001), the composition based on Fe_2O_3 (70% by mass) and Al_2O_3 (30% by mass) with several technological admixtures was chosen as the sacrificial material for the VVER-1000 ex-vessel corium catcher of the Tyanvan nuclear power plant.

2.4.6 Core Catcher for Future FBRs

Though the composition of fuel, clad and structural material and the coolant are different for sodium cooled FBRs, the core catcher concepts used for high power ALWR can be adopted for FBR with suitable modifications, after ensuring the compatibility of core catcher materials with sodium at high temperatures, during accidental conditions. Making such a bold attempt, a multi layer core catcher consisting of a top sacrificial layer, a middle refractory ceramic layer (which can itself be single or multiple layers) and a base layer is proposed for future FBRs.

2.5 CLOSURE

In this chapter review of literature in relevant fields is presented concisely. The solution methodology to be adopted for the research work is highlighted along with reasons for the particular choice. Low Reynolds number k-ε model is proposed for CFD simulation of turbulent natural convection of sodium. Enthalpy formulation discretised using finite difference method is to be employed for developing a computer code to study the grid plate melting phenomenon. Analysis of PLOHS will be done using porous body formulation with effective properties. For enhancing the core debris retention capacity of the core catcher, a multi layer core catcher is considered and its capability is to be proved by heat transfer analysis.

CHAPTER 3

MATHEMATICAL FORMULATION

3.1 INTRODUCTION

The research work involves three parts namely, natural convection studies, core-melt relocation studies and thermal studies on the multi layer core catcher. The mathematical formulation of the three problems along with governing equations and other relevant input conditions are presented in this chapter.

3.2 NATURAL CONVECTION AND CONJUGATE HEAT TRANSFER STUDIES

The commercial Computational Fluid Dynamics code PHOENICS is employed for this part of the study. Natural convective heat transfer is solved for thin plate approximation of the sodium enclosed cavity. However, conjugate heat transfer analysis solving for heat conduction in the top plate and convection in enclosed sodium is carried out when the top plate has finite thickness with Bi > 0.1. The schematic of the problem in axi-symmetric geometry for thick top plate configuration is depicted in Fig. 3.1. Transient heat transfer computations are performed solving the conservation equations of mass, momentum and energy with appropriate initial and boundary conditions described in the next section. Boussinesq approximation is incorporated in the vertical momentum equation to take care of the buoyancy effect in sodium. The maximum temperature difference (ΔT) that the sodium in the confined cavity is likely to experience is less than 300 K. Therefore the condition $\beta \times \Delta T < 0.1$ is satisfied for applying Boussinesq approximation where β is the coefficient of volumetric expansion of sodium. Low Reynolds number k-ε model is invoked to handle turbulence. This model is suitable for natural convection boundary layers, where well defined wall functions are not available. However, fine grids have to be adopted with y^+ close to unity (Wilcox, 1994). The intention of the study is to obtain natural convective heat transfer correlations in the given geometry.

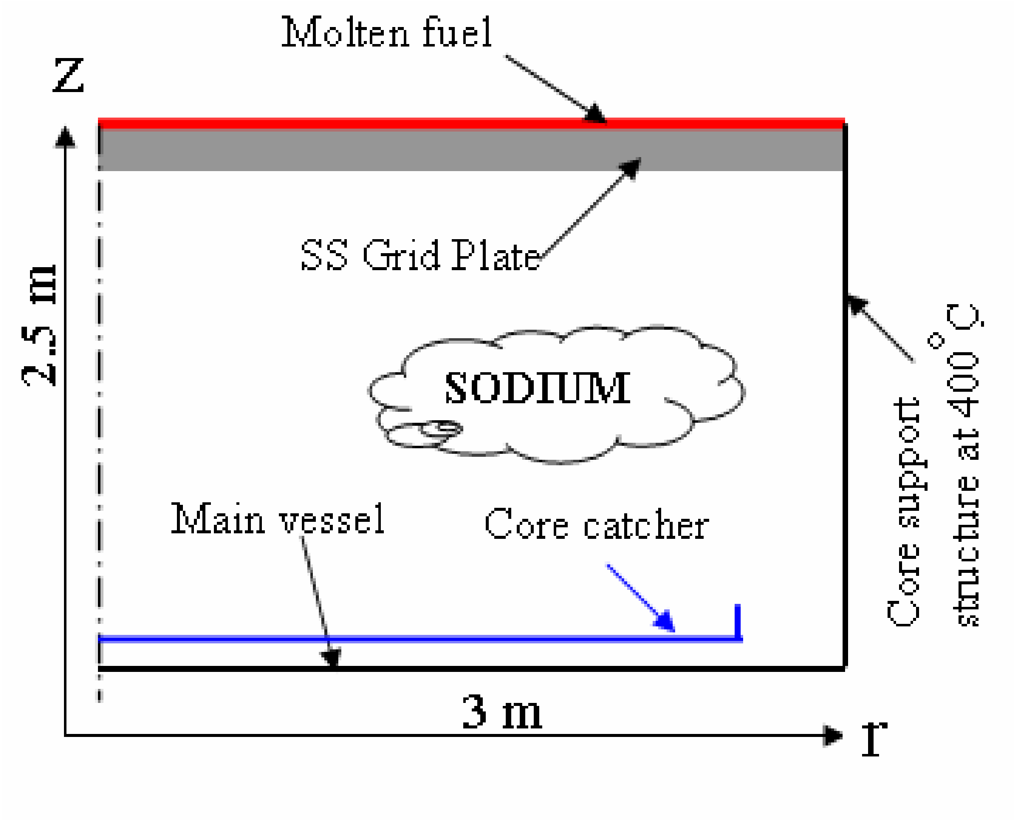

Fig. 3.1 Schematic of computational domain for natural convection studies

From the boundary layer theory for liquid metals, it is known that Nusselt number correlates with Boussinesq number (Bejan, 2004). Therefore, Boussinesq number is varied by altering the source temperature and also the enclosure size, preserving the aspect ratio. In the first part of the study with isothermal and isoflux conditions on the top plate, the thickness of the heated top wall is neglected. Steady state natural convection correlations are developed for Nusselt number in terms of Boussinesq number. Even for steady state analysis, false transient method has been used to promote smooth convergence. In the third case, wall thickness effect has been investigated both for steady and transient cases.

3.2.1 Governing Equations

For unsteady incompressible turbulent flow of sodium, mass conservation equation, Reynolds Averaged Navier-Stokes equations, energy equation, turbulent kinetic energy and its dissipation rate equations are as follows:

Continuity

$$\frac{1}{r}\frac{\partial(ru)}{\partial r}+\frac{\partial v}{\partial z}=0 \tag{3.1}$$

Radial Momentum

$$\frac{\partial(\rho_{Na}u)}{\partial t}+\frac{\partial(\rho_{Na}uu)}{\partial r}+\frac{\partial(\rho_{Na}vu)}{\partial z}=-\frac{\partial p}{\partial r}+\frac{1}{r}\frac{\partial}{\partial r}(r\mu_{eff}\frac{\partial u}{\partial r})+\frac{\partial}{\partial z}(\mu_{eff}\frac{\partial u}{\partial z})-\mu_{eff}\frac{u}{r^2} \tag{3.2}$$

Axial momentum

$$\frac{\partial(\rho_{Na}v)}{\partial t}+\frac{\partial(\rho_{Na}uv)}{\partial r}+\frac{\partial(\rho_{Na}vv)}{\partial z}=-\frac{\partial p}{\partial z}+\frac{1}{r}\frac{\partial}{\partial r}(r\mu_{eff}\frac{\partial v}{\partial r})+\frac{\partial}{\partial z}(\mu_{eff}\frac{\partial v}{\partial z})+g\rho\beta(T-T_{ref}) \tag{3.3}$$

Energy equation

$$\frac{\partial}{\partial t}(\rho_{Na}C_{Na}T_{Na})+\frac{\partial}{\partial r}(\rho_{Na}C_{Na}u_{Na})+\frac{\partial}{\partial z}(\rho_{Na}C_{Na}v_{Na})=\frac{1}{r}\frac{\partial}{\partial r}\left(r\kappa_{eff}\frac{\partial T_{Na}}{\partial r}\right)+\frac{\partial}{\partial z}\left(\kappa_{eff}\frac{\partial T_{Na}}{\partial z}\right) \tag{3.4}$$

Turbulent kinetic energy

$$\frac{\partial}{\partial t}(\rho_{Na}k)+\frac{\partial}{\partial r}(\rho_{Na}uk)+\frac{\partial}{\partial z}(\rho_{Na}vk)=\frac{1}{r}\frac{\partial}{\partial r}[r(\mu+\frac{\mu_t}{\sigma_k})\frac{\partial k}{\partial r}]+\frac{\partial}{\partial z}[(\mu+\frac{\mu_t}{\sigma_k})]\frac{\partial k}{\partial z}+p_k+G_k \tag{3.5}$$

Dissipation rate of turbulent kinetic energy

$$\begin{aligned}\frac{\partial}{\partial t}(\rho_{Na}\varepsilon)+\frac{\partial}{\partial r}(\rho_{Na}u\varepsilon)+\frac{\partial}{\partial z}(\rho_{Na}v\varepsilon)&=\frac{1}{r}\frac{\partial}{\partial r}[r(\mu+\frac{\mu_t}{\sigma_\varepsilon})\frac{\partial \varepsilon}{\partial r}]+\frac{\partial}{\partial z}[(\mu+\frac{\mu_t}{\sigma_\varepsilon})]\frac{\partial \varepsilon}{\partial z}\\&+[c_{\varepsilon1}f_1(P_k+C_{\varepsilon3}G_k)-C_{\varepsilon2}f_2\varepsilon]\frac{\varepsilon}{k}\end{aligned} \tag{3.6}$$

where $$P_k=\mu_t\left[2\left(\frac{\partial u}{\partial r}\right)^2+2\left(\frac{\partial v}{\partial z}\right)^2+\left(\frac{\partial u}{\partial z}+\frac{\partial v}{\partial r}\right)^2+2\left(\frac{u}{r}\right)^2\right]$$

$$G_k=-\frac{\mu_T}{\sigma_T}g\beta\frac{\partial T}{\partial z}$$

$$\nu_t = \frac{\mu_t}{\rho} = c_\mu f_\mu \frac{k^2}{\varepsilon}$$

$$C_{\varepsilon 1} = 1.44,\ C_{\varepsilon 2} = 1.92,\ C_\mu = 0.09,\ \sigma_k = 1.0,\ \ \sigma_\varepsilon = 1.3$$

$$f_\mu = \left(1 - e^{-0.0165 R_y}\right)^2 \left(1 + \frac{20.5}{\mathrm{Re}_T}\right)$$

$$f_1 = 1 + \left(\frac{0.05}{f_\mu}\right)^3$$

$$f_2 = 1 - e^{-\mathrm{Re}_T^2}$$

$$\mathrm{Re}_T = \frac{k^2}{\varepsilon \nu}; \quad R_y = \frac{k^{0.5} y}{\nu}$$

The model constants for the low Reynolds number k-ε model are functions of local turbulent Reynolds number as given above (Henkes, 1991 and PHOENICS user's manual, 2005). In particular, Lam Bremhorst model is adopted in the present study (Wilcox, 1994). This set of equations is solved using the elliptic staggered grid formulation using a CFD code PHOENICS. SIMPLE algorithm is used to resolve pressure-velocity coupling. In the conjugate heat transfer study, transient temperature field in the solid stainless plate is governed by the following heat conduction equation:

$$\frac{\partial(\rho_{ss} C_{ss} T_{ss})}{\partial t} = \frac{1}{r}\frac{\partial}{\partial r}\left(r \kappa_{ss} \frac{\partial T_{ss}}{\partial r}\right) + \frac{\partial}{\partial z}\left(\kappa_{ss} \frac{\partial T_{ss}}{\partial z}\right) \tag{3.7}$$

3.3 CORE-MELT RELOCATION AFTER ULOFA

An explicit finite difference transient heat conduction code including latent heat viz, HEATRAN-1 is developed to solve the grid plate melting phenomenon. The mathematical formulation of phase change problem is governed by partial differential equation of parabolic type. The location of the moving solid – liquid interface has to be obtained as a part of the solution (Venkateshan, 2004 and Ozisik, 1977). The enthalpy method is adopted in the present study due to its advantage that the position of the interface can be found by comparing the enthalpy between the successive nodes. (Ozisik, 1994). The schematic of the model is depicted in Fig 3.2. Voller's algorithm which is used to smoothen out the melt front is explained in the next section.

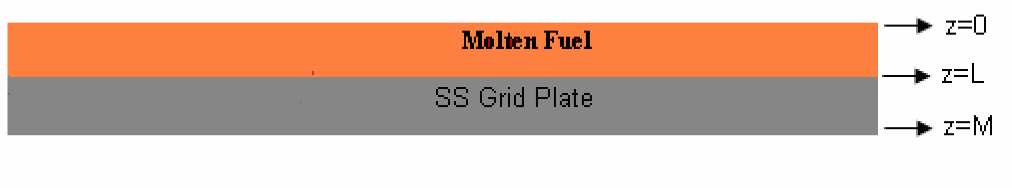

Fig 3.2 Schematic of the computational model

The governing equations are:

Fuel (core-melt) region

$$\rho_f \frac{\partial H_f}{\partial t} = \frac{\partial}{\partial z}\left(\kappa_f \frac{\partial T_f}{\partial z}\right) + \dot{q}''' \tag{3.8}$$

Initial and boundary conditions

$$T_f = (T_o)_f = 3020\,K \tag{3.9}$$

$$H_f = (H_o)_f = C_f\left((T_o)_f - (T_m)_f\right) \quad \text{at } t=0;\ 0 \le z \le L \tag{3.10}$$

At z = 0, the fuel layer is adiabatic

At z = L,

$$-\kappa_f\left(\frac{\partial T_f}{\partial z}\right) = -\kappa_{ss}\left(\frac{\partial T_{ss}}{\partial z}\right) \tag{3.11}$$

Grid plate region

$$\rho_{ss} \frac{\partial H_{ss}}{\partial t} = \frac{\partial}{\partial z}\left(\kappa_{ss} \frac{\partial T_{ss}}{\partial z}\right) \tag{3.12}$$

Initial and boundary conditions

$$T_{ss} = (T_o)_{ss} = 673\,K \tag{3.13}$$

$$H_{ss} = (H_o)_{ss} = C_{ss}((T_o)_{ss} - (T_m)_{ss}) \quad \text{at t=0 ; L} \leq z \leq \text{M} \tag{3.14}$$

At z = M

$$-\kappa_{ss}\left(\frac{\partial T_{ss}}{\partial z}\right) = 0 \tag{3.15}$$

(or)

$$-\kappa_{ss}\left(\frac{\partial T_{ss}}{\partial z}\right) = h(T - T_{Na}) \tag{3.16}$$

At melting point, enthalpy includes latent heat of fusion. Considering the melting temperature of fuel / stainless steel (depending upon the region) as the reference temperature for calculation of enthalpy,

$$H = C_p(T - T_m) \qquad for T \leq T_m \tag{3.17}$$

$$H = C_p(T_f - T_m) + L \qquad for T > T_m \tag{3.18}$$

The definition of enthalpy as indicated above helps in minimising the temperature oscillations usually encountered with the enthalpy method around the phase change temperature and it is termed relative enthalpy method. The inverse relationships to calculate temperature from enthalpy is given by

$$T = T_m + \frac{H}{C_p} \qquad for\, H < 0 \tag{3.19}$$

$$T = T_m \qquad for 0 \leq H \leq L \tag{3.20}$$

$$T = T_m + \frac{H - L}{C_p} \qquad for H > L \tag{3.21}$$

Since an explicit scheme is used for time marching, the restriction imposed on the time step is that cell Fourier number, Fo ≤ 1/2 for a stable solution. The governing equations are discretised using finite difference method in HEATRAN-1 code. Heat transfer coefficient between the grid plate bottom and liquid sodium, h is estimated through correlations obtained from the conjugate heat transfer study explained in Section 3.2.

3.3.1 Source Term

The core-melt is a source of heat by internal volumetric heat generation arising from the radioactive decay of the fission products which it contains. Reactor physics calculations for the fuel indicate that decay power is as high as 21% of reactor operating power one second after the accident. But it comes down rapidly to about 6% after one minute and 1.5% after an hour (Sridharan, 2002). Taking into account such time variations, the decay heat content is approximated by a function of the form

$$\dot{q}''' = 86.5 \times 10^{6} \,/ (t^{0.31}) \tag{3.22}$$

as illustrated in Fig. 3.3, where $\dot{q}'''$ is the volumetric heat source in W/m^3 and t is the time in seconds after the CDA.. This forms the volumetric heat generation source term which rapidly decreases with time. It is assumed that core-melt reaches the grid plate at times ranging from 1s to 100s after CDA which implicitly alters the initial heat load on the grid plate.

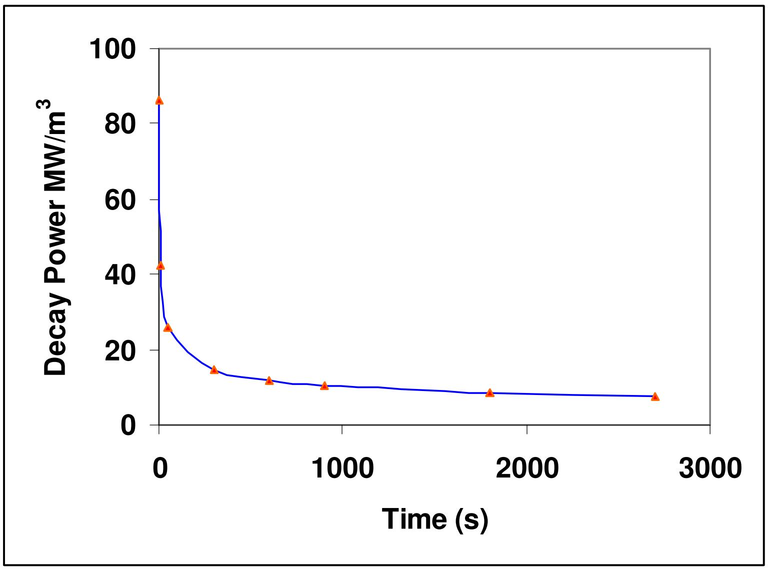

Fig. 3.3 Decay heat as a function of time

3.3.2 Voller's Algorithm for Tracking Interface

In enthalpy method, the phase boundary or the melt front cannot be located precisely within a mesh at a particular time. If the moving melt front has to be accurately tracked, suitable interpolation has to be adopted. The algorithm proposed by Voller and Cross for accurate tracking of solid-liquid moving interface is incorporated in the code (Ozisik, 1994).

Considering a node *i* of width Δz with its neighbouring nodes *i-1* and *i+1* as illustrated in Fig. 3.4, containing the solid liquid interface at the position z=s(t) at any time *t*, one dimensional control volumes represented by *e* are drawn around each node. Let *f* be the fraction of this element which is solid and *(1-f)* the fraction of the element which is liquid and let L be the latent heat of fusion. The melt front is moving in the positive *z* direction. The total heat content of the element e_i at any time *t* can be approximated as $H_i \Delta z$ where H_i is the nodal enthalpy.

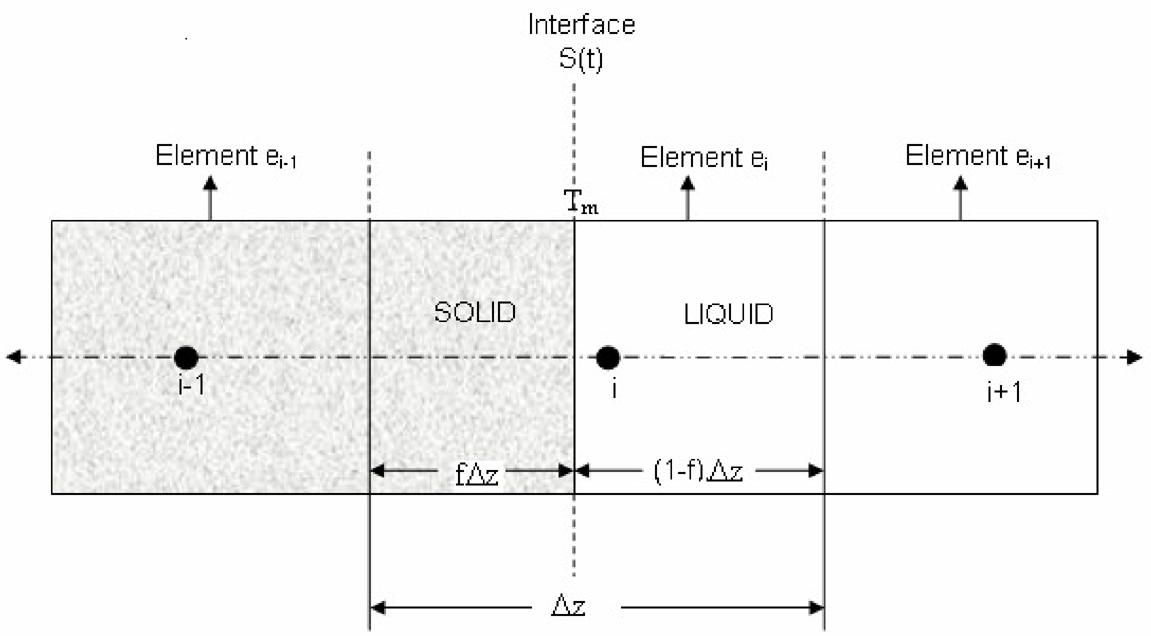

Fig. 3.4 Interpretation of Interface in Enthalpy Method

This total heat of the element may also be approximated as the sum of the heat in the solid and liquid parts of the element as

$$\left(C_pT_lf + (C_pT_l + L)(1-f)\right)\Delta z$$

This implies that

$$H_l = C_pT_lf + (C_pT_l + L)(1-f) \tag{3.23}$$

When the melt-front reaches the node i and is at the mid point, we have f_i=1/2 and T_i=T_m, then H_i can be rewritten as

$$H_l = C_pT_m + \frac{L}{2} \tag{3.24}$$

This result indicates that when the nodal enthalpy satisfies the above condition, the interface can be regarded as located on the node i.

Based on the above interpretation of nodal enthalpy, Voller and Cross proposed the improved algorithm for tracking of the interface (Voller, 1981). Whenever the enthalpy at the node point i is such that

$$H_i^n < \left(C_pT_m + \frac{L}{2}\right) \quad \text{and} \quad H_i^{n+1} > \left(C_pT_m + \frac{L}{2}\right)$$

The phase change boundary has crossed the node within that Δt. Assuming that the enthalpy changes linearly in any time interval, the time at which the the interface is on the node 'i' is given by

$$t_i = (n+\beta)\Delta t \tag{3.25}$$

where the fractional time β<1 and is given by the linear interpolation

$$\beta = \frac{(C_pT_m + \frac{L}{2}) - H_i^n}{H_i^{n+1} - H_i^n} \tag{3.26}$$

Using this algorithm, t_i the time at which the moving interface crosses the node i can be evaluated. For the relative enthalpy method the criterion for melt front crossing the node will be

$$H_i^n < \left(\frac{L}{2}\right) \ and \ H_i^{n+1} > \left(\frac{L}{2}\right)$$

and the fractional time is also modified accordingly. Figure 3.5(a) shows the typical staircase pattern of time history of location of the melt interface for a case study of 5 cm thick stainless steel plate constantly exposed to core-melt attack at 3020 K on its top side.

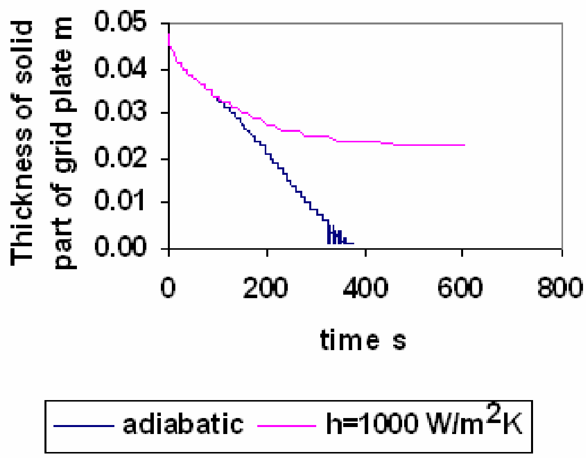

(a)

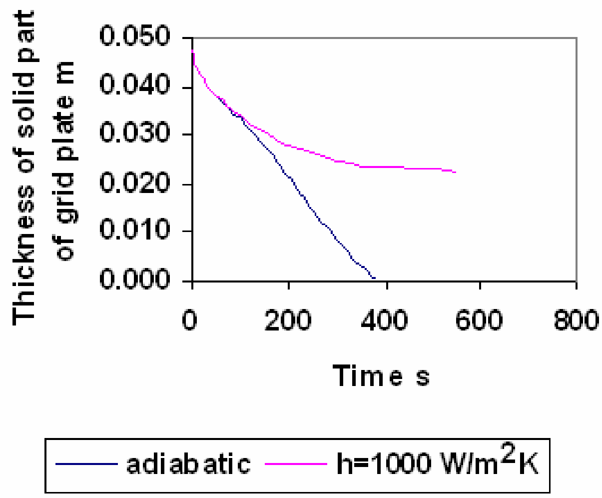

(b)

Fig. 3.5 Interface Tracking a) Normal enthalpy method and b) with Voller's algorithm

Figure 3.5(b) depicts the interface locations after applying Voller's algorithm. It is clear that the Voller's algorithm predicts a smoother interface movement.

3.3.3. Numerical Modelling of Molten Material Displacement

Molten stainless steel is lighter than the core-melt. Therefore molten steel gets displaced by the hot core-melt as depicted in Fig. 3 6 which can accelerate melting rate of

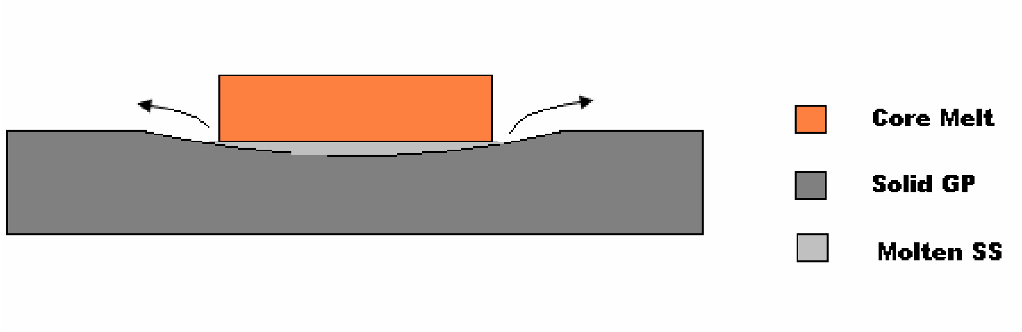

Fig. 3.6 Molten stainless steel displaced by hot core-melt

the grid plate. It is known that contact melting is a wide and complex area of study (Moallemi and Viskanta 1985). Moallemi in his study has obtained an expression for the film thickness δ of the melting object in contact with an isothermal heat source in terms of force due to apparent weight *F* and Stefan number *Ste* as an expression given below (Moallemi and Viskanta, 1985).

$$\delta = \left(\frac{16 \times Ste}{5F}\right)^{0.25} \tag{3.27}$$

In a similar study Chen et al (2008) have pointed out that in this thin molten film, heat transfer is mainly by conduction. Hence, using a conduction code to such melting problems is justified. In the present study, the interface between the core-melt and steel is not at constant temperature. Hence film thickness was calculated for the initial source temperature of 3020 K and also for the minimum interface temperature of 1720 K. It is found that the film thickness varies from 1.55 mm to 0.55 mm. Therefore, displacement is implemented in a simplified manner by allowing the node of thickness 2 mm to melt completely and then removing it from the computational domain. Essentially, the thickness of the grid plate is redefined each time one of the nodes crosses the melting temperature. That is when the molten stainless steel film thickness exceeds 2 mm, it is assumed to be displaced by the heavier core-melt and then the film thickness is allowed to grow till 2 mm after which it is displaced. The same study is repeated by restricting the film thickness to 1 mm and the deviation in the melt-through time is found to be less than 1%.

3.4 CORE-MELT RELOCATION AFTER PLOHS

The core-melt is assumed to be in perfect contact with the lower axial blanket region heating it and the schematic of the model is shown in Fig. 1.5. The other regions lying below it are the fission gas plenum, tail piece containing the coolant entry tube, discriminator made of solid steel at the foot of subassembly and finally comes the top portion of the grid plate. PLOHS study is carried out by considering the each region as a porous body with two or more materials arranged in parallel connection.

3.4.1 Initial and Boundary Conditions

The problem is formulated based upon the following assumptions.

- Initially the whole domain is at a uniform temperature of 673 K. This assumption is justified since the domain under consideration lies below the active core region and cold sodium is pumped into the subassemblies at this temperature.
- At the start of the transient, boiling fuel is in constant touch with the lower axial blanket region. Constant temperature boundary of 3600 K is prescribed as the top boundary condition.
- Decay heat is not considered explicitly because the molten core region is not modeled as one of the regions. But constant boiling of fuel in the core region implies that the decay heat is large enough to maintain the fuel at its boiling point.

This imposed condition is conservative with respect to prediction of core-melt relocation time. In reality, decay heat decreases with time.

- Grid plate bottom surface is considered to be adiabatic, without any heat transfer to underlying sodium. But sodium rewetting within the subassembly components is considered even after sodium boiling temperature is reached.

The main reason behind this choice of top and bottom boundary conditions is that this data set will yield a conservative value i.e., minimum value of core-melt relocation time.

3.4.2 Calculation of Effective Thermophysical Properties

As stated earlier, each region which comprises of two or three materials has to be treated as a single medium by defining effective properties. The properties of individual materials which are assumed to be constants are listed in Table 3.1.

Table 3.1 Thermophysical properties

Property	UO_2	Helium	Sodium	Stainless Steel
k (W/m.K)	3	0.2	75	20
ρ (kg/m^3)	10970	0.18	820	7800
C (J/kg.K)	350	5195	1200	500

Volume averaging is adopted for thermal conductivity and mass averaging is done for other properties namely, density and specific heat. In the present problem, the different materials are arranged in parallel, hence parallel conductivity is taken into account. The volume fractions of each component in the various regions and the corresponding effective properties are outlined in Table 3.2.

Table 3.2 Effective thermophysical properties

<table>
<tr><th>Sl. No.</th><th>Region</th><th>Compo- -sition</th><th>Volume fraction (%)</th><th>r mm</th><th>h mm</th><th>K W/mK</th><th>ρ kg/m³</th><th>C J/kg.K</th></tr>
<tr><td rowspan="3">1</td><td rowspan="3">Lower Axial blanket</td><td>UO_2</td><td>32</td><td rowspan="3">67.5</td><td rowspan="3">300</td><td rowspan="3">39.7</td><td rowspan="3">9309</td><td rowspan="3">456</td></tr>
<tr><td>Na</td><td>46</td></tr>
<tr><td>SS</td><td>22</td></tr>
<tr><td rowspan="3">2</td><td rowspan="3">Fission Gas plenum</td><td>He</td><td>32</td><td rowspan="3">67.5</td><td rowspan="3">750</td><td rowspan="3">39</td><td rowspan="3">6541</td><td rowspan="3">627</td></tr>
<tr><td>Na</td><td>46</td></tr>
<tr><td>SS</td><td>22</td></tr>
<tr><td rowspan="2">3</td><td rowspan="2">Tail piece of Subassembly</td><td>Na</td><td>50</td><td rowspan="2">110-60 (frustum of cone)
60 (cylinder)</td><td rowspan="2">200
450</td><td rowspan="2">47.5</td><td rowspan="2">7136</td><td rowspan="2">567</td></tr>
<tr><td>SS</td><td>50</td></tr>
<tr><td>4</td><td>SA discriminator</td><td>SS</td><td>100</td><td>60</td><td>200</td><td>20</td><td>7800</td><td>500</td></tr>
<tr><td>5</td><td>Grid plate Top plate</td><td>SS</td><td>100</td><td>-</td><td>50</td><td>20</td><td>7800</td><td>500</td></tr>
</table>

3.4.3 Computational Model

Unsteady conduction heat transfer is modeled in all the five regions with constant temperature equal to fuel boiling temperature prescribed as constant temperature boundary at the top of lower axial blanket region. Radial power profile is assumed to be flat across the core. Initiation of melting starts simultaneously in all subassemblies and so the computation is carried out along the vertical axial direction. Energy equation in temperature formulation is solved in all the regions using a commercial CFD code. Heat flux matching boundary condition is applied at the interfaces. The bottom of grid plate Is not allowed to exchange heat with the sodium plenum.

$$(\rho C_p)_{eff} \frac{\partial T}{\partial t} = \frac{\partial}{\partial z}(\kappa_{eff} \frac{\partial T}{\partial z}) \qquad (3.28)$$

At the interface between ith and i+1st region,

$$T_i = T_{i+1} \qquad (3.29)$$

$$\left[\kappa_{eff} \frac{\partial T}{\partial z}\right]_i = \left[\kappa_{eff} \frac{\partial T}{\partial z}\right]_{i+1} \qquad (3.30)$$

3.5 MULTI LAYER CORE CATCHER

The schematic of the model for multi layer core catcher is depicted in Fig. 3.7. Figure 3.7(a) denotes the domain for one dimensional computations where the core-melt is evenly spread on the entire core catcher. In the two dimensional case, the core-melt is lumped to two third radius on the core catcher plate.

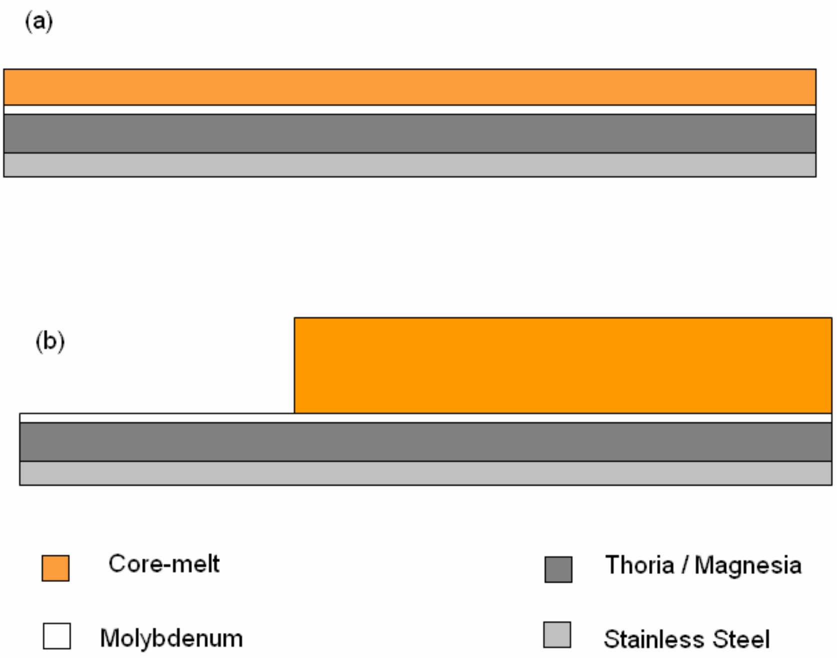

Fig. 3.7 Schematic of the model for multi layer core catcher

For the proposed triple layer core catcher, 5 mm thick Molybdenum forms the top most layer, followed by a layer of thoria whose thickness is to be optimized so that the maximum temperature on the base layer of 2 cm thick stainless steel structure is within design safety limit. Transient heat conduction analysis is carried out using a commercial CFD code for this composite core catcher assembly. Temperature and heat flux continuity are maintained at the interfaces between layers. Initial temperature of the composite core catcher is the cold sodium pool temperature which is 673 K. The initial temperature in the core-melt region is 3020 K which is the melting temperature of MOX fuel.

$$(\rho C_p)_i \frac{\partial T_i}{\partial t} = \frac{\partial}{\partial z}(\kappa_i \frac{\partial T_i}{\partial z}) + \dot{q}''' \tag{3.31}$$

Here κ, ρ, C, T and t refer to thermal conductivity, density and specific heat capacity, temperature and time respectively. Based on reactor physics calculations (Sridharan, 2002), the decay heat content is approximated by the function

$$\dot{q}''' = 86.5 t^{-0.31} MW/m^3 \tag{3.32}$$

$q''' = 0$ for all the other regions

where q''' is the volumetric heat source in the core debris and t is the time elapsed after neuronic shut down of the reactor following an accident.

3.6 CLOSURE

The problem formulation is elaborated in this chapter by defining governing equations and along with initial and boundary conditions. Commercial CFD codes are to be employed for solving conduction / convection problems because of their robustness. But when melting of grid plate is considered, a computer code is proposed to be developed specifically for the problem. The advantages would be the flexibility offered by the code to include temperature dependent properties and time varying source and boundary conditions. Melt-front tracking and contact melting phenomenon are also modelled adding strength to the code.

CHAPTER 4

CFD STUDIES ON NATURAL CONVECTION IN SODIUM FILLED CYLINDRICAL ENCLOSURES

4.1 INTRODUCTION

The main objective of this numerical study is to develop heat transfer correlations for natural convection in sodium filled cylindrical cavities heated on the top side and cooled at the cylindrical wall. Both thin plate and thick plate conditions of the top wall are considered as shown in Figs. 4.1(a) and Fig. 4.1(b). Conjugate heat transfer analysis is carried out for the case of thick top plate configuration. The computational model is built and solved using a commercial CFD code PHOENICS. Grid optimization has been carried out. The details of model validation for two case studies viz., differentially heated cavity and bottom heated cavity are also described.

4.2 GRID OPTIMISATION

In any numerical study grid optimization is carried out with a view to minimize the errors. The spatial grid size is decreased in steps until no appreciable change in the output parameter, say, temperature at a selected point is reached. In the present study, turbulence is modeled by a low Reynolds number k-ε model. Therefore, the grid size is so chosen that mesh points extend upto the conduction dominated laminar sub layer. This implies that computations are extended through the viscous sub-layer close enough to the wall and excludes the use of wall functions. The number of nodes in the axial direction is optimized such that the typical value of y^+ is close to one, as required by the turbulence model. For the reactor sodium plenum, 100 nodes along axial direction and 50 nodes along radial direction are taken. Increasing the number of nodes to 100 in radial direction did not alter the solution appreciably. Therefore the domain was discretised by 50×100 nodes. Global convergence criterion is fixed at 10^{-3}. Reducing this value to 10^{-4} did not produce perceptible change in heat transfer rates.

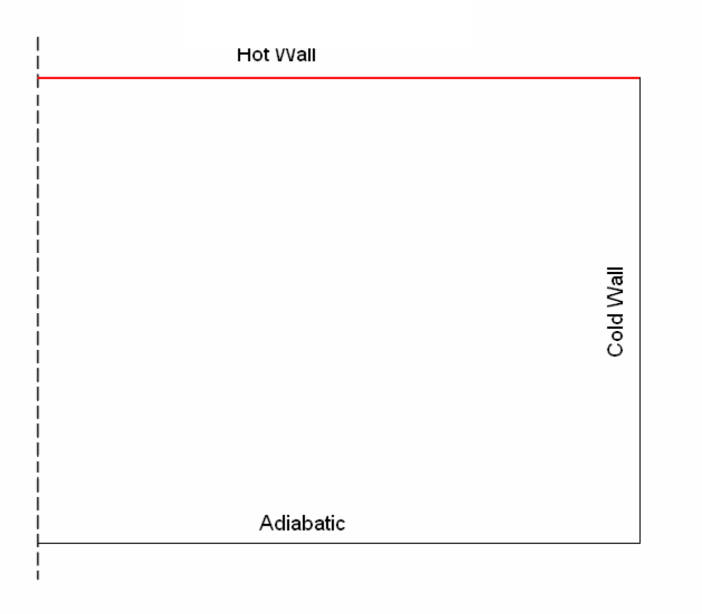

(a)

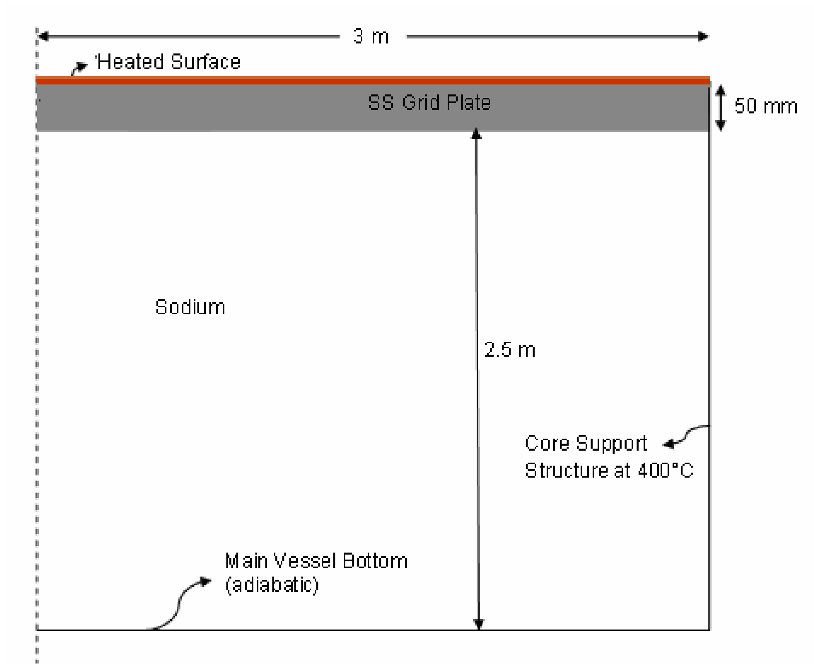

(b)

Fig. 4.1 Schematic of computational domain (a) Thin top plate and (b)Reactor sodium plenum with thick top plate

Computations are carried out upto 500 s, adopting a time marching approach for steady state solutions. Before this time, steady state has been attained in all the cases.

Typical values of y+ along the lateral wall for the reactor cavity were found to lie between 0.2 and 3 as discussed later in Section 4.5.

4.3 VALIDATION

Natural convection results for top wall heated and side wall cooled sodium filled enclosures are not available in open literature. Hence, for the validation of computational procedure used, two rectangular enclosures with well established benchmark results are considered. In one of the enclosures, the vertical walls are differentially heated, while the horizontal walls are maintained adiabatic. Mohamad and Viskanta (1993) have studied natural circulation in such differentially heated enclosures in detail and proposed a correlation for Nusselt number in terms of Boussinesq number given by Eqn. (2.7). Considering the test fluid to be sodium with Boussinesq number 3.7×10^8, results obtained in the present study are compared with their correlation. The comparison is given in Table 4.1. The steady state velocity vectors and temperature field obtained for this case from the present study are illustrated in Fig. 4.2 and Fig. 4.3 respectively. Next, the present model is run for Viskanta's case study of $Ra=10^6$ and $Pr=0.02$ to compare flow and temperature patterns (Viskanta et al., 1986). The comparison of results is illustrated in Fig. 4.4 and Fig. 4.5. The flow and temperature patterns obtained from the present study compare very well with the benchmark patterns.

In the next case, the bottom wall of the enclosure is heated and top wall is cooled isothermally. Rossby (Kek and Muller, 1993) has studied natural circulation driven by vertical temperature gradient in these enclosures and proposed a correlation given by Eqn. (2.8). The same problem was analysed by the present method and the predicted Nusselt number is given in Table 4.1.

Table 4.1: Comparison of present results with benchmark data for liquid metals

Square cavity	Configuration	Bo	Empirical Nu	Computed Nu from present study	% Error
Bottom Heated (Rossby et al. referred by Kek and Muller, 1993)	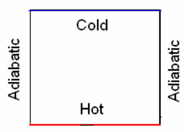	1.48×10^{6}	23.4	24.3	3.5
Differentially Heated (Mohamad and Viskanta, 1993)	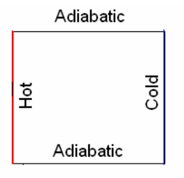	3.7×10^{8}	19.7	18.7	5

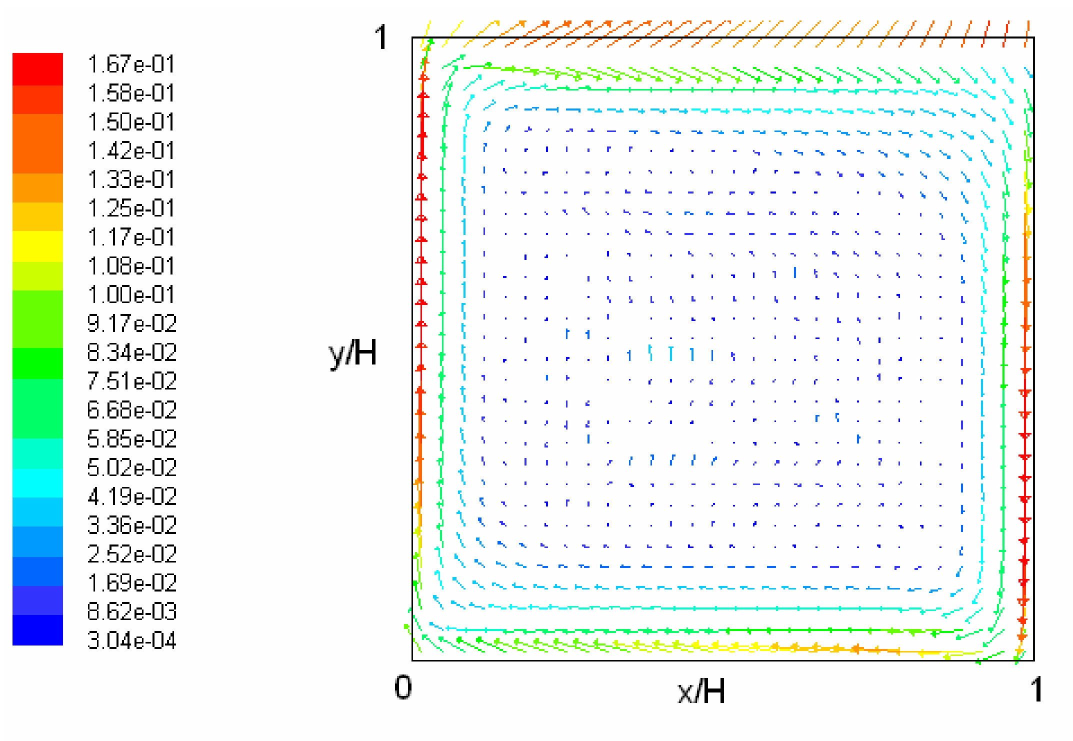

Fig. 4.2 Velocity vectors (m/s) in a differentially heated cavity ($Bo=3.7\times10^{8}$)

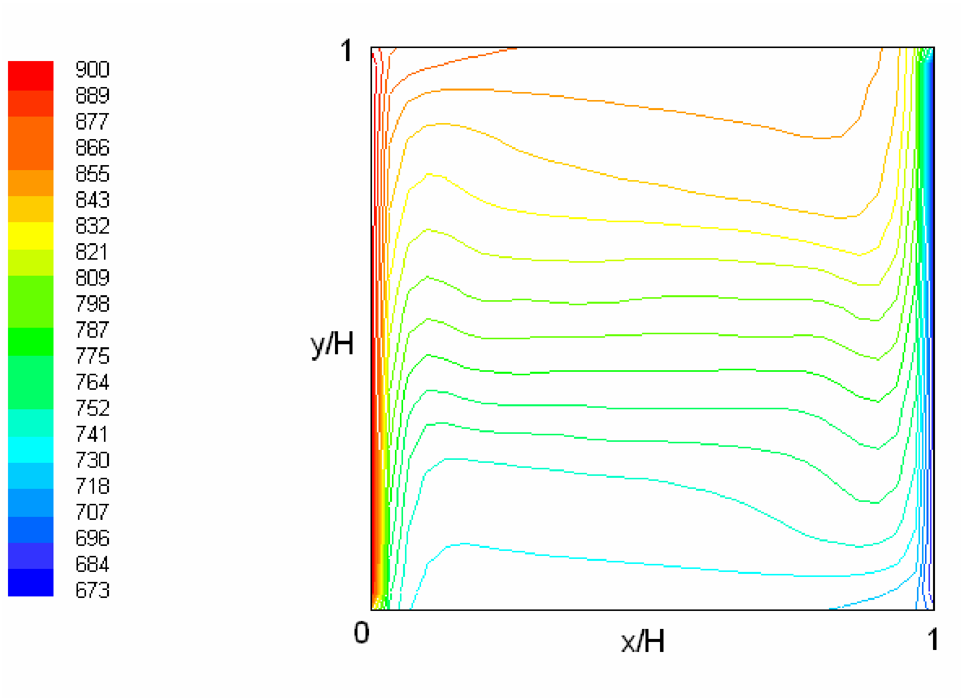

Fig. 4.3 Temperature Field (K) in a differentially heated cavity (Bo=3.7×10^{8})

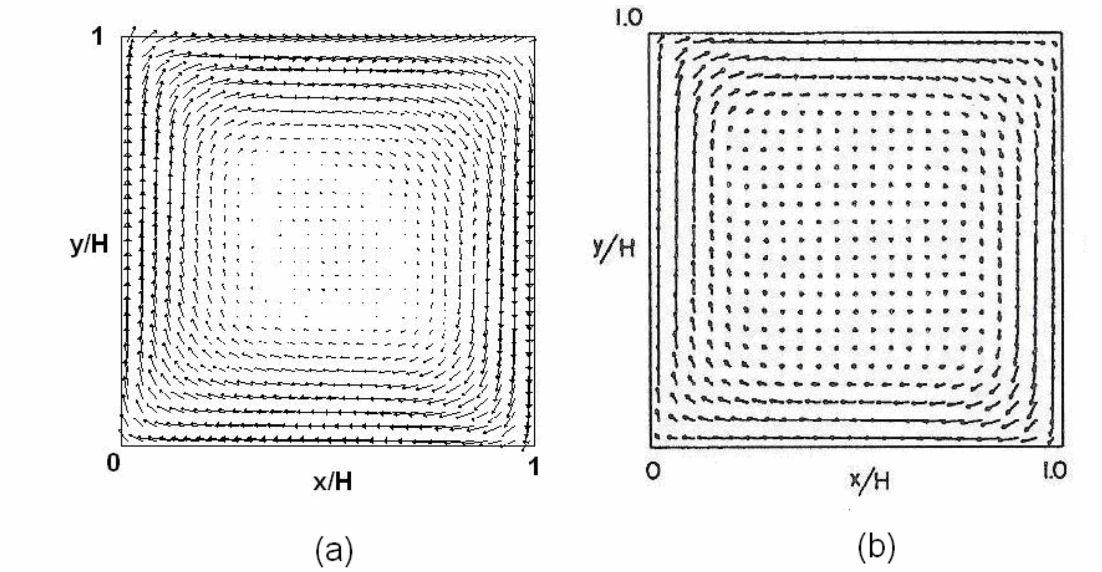

Fig. 4.4 Comparison of velocity field of present work with that of Viskanta's work

(Ra=10^{6}, Pr=0.02)

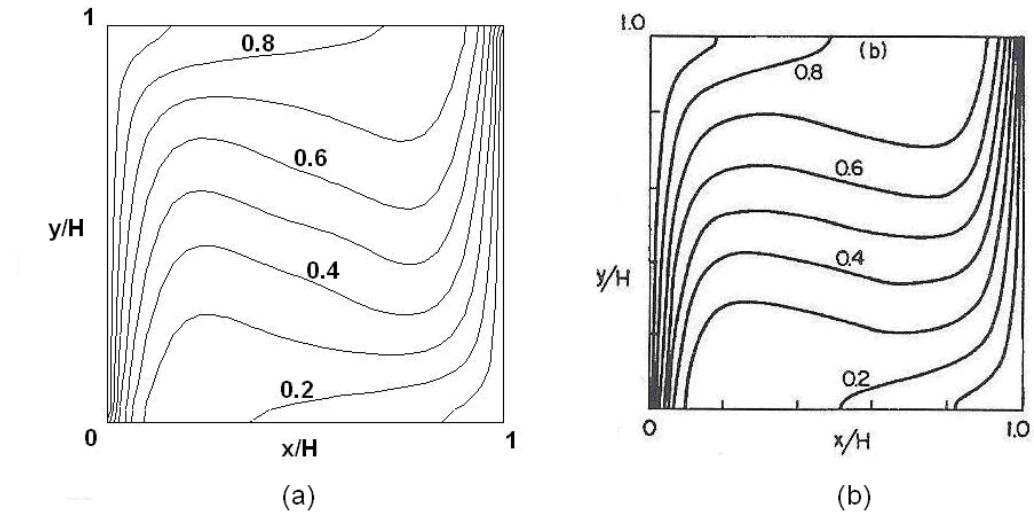

Fig. 4.5 Comparison of non dimensional temperature field of present work with that Viskanta's work (Ra=10^6, Pr=0.02)

For the bottom heated cavity, velocity and temperature fields for this problem are depicted in Fig. 4.6 and Fig. 4.7. Two counter rotating vortices are predicted in the enclosure with the temperature field symmetric about x/H=0.5, as expected for the boundary conditions employed. From the validation cases, it is found that present results differ from the published data only by 5%.

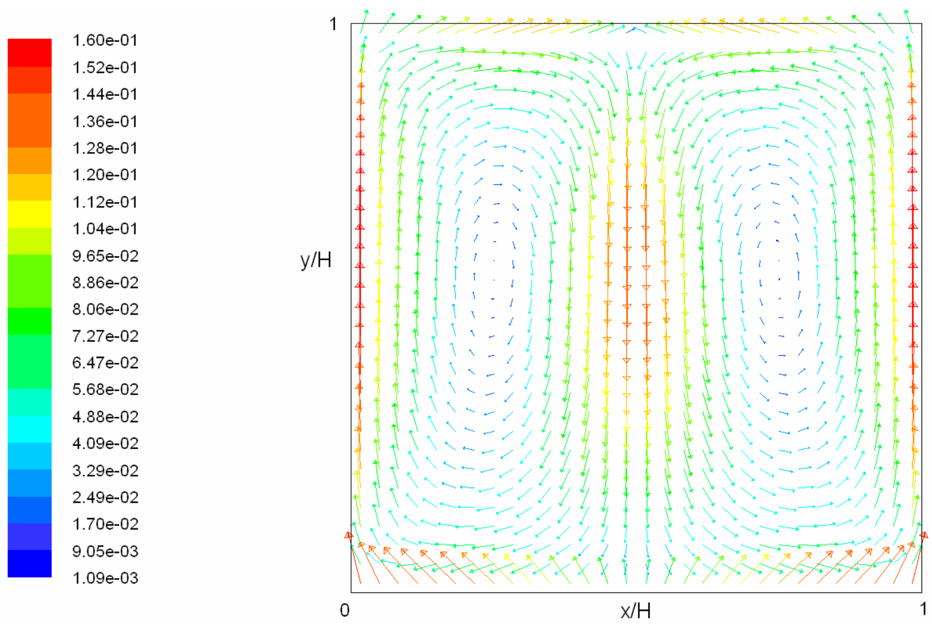

Fig. 4.6 Velocity vectors (m/s) for a bottom heated cavity (Bo=1.48×10^6)

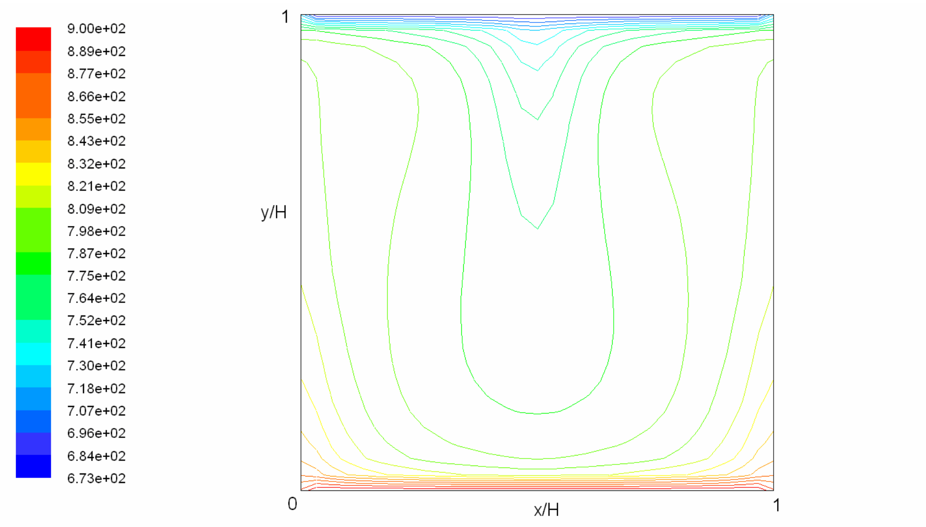

Fig. 4.7 Temperature field (K) for a bottom heated cavity (Bo=1.48×10^6)

4.4 RESULTS AND DISCUSSION FOR THIN PLATE ENCLOSURE

After satisfactory validation of the present low Reynolds number k-ε model for both laminar and turbulent regimes, detailed parametric studies have been carried out for axisymmetric cylindrical enclosures for Pr=0.004.

4.4.1 Calculation of Nusselt Number

Steady state analysis is carried out in cylindrical enclosures depicted in Fig. 4.1(a). The top surface is the heat source maintained either at constant temperature or at constant heating rate, and the cylindrical side wall is the isothermal heat sink. The thickness of the top wall is considered to be negligible. Heat transfer coefficient (*h*) in liquid sodium below this plate is estimated by equating the conductive heat transfer rate to convective heat transfer rate as given in the following equation.

$$h_i = \frac{\kappa_{Na}\left(\frac{\partial T}{\partial z}\right)_i}{T_p - T_{amb}} \tag{4.1}$$

$$h_{ave} = \frac{\sum_{i=1}^{N} h_i dA_i}{\sum_{i=1}^{N} dA_i} \tag{4.2}$$

where, dA_i is the area associated with i^{th} node, N is the number of radial nodes, T_p is the hot plate temperature, h_i is local heat transfer coefficient and h_{ave} is the average heat transfer coefficient.

Using this heat transfer coefficient, Nusselt number is estimated as

$$Nu_{ave} = \frac{h_{ave} L}{\kappa_{Na}} \tag{4.3}$$

where the characteristic length L is taken as the diameter of the cylindrical enclosure. In liquid metals since Pr << 1, Nusselt number is correlated with Boussinesq number (Bejan, 2004) where Boussinesq number is defined as

$$Bo = \frac{g\,\beta\,\Delta T\,L^3}{\alpha^2} \tag{4.4}$$

Hence, the analysis is carried out with the view to arrive at such a correlation between Nusselt number and Boussinesq number.

4.4.2 Isothermal Top Surface

In the first case, natural convective heat transfer in liquid sodium is studied by prescribing constant temperature boundary condition on the top surface of the cylindrical cavity. The side cylindrical wall is kept at 673 K which is the typical temperature prevailing in the lower plenum of a fast breeder reactor. The aspect ratio of the cylindrical enclosure is 0.4. Based on systematic parametric studies, the mean Nusselt number is computed for a large range of Boussinesq number which is of interest in the accident analysis of a fast breeder reactor.

For a typical case with hot wall at 800 K, the predicted results of velocity field and isotherms are presented in Fig. 4.8 and Fig. 4.9 respectively. Liquid sodium upon getting cooled near the side wall descends due to gravity. This descending flow induces a weak circulation in the cavity which is otherwise stably stratified with hot sodium at the top. The maximum value of sodium velocity at Bo=1.38×10^{10} is 8 cm/s as can be seen in

Fig. 4.8. From the corresponding isotherms depicted in Fig. 4.9, it is observed that the region close to the axis of symmetry is unaffected by the weak natural convection.

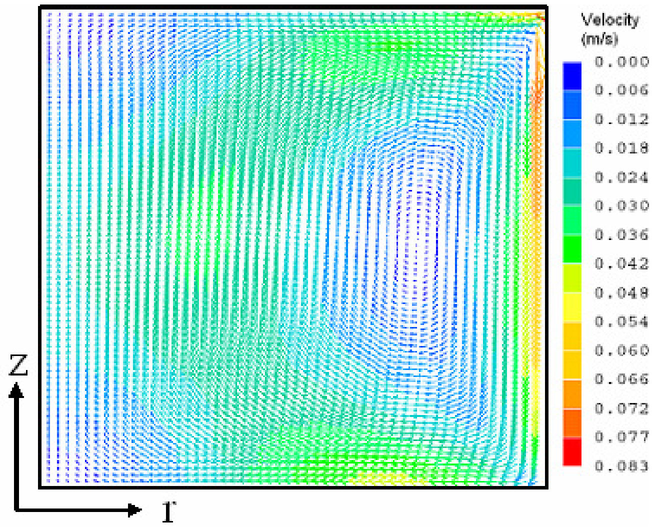

Fig. 4.8 Velocity vectors (m/s) in top heated cylindrical cavity (Bo=1.38×10^{10})

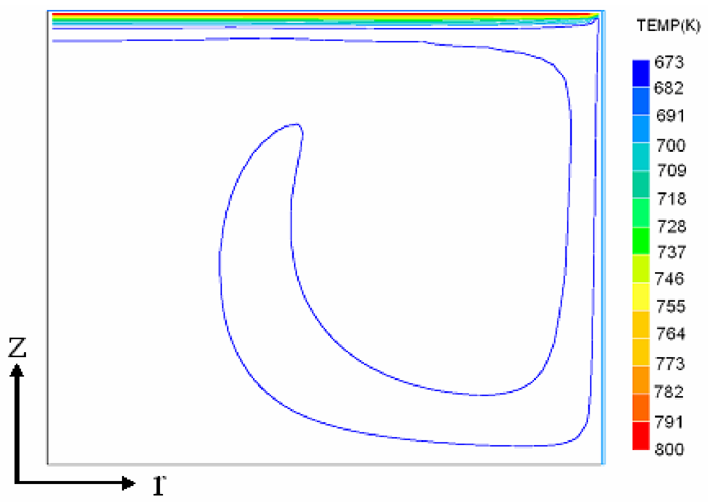

Fig. 4.9 Isotherms (K) in top heated cylindrical cavity (Bo=1.38×10^{10})

The temperature difference between the hot and cold walls which is the driving force for convection is not strong enough to encompass the entire enclosure. The bulk temperature of the enclosure is close to 673 K. The dependence of mean Nusselt number on Boussinesq number is seen to vary as

$$Nu = 3.6811(Bo)^{0.1022} \qquad for\ 2\times10^{3} < Bo < 2\times10^{6} \tag{4.5}$$

as shown in Fig. 4.10. Turbulence is found to be dominant for higher Boussinesq numbers and Nusselt number is seen to exhibit a stronger dependence on Boussinesq number as given by

$$Nu = 0.8715(Bo)^{0.2029} \qquad for\ 2\times10^{6} < Bo < 2\times10^{11} \tag{4.6}$$

The regression coefficient for both the equations is 0.99. The graphical representation of these results is given in Fig. 4.10.

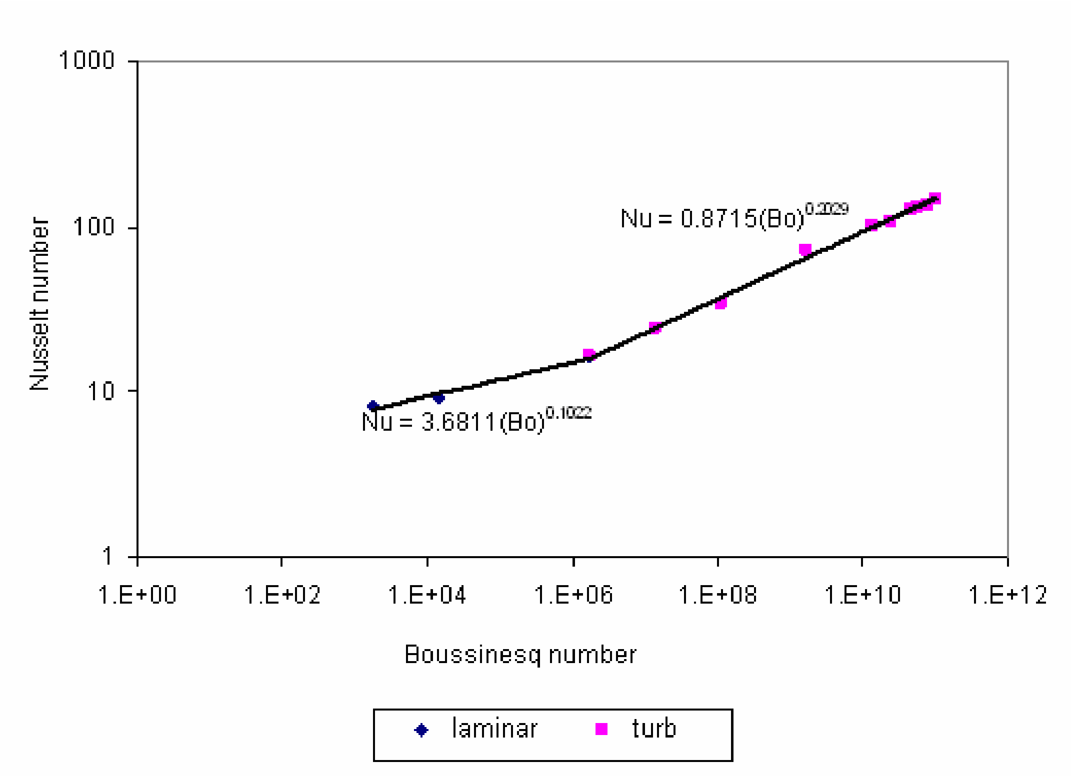

Fig. 4.10 Nusselt number vs Boussinesq number for isothermal top wall

4.4.3 Comparison of Present Results with Published Data

The works of Sheriff and Davies (1979) and that of Rigoleur (1982) which are focused towards nuclear reactor accident analysis are taken for comparison with the present work. Both of them have presented their results for downward facing hot plate in a pool of liquid metal. The exact ranges of applicability of these empirical correlations are not explicitly reported in the published literature. However, the Nusselt number predicted by the present study is compared with that reported by Sheriff and Davies and Rigoleur for Boussinesq number in the range of 10^6 to 10^{11}, in Fig. 4.11.

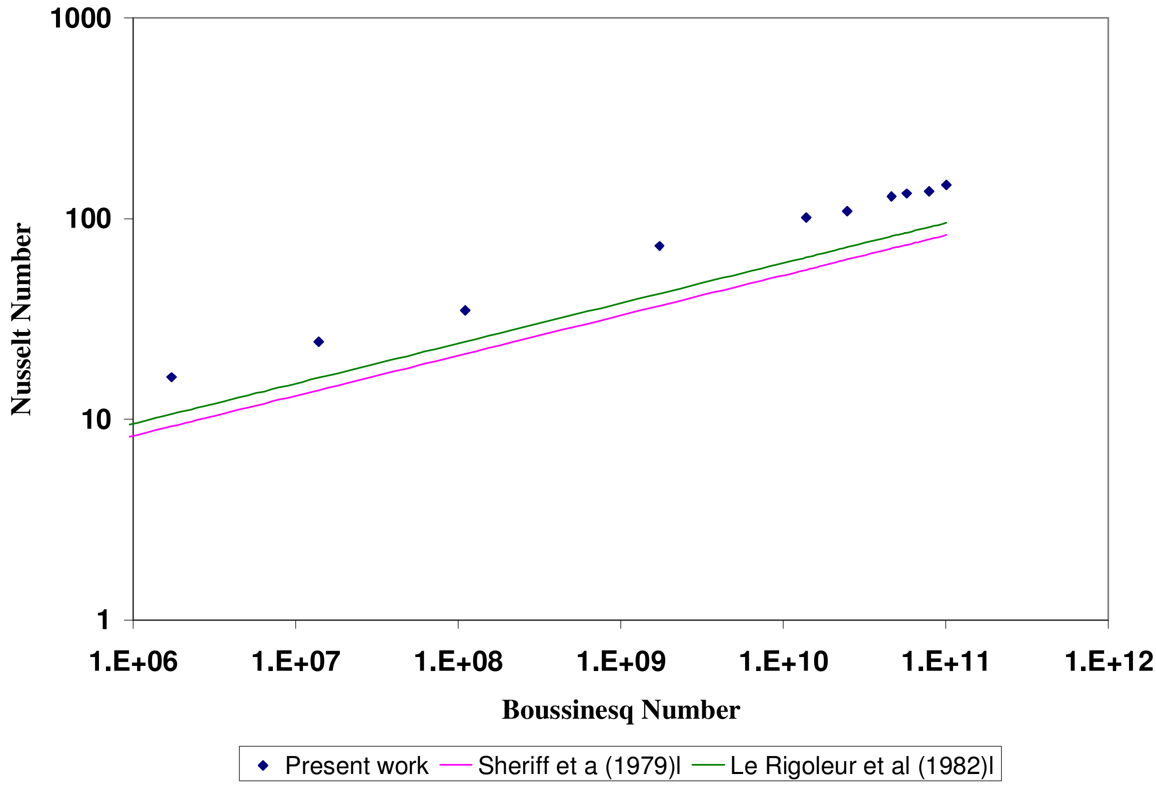

Fig. 4.11 Comparison of present work against published data

The Nusselt number predicted by the present study for a vertical cylindrical enclosure is higher than the reported results for downward facing hot plate in an infinite ambient liquid. The reason for this difference can be attributed to the presence of a heat sink at the side wall which lowers the plate edge temperature and hence increases the convective velocity near the edge of the plate. For a hot plate in a pool of liquid, the velocity at the edge of the plate is not enhanced by a temperature difference as in this geometry but rather from buoyancy of the hotter liquid tending to rise due to gravity. Predicted local heat transfer coefficient as a function of radial distance is shown in Fig. 4.12. It is observed that near the top extreme edge of the cavity, the local heat transfer coefficient is high because of the enhanced natural circulation. This contributes to the higher proportionality constant in the present side wall cooled enclosure. Nevertheless, it is observed that the power law dependence is the same for all the results.

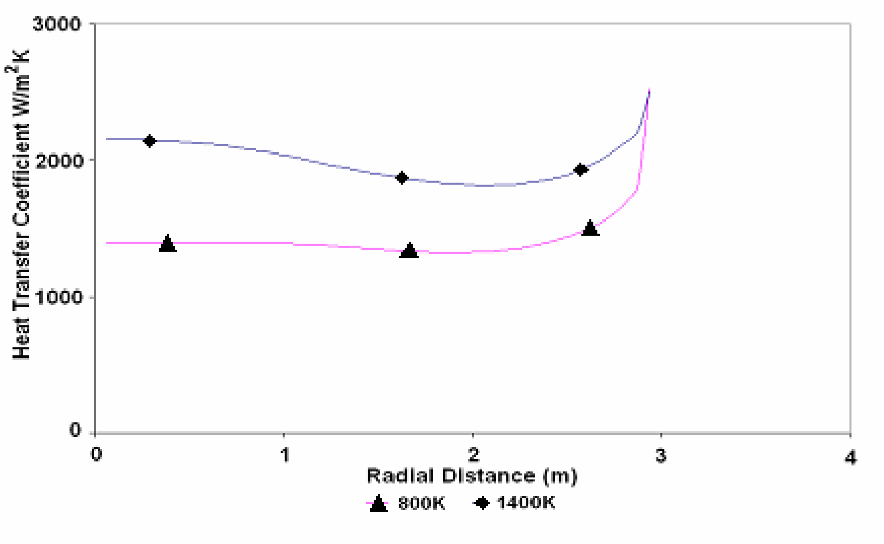

Fig. 4.12 Radial variation of local heat transfer coefficient

4.4.4 Isoflux Top Surface

In this part of the study, a constant heat flux is imposed on the top wall of the cylindrical enclosure. All the other conditions are the same as in the previous case. Rigoleur and Tenchine (1982) have developed an empirical correlation using modified Boussinesq number Bo* as

$$Nu = 0.59(Bo^*)^{\frac{1}{6}} \qquad for\, 8.6\times10^5 < Gr\,\mathrm{Pr}^2 < 3\times10^6 \tag{4.7}$$

where $\quad Bo^* = Gr^*\mathrm{Pr}^2 = g\beta \dot{q}'' L^4/(\kappa\alpha^2)$

In the case of constant heat flux boundary in the present study, Bo* is varied from 4×10^4 to 2×10^9. Based on the computed temperature distribution, the Nusselt number is seen to have 1/10 power law dependence on Boussinesq number. The Nusselt number is seen to correlate with modified Boussinesq number as per the relation,

$$Nu = 2.9(Bo^*)^{0.096} \qquad for\ 4\times10^4 < Bo^* < 2\times10^9 \tag{4.8}$$

with the regression coefficient of 0.98. The difference between the correlations represented by Eqn. (4.7) and Eqn. (4.8) is attributed to the fact that the present study is for an enclosure with hot top wall and cold side wall, while that of Rigoleur is for a downward facing hot plate immersed in a large pool. The comparison of present result with the empirical correlations of Rigoleur and Tenchine (1982) and Shereiff and Davies (1979)is given in Fig. 4.13.

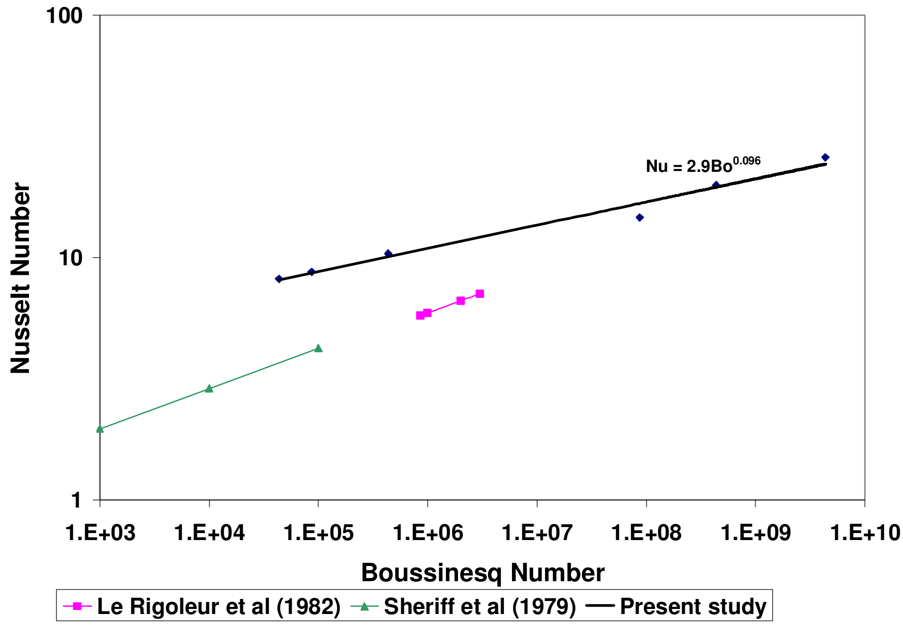

Fig. 4.13 Nusselt number vs Boussinesq number for constant flux heating

4.5 RESULTS AND DISCUSSION FOR THICK PLATE ENCLOSURE

Results presented in the previous sections correspond to thin plate consideration. However in reactor designs, the grid plate is of finite thickness. For example in BN 800 reactor, the grid plate thickness is 11 cm. The corresponding value in Indian FBR is 5 cm (Chetal et al., 2006). The finite thickness of the grid plate necessitates a conjugate heat transfer analysis. Therefore, conjugate heat transfer analysis has been carried out for transient as well as steady state conditions for the geometry depicted in Fig 4.1(b). As explained in Section 3.2, low Reynolds number *k*-ε model is used to account for turbulence effects. A typical plot of y^+ close to the top horizontal wall is given in

Fig. 4.14. The values ranging from 0.2 to 3 indicate that the laminar sub-layer is well resolved by the adopted mesh and gradients along the wall are adequately captured without the use of wall functions.

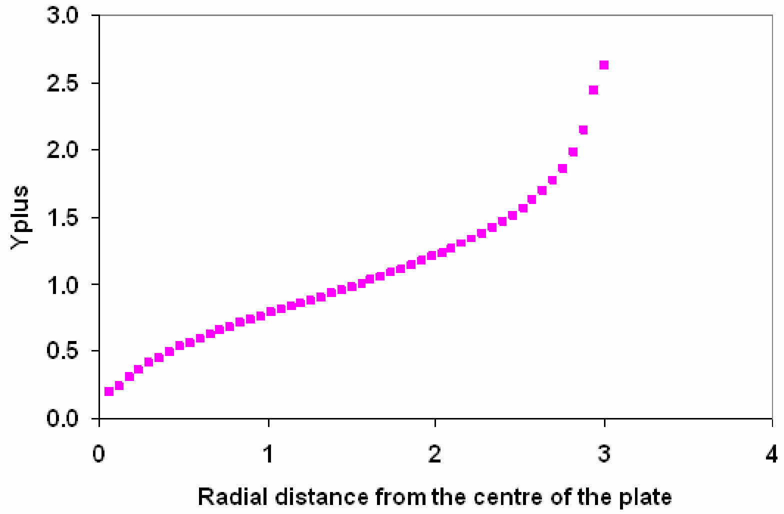

Fig. 4.14 Plot of y^+ along the lateral hot wall

4.5.1 Transient and Steady State Analysis for Sudden Heating of Top Plate

Usually steady state heat transfer correlations serve a majority of practical purposes, barring a few applications namely, start up and shut down of heat transfer equipments and in processes with time varying boundary conditions. In such cases transient analysis assumes importance. Here, we have considered transient analysis to understand if finite thickness of the plate has any bearing on the transient stage of heat transfer. The evolution of heat transfer coefficient for the case of plate thickness 50 mm and Boussinesq number 7.9×10^{10} is given in Fig. 4.15.

Due to the resistance offered by the plate to heat transfer, there is a time delay before the effect of heating on top surface of the plate is first felt at its bottom surface. Time for heat penetration to the first node in liquid sodium is found to be 12 s. At 12 s, the heat transfer coefficient (h) is 2500 W/m^{2}K and it reduces rapidly with increasing time. At steady state, when the plate temperature is 894 K, this value is 780 W/m^{2}K.

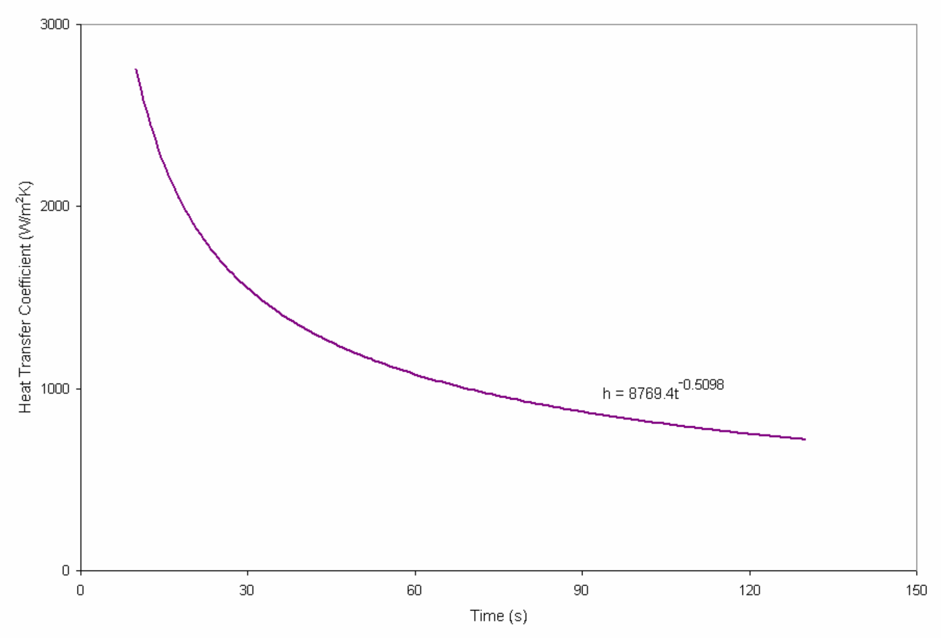

Fig. 4.15 Transient heat transfer coefficient

To understand the dependence of heat transfer coefficient with time in the initial unsteady state, a power law fit with respect to time was attempted for computed *h* value. The graph indicates that it varies inversely as square root of time. The predicted value of *h* is found to compare well with the equivalent heat transfer coefficient representing transient heat conduction defined as

$$h_{eq} = \frac{\kappa_{Na}}{\sqrt{\alpha t}} \tag{4.9}$$

upto the first 120 s.

This clearly indicates that conduction is the dominant heat transfer mechanism during this time interval. Equivalently, it can be stated that Nusselt number is inversely proportional to square root of dimensionless time

$$Nu = \left(\frac{t}{\tau}\right)^{-\frac{1}{2}} \tag{4.10}$$

where, τ is the time constant of the entire sodium column (of height *z*). Transient heat transfer coefficient is primarily a characteristic of the liquid and is not dependent on the wall thickness or temperature variation - whether it is steady or changing. This is true for a thin wall approximation case also. But the boundary wall temperature and its variation do have an influence on the final steady state heat transfer. By carrying out a parametric study by varying the source temperature, it is found that for thick plate configuration the steady state Nusselt number is correlated with Boussinesq number as

$$Nu = 0.4(Bo)^{0.2} \tag{4.11}$$

The hot plate temperature used in arriving at this correlation is the average temperature of the lower surface of the hot plate. This final steady state heat transfer correlation is compared with that calculated using an empirical correlation suggested by Rigoleur for a downward facing hot plate in liquid sodium which is given by

$$Nu = 0.6(Bo)^{0.2} \tag{4.12}$$

Comparing Eqn. 4.11 with Eqn. 4.12, it is evident that the present Nusselt number is ~33% lower than that of Rigoleur's prediction. The reason for this deviation is that the empirical correlation is valid for plates at uniform steady temperatures only in a pool geometry. In this particular configuration of thick top plate, the temperature of the surface in contact with the liquid is a slowly increasing one due to the resistance offered by the thickness of the plate. On comparing the correlation in Eqn. 4.11 for thick top plate with that of thin top plate given by Eqn. (4.6), it is found that the reduction in heat transfer is about 50% in case of the thick plate. The velocity vectors obtained for the same Boussinesq number for thick and thin plates shown in Figs. 4.16 and 4.17 respectively. The comparison of velocity vectors qualitatively explains the reduced heat transfer coefficient with the thick plate. It is seen that natural convective velocity is almost one half of that in the case of a thin plate and the reduced convective velocity in the case of a thick plate, leads to a lower heat transfer coefficient.

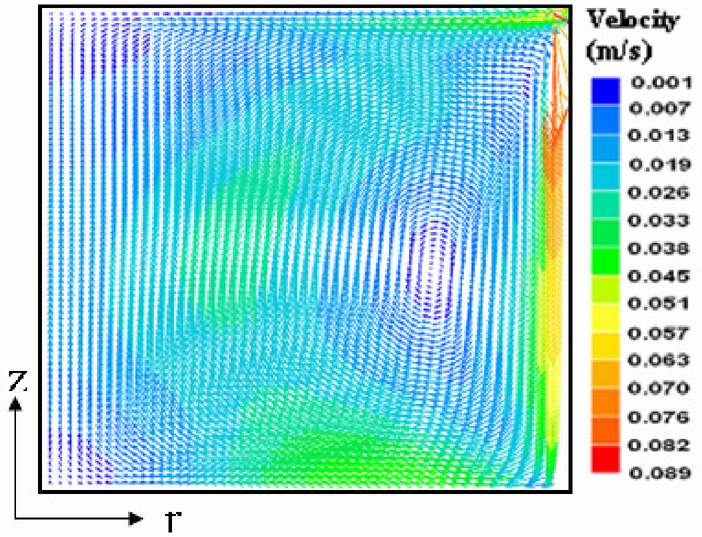

Fig. 4.16 Velocity vectors for Bo =7.9×10^{10} with thick plate configuration

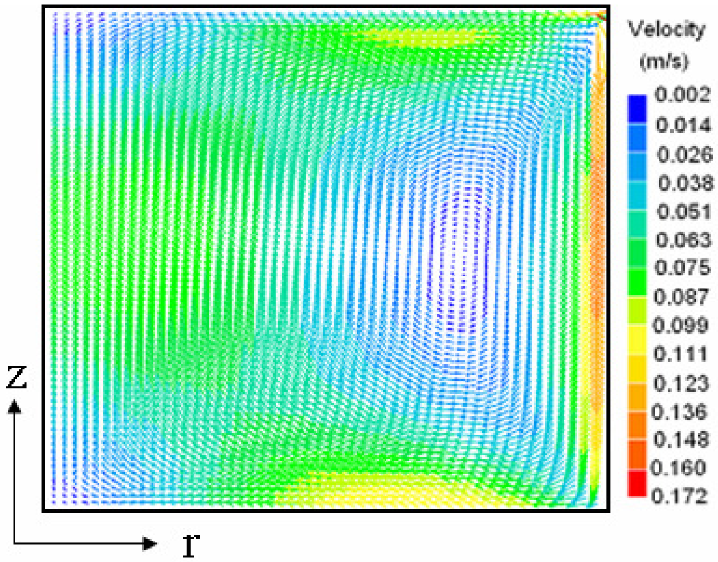

Fig. 4.17 Velocity vectors for Bo=7.9×10^{10} with thin plate configuration

4.5.2 Steady State Analysis

An attempt has been made to develop a single correlation for the Nusselt number combining the influence of defining parameters, viz., Boussinesq number, conductivity ratio and height ratio by carrying out another parametric study by varying the source temperature, material of the plate and thickness of the plate one by one. The aspect ratio (height/diameter) of the cavity is 0.4 and is preserved in all the cases. Height ratio or non dimensional plate thickness is defined as the ratio between the thickness of the plate and the height of the cylindrical enclosure. Conductivity ratio is the ratio of the thermal conductivity of the plate to that of sodium liquid.

Steady state analysis is carried out for different conductivity ratio between the solid plate and the liquid. Three different metals are considered and predicted Nu – Bo dependence is presented in Fig. 4.18.

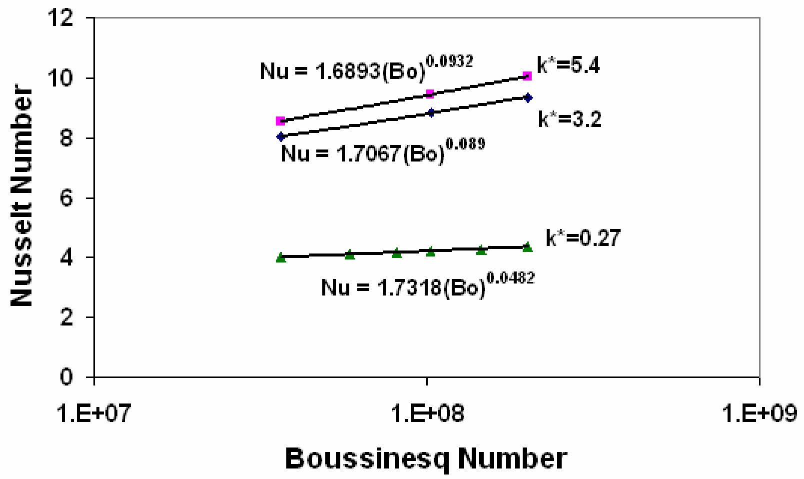

Fig. 4.18 Effect of conductivity ratio on Nu-Bo Correlation

The thickness of the plate is also varied as a parameter ranging between 10 mm and 50 mm. A graph showing the variation of the Biot number with Nusselt number is given in Fig. 4 19. It is observed that when the Biot number is large, the temperature drop across the plate increases. Therefore, the temperature at the bottom of the plate is low which leads to low heat transfer coefficient and hence small Nusselt number.

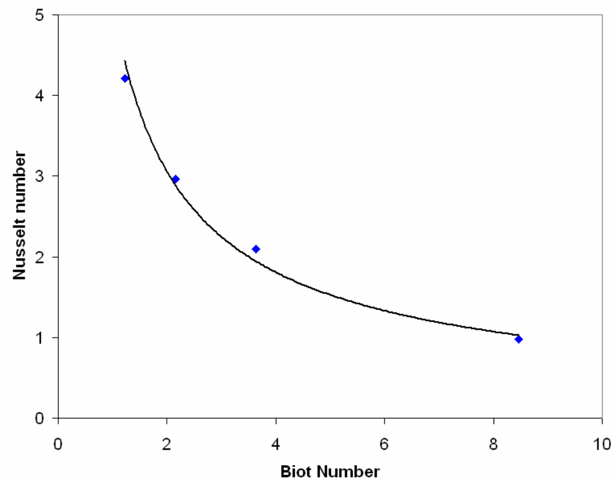

Fig. 4.19 Nu-Bi relationship for varying thickness of plate

The developed correlation indicates the reduced significance of Boussinesq number on heat transfer in case of thick plates. While developing this correlation, the constant temperature imposed on top surface of the hot plate is considered as the plate temperature, so that the influence of the thickness of the plate is included in the analysis. The correlation developed using multi variable regression analysis is given below.

$$Nu = 0.15(Bo)^{0.07}(l^*)^{-0.6}(\kappa^*)^{0.27} \tag{4.13}$$

The goodness of fit of the correlation is shown in Fig. 4.20. The correlation coefficient between the exact and the fitted data is 0.99. To further check the validity and applicability of the above correlation, two cases are chosen with different conductivity ratio κ^* and one case with a different scale and conjugate heat transfer analysis is carried out to estimate heat transfer coefficient. The estimated heat transfer coefficient is compared with that obtained using the correlation and the error was found to be less than 3% as shown in Table 4.2.

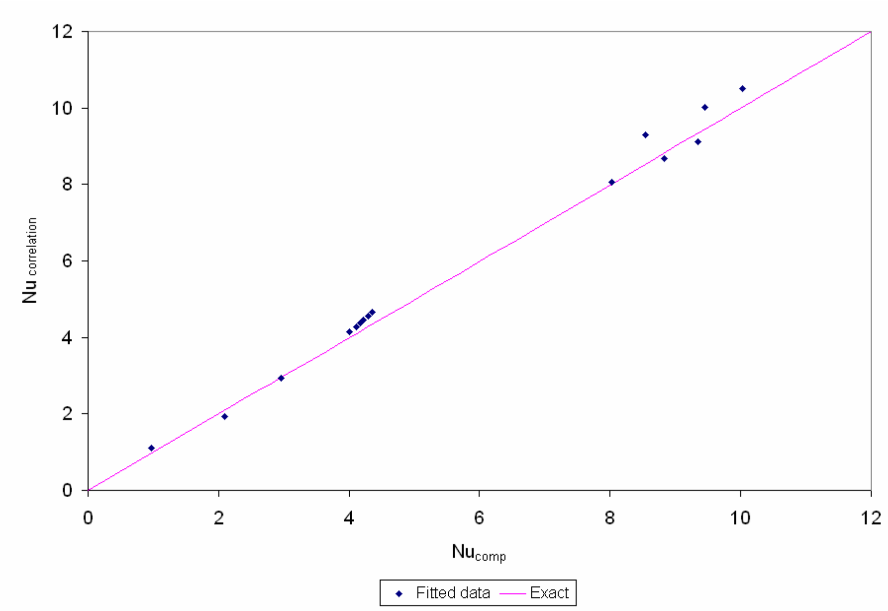

Fig. 4.20 Comparison of computed and correlated Nusselt numbers

This numerical study clearly points out that using thin plate approximated correlations for thick plates can lead to erroneous results. Hence, it is prudent to carry out a conjugate heat transfer study accounting for the conduction heat transfer in the plate or to use correlations that are specific for such thick plate configuration. The set of correlations developed in the present study for thin and thick plates and the ranges of their validity in terms of corresponding independent non-dimensional numbers are summarized in Table 4.3. For thick plates, the reduced influence of Boussinesq number on convective heat transfer is evident from the developed corelations.

Table 4.2 Validation of the developed correlation

Bo	Heat Transfer Coefficient (W/m^2K)		% deviation
	Conjugate heat transfer study	Predicted by Eqn. (4.13)	
5.48×10^{7}	927	910	+ 1.8
1.19×10^{8}	990	966	+ 2.4
3.76×10^{10}	200	198	+ 1.0

Table 4.3 Correlations developed and their ranges of validity

Plate	Top boundary condition	Correlation	Range
Thin	Isothermal	$Nu = 3.6811(Bo)^{0.1022}$ $Nu = 0.8715(Bo)^{0.2029}$	$2\times10^{3} < Bo < 2\times10^{6}$ $2\times10^{6} < Bo < 2\times10^{11}$
Thin	Isoflux	$Nu = 2.9(Bo)^{0.096}$	$4\times10^{4} < Bo < 2\times10^{9}$
Thick	Isothermal	$Nu = 0.15(Bo)^{0.07}(l^*)^{-0.6}(\kappa^*)^{0.27}$	$3.6\times10^{7} < Bo < 2\times10^{8}$ $0.27 < \kappa^* < 5.4$ $6 < l^* < 60$

4.6 CLOSURE

Natural convection heat transfer studies have been carried out numerically for a top surface heated and side wall cooled sodium filled cylindrical enclosures. Nusselt number correlations are obtained both for thin and thick plates forming the top boundary. The study on the thick top plate enclosure has revealed that conductivity ratio and height ratio also significantly affect the Nusselt number other than the Boussinesq number. In the thick top plate configuration, lower sodium plenum of the reactor main vessel is also investigated and there can be reduction in heat transfer upto even 50% because of the sluggish sodium natural convection velocity. A few of these developed correlations are further to be used in the core-melt relocation studies to be discussed in the next chapter.

CHAPTER 5

CORE-MELT RELOCATION STUDIES

5.1 INTRODUCTION

The mathematical model explained in section 3.3 is formulated into a computer code named HEATRAN-1. The code is validated and applied to the core-melt relocation studies following a ULOFA. As already explained, it is an explicit enthalpy based finite difference code. The Voller's algorithm for the phase front tracking and a dynamic molten material displacement model are the special features of the code. Melting of grid plate is analysed using HEATRAN-1 code. Time varying heat transfer coefficient developed in the previous chapter is applied as the boundary condition at the grid plate bottom. In case of ULOFA, core-melt is initially assumed to have settled upon grid plate and the grid plate melt-through time is taken as core-melt relocation time to the core catcher.

On the other hand, molten core material relocation is different in the case of a PLOHS accident where core-melt has to move downwards by melting all the underlying structures below the active fuel zone. For this case conduction heat transfer analysis is carried out using a commercial CFD code. This chapter explains the results obtained from the analyses of both these accidents. Another major difference between the two analyses is that decay heat is simulated in the ULOFA study but a time invariant boiling fuel is assumed in case of PLOHS accident. It is worth mentioning here that ULOFA and PLOHS accident constitute the bounding events to estimate the lower and upper limits of core-melt relocation time to the core catcher.

5.2 RATIONALE FOR 1-D APPROXIMATION

In core-melt relocation studies, the primary objective is to estimate the time taken by the molten fuel material to get relocated in the downward direction to the core catcher placed at the bottom of the main vessel. Therefore, the heat transfer analysis is carried out in the axial direction only. To check the adequacy of these one dimensional computations, two dimensional transient heat transfer computations have been carried out using PHOENICS code, on the grid plate. Since the code does not handle phase change, it is not possible to include latent heat in the calculations. However, the obtained temperature contours were useful in justifying the 1 D approximation used in the development of HEATRAN-1 code.

5.2.1 Axisymmetric Computations with PHOENICS

Computation was performed in two dimensional axisymmetric geometry with grid plate extending to 3 m in radial direction with its thickness being 5 cm. The core-melt which is maintained at its melting point is assumed to occupy 1 m radius on its top. Constant thermophysical properties have been assumed. The grid plate bottom is considered to be adiabatic. Energy equation is solved using the implicit method considering 20 nodes along axial direction and 100 along radial direction. Temperature contours have been obtained in the r-z plane and temperature time histories obtained at the node close to the top boundary and at the bottom most node of the grid plate.

Temperature contours are shown at a few instants of time to observe the propagation of heat in the radial as well as axial directions in Fig. 5.1. At the time of around 170 s, the melt front touches the last grid as seen from the contours. The exact time of last node touching melting point is 173.2 s which is determined from the temperature time history of the last node. The magnified image of temperature contours at 170 s is shown in Fig. 5.2.

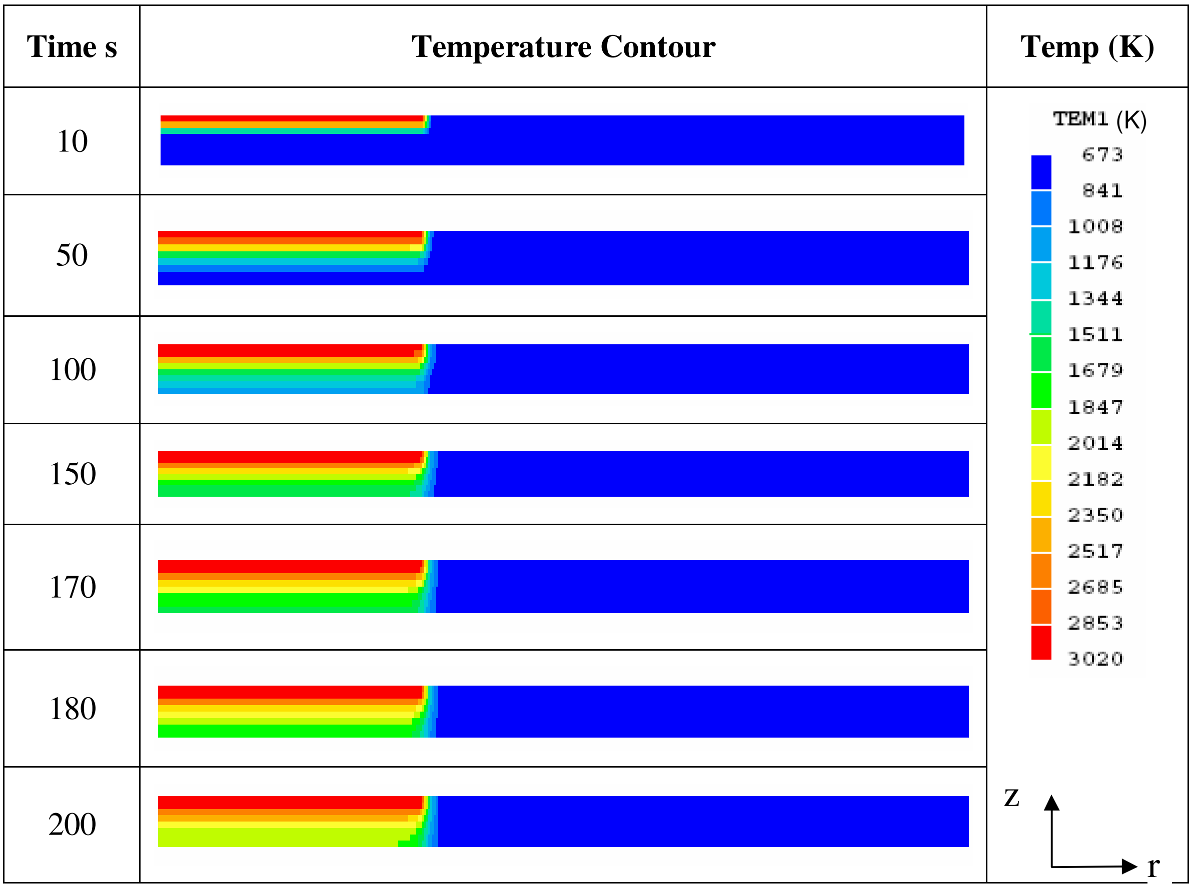

Fig. 5.1 Temperature Contours across r-z plane at different instants

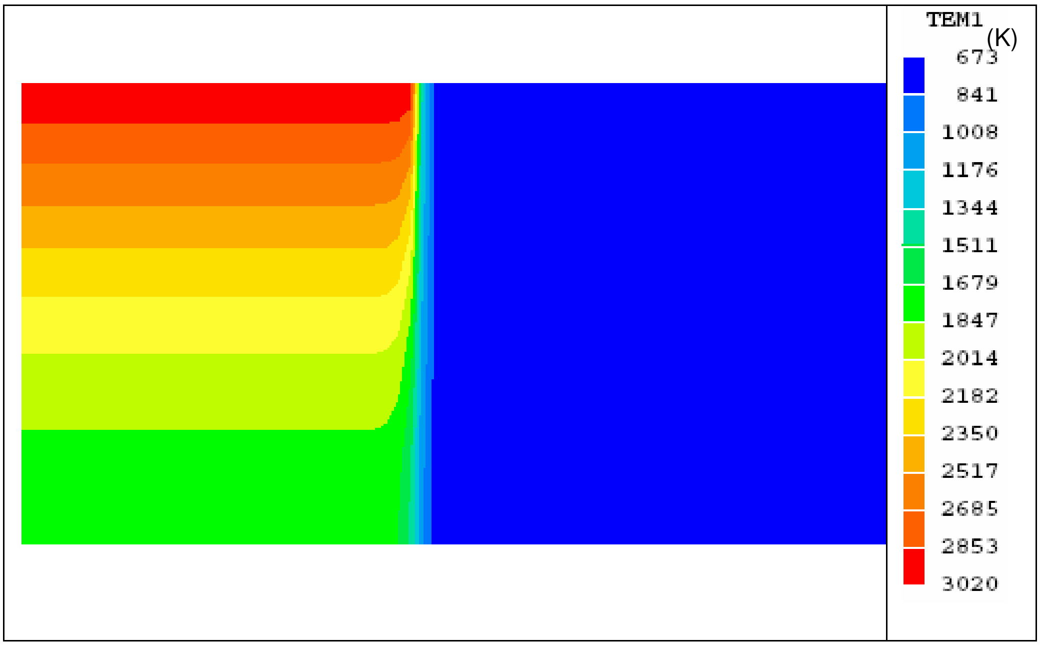

Fig. 5.2 Temperature Contours in r-z plane at 170 s

At 170 s, the radial extent upto which the effect of the source on the top surface was felt was assessed. It is seen that for the source prescribed upto 1 m radius, the effect was felt upto a radius of 1.15 m where the temperature had increased at least by a single degree. Similarly, the radius of the melt front at the bottom most node in grid plate was found to be 9 cm short of source radius on top. A portion of the domain capturing 1700 K isotherm is shown in the Fig. 5.3. Figure 5.4 shows a few isotherms at the instant of 170 s when the last node comes close to melting temperature of stainless steel.

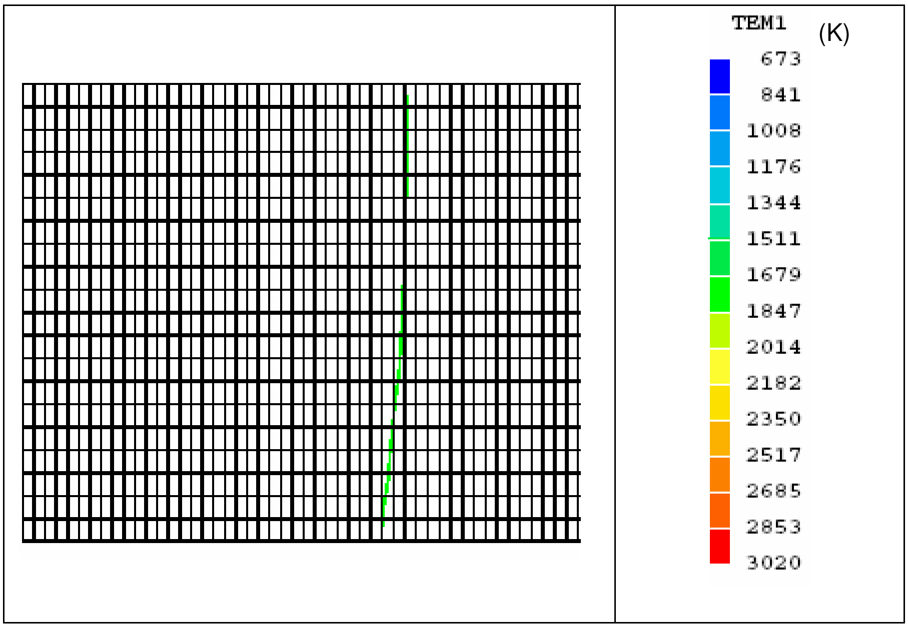

Fig. 5.3 Isotherm of 1700 K at time 170 s

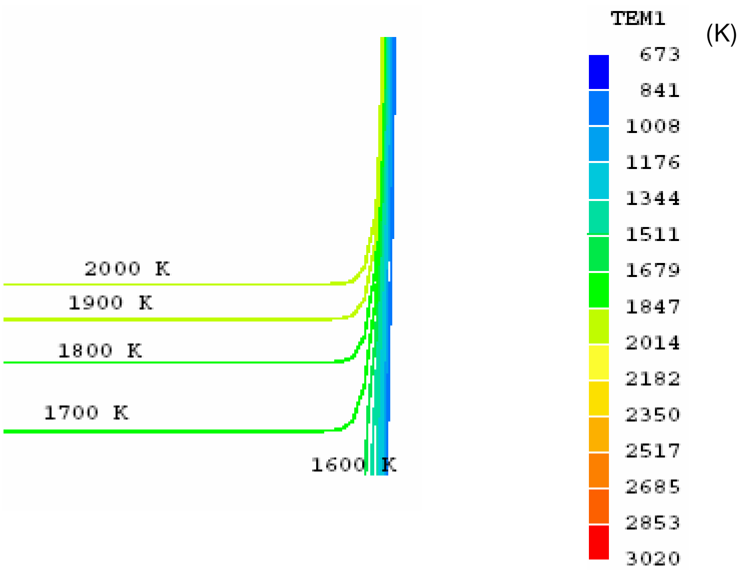

Fig. 5.4 Expanded view of isotherms at 170 s

These computations reveal that the one dimensional approximation used in HEATRAN1 calculations are quite justified since it has missed only a narrow margin of

5 % and 3 % in defining the heat affected zone in the radial direction and the melting radius at the bottom of the plate respectively.

5.3 DEVELOPMENT OF HEATRAN-1 CODE

The difficulties associated with inclusion of latent heat and tracking the melt front in the PHOENICS code has made it necessary to develop a phase change code to deal with grid plate melting due to heating on top by a layer of core-melt with decay heat. Temperature dependent thermo physical properties have been used in the solid phase and constant properties are prescribed for the liquid phase (Chawla et al., 1981).

5.3.1Thermophysical Properties

Thermophysical properties of stainless steel (SS316LN) as a function of temperature are taken into consideration. The variation of thermal conductivity, density and specific heat as a function of temperature are depicted in Figs. 5.5 – 5.7 respectively.

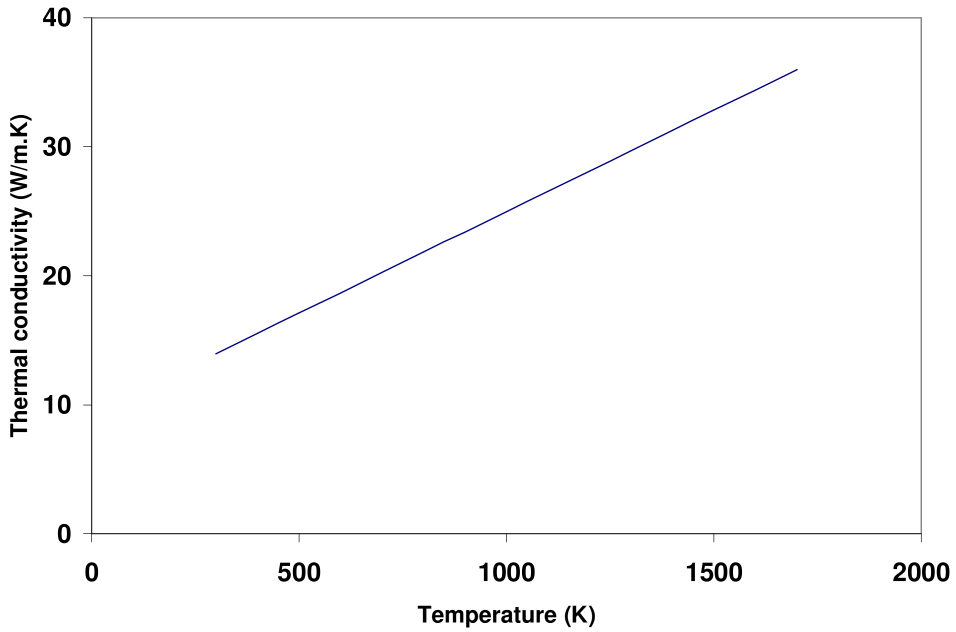

Fig. 5.5 Temperature Dependent Thermal Conductivity of SS 316

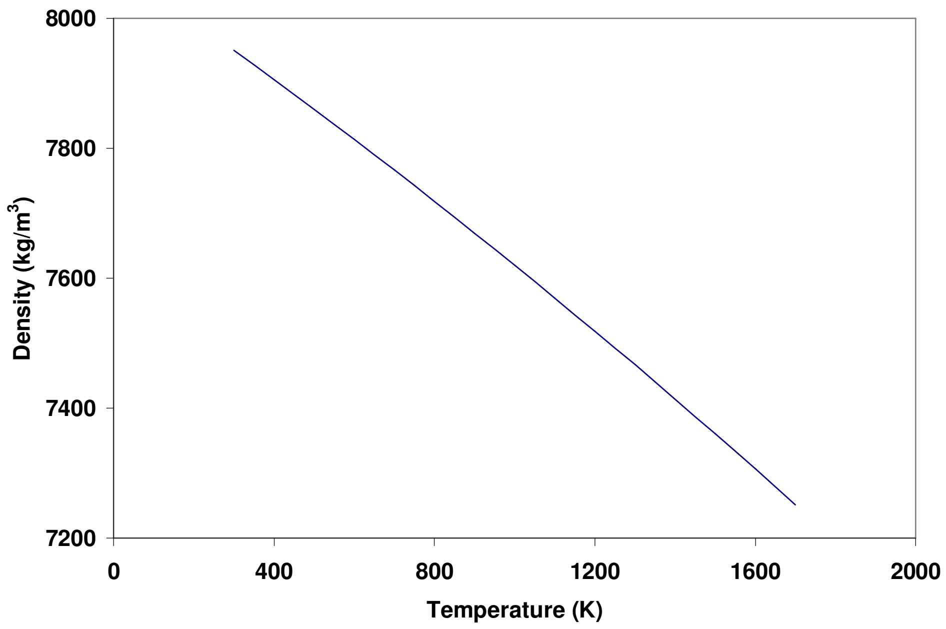

Fig. 5.6 Density Variation of SS 316 with Temperature

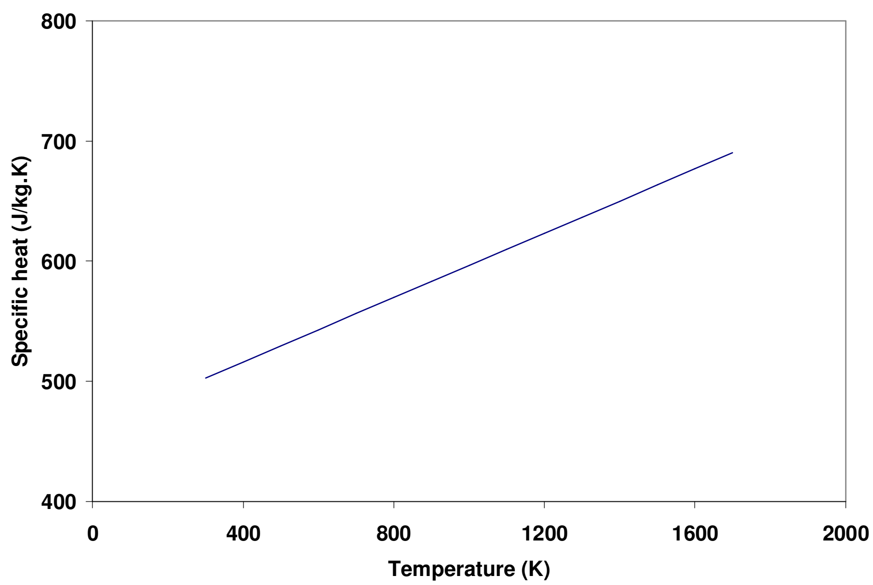

Fig. 5.7 Temperature Dependance of Specific Heat of SS 316

Thermophysical properties of mixed oxide fuel as a function of temperature are taken into consideration. The variation of thermal conductivity, density and specific heat as a function of temperature adopted in the present computation are depicted in Figs. 5.8-5.10.

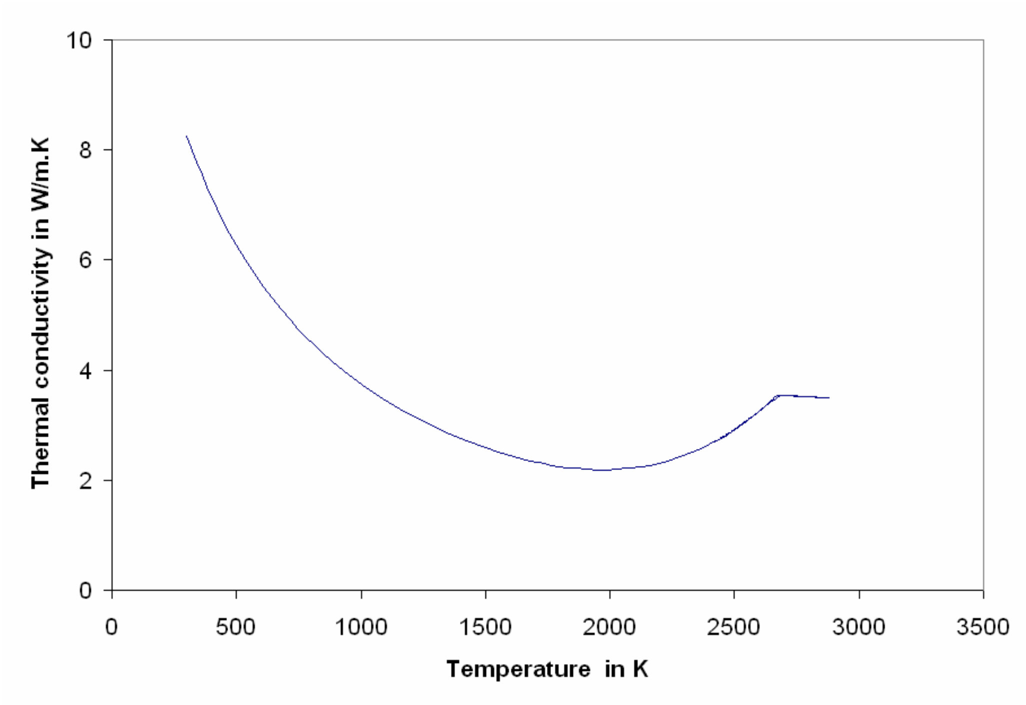

Fig. 5.8 Thermal conductivity of core-melt

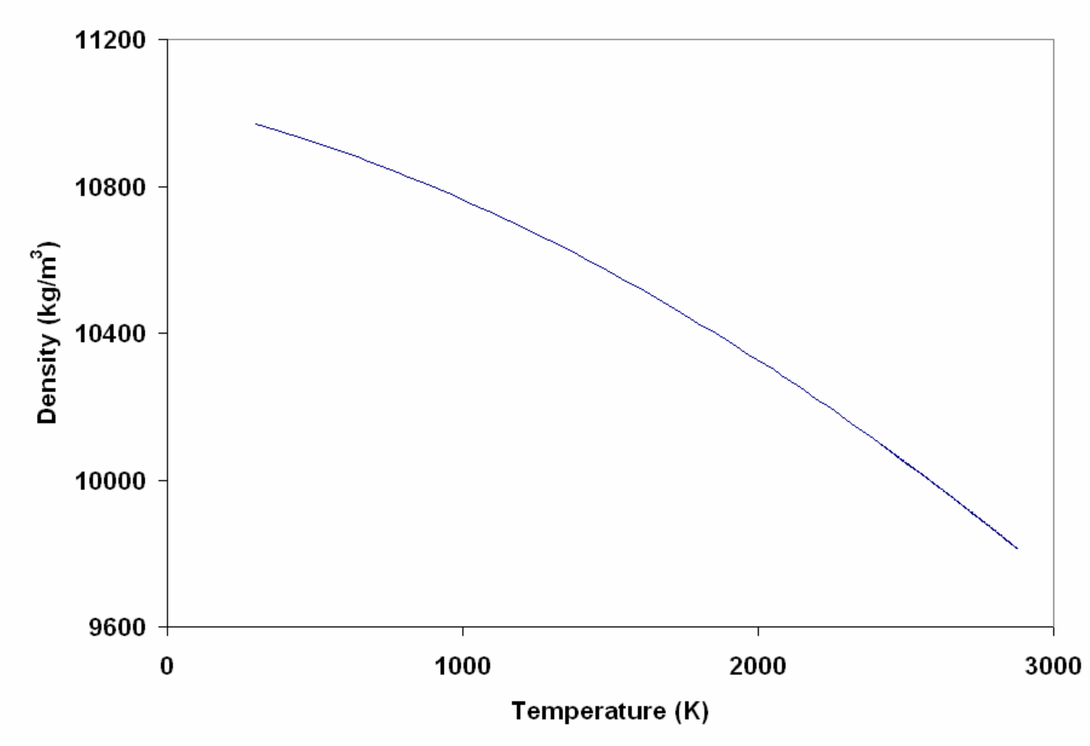

Fig. 5.9 Density of core-melt

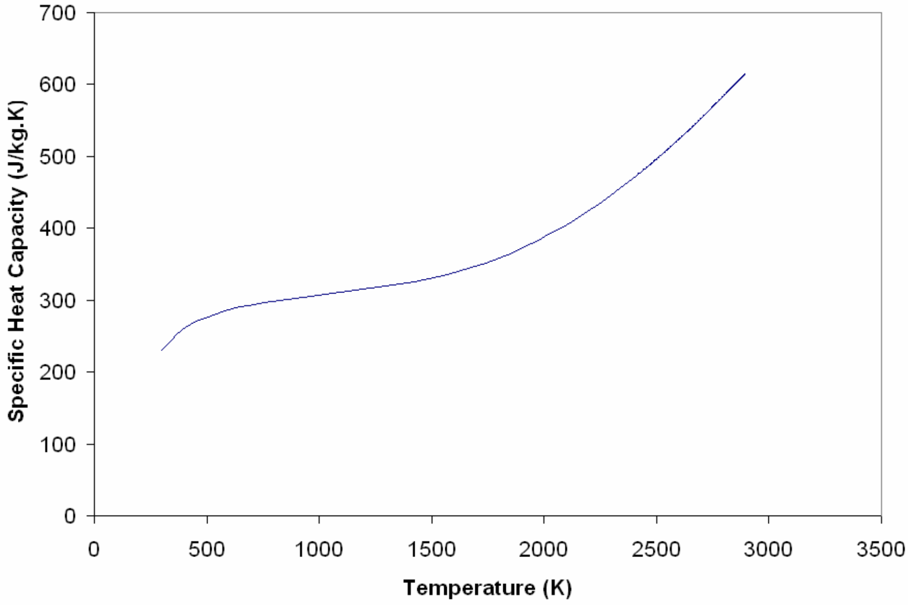

Fig. 5.10 Specific heat capacity of core-melt

5.3.2 Treatment of Nonlinearity

Thermophysical properties namely κ, ρ and C_p being functions of temperatures, render the energy equation nonlinear. The method of lagging the properties by one time step has been used to linearise the problem. That is, when calculations are carried out for $(n+1)^{th}$ time step, properties are evaluated using the nodal temperatures prevailing at the n^{th} time step.

5.4 VALIDATION OF HEATRAN – 1 CODE

HEATRAN-1 code is validated extensively with analytical solution as well as with benchmark data which is explained in the next few sections. The results of the validation exercise are summed up in Table 5.1.

5.4.1 Stefan Problem

The formula for melt penetration depth in a semi infinite medium for the classical Stefan problem is given by $\mu = \dfrac{s}{2\sqrt{\alpha_l t}}$

where μ is the dimensionless parameter so chosen to satisfy the following condition at the interface.

$$Ste = \sqrt{\pi}\mu e^{\mu^2} erf(\mu) \quad (5.1)$$

In the present case with Stefan number lying close to four, μ is calculated to be 0.984. Therefore, the time for melt penetration can be obtained from

$$t = \frac{s^2}{4\alpha_l \mu^2} \quad (5.2)$$

The time taken for 5 cm melt penetration is 194.4 s from this analytical solution. For validating HEATRAN-1 code with Stefan problem, a stainless plate of thickness 50 cm was considered and the time to melt 5 cm thickness is estimated. Adiabatic bottom is assumed instead of an infinitely extending medium considered in developing analytical solutions and the case was solved using HEATRAN-1 code. Thickness of 50 cm was found to be sufficiently large compared to the 5 cm thickness which is to be melted and the effect of heating at the top surface was not felt at the adiabatic bottom, till the 5 cm thickness was molten. Melting temperature of stainless steel (1700 K) was imposed as the initial condition and the top boundary was held constant at 3020 K. Constant properties were used. The time taken for melt penetration upto 5 cm thickness was estimated from the code to be 189.2 s and the discrepancy from the analytical solution is only 2.7%. The discrepancy is attributed to the assumption of semi infinite medium in analytical solution, whereas it is a slab with adiabatic boundary in the computation.

5.4.2 BN 800 Benchmark Data

Transient heat conduction and melt through of lower portion of grid plate have been evaluated numerically for BN 800 reactor using a one dimensional code (Voronov, 1994). Voronov has reported that under the most conservative assumptions of coremelt lying above the grid plate at its boiling temperature and grid plate bottom assumed adiabatic, the time taken to melt the 11 cm thick grid plate is1020 s. Using HEATRAN-1, the same has been estimated as 1056 s and the discrepancy is only 3%.

5.4.3 Validation with PHOENICS Model

The time to reach the melting temperature at the bottom of the grid plate has been estimated using PHOENICS code to be 173.2 s with constant thermophysical properties and without including the latent heat of fusion. The problem with the same set of input data was solved using HEATRAN-1 and the grid plate bottom reached 1700 K in 170 s.

5.5 GRID SENSITIVITY STUDY

Grid independence study is carried out to minimize the errors involved in the computation. The number of nodes in the 5 cm thick grid plate region is increased from a minimum of 5 nodes to a maximum of 80 nodes. The error shows an upward trend when the number of nodes is increased from 40 to 80. It is observed that between 20 nodes and 40 nodes barely 1% deviation is observed in the melt-through time. Hence the number of axial nodes has been fixed at 20 nodes.

Table 5.1 Validation of HEATRAN-1 code

Case	Time to melt (s)	
	ORIGINAL	HEATRAN 1
Stefan's problem (semi infinite medium approximation) (5 cm stainless steel plate)	194.4	189.2
BN – 800 Benchmark data (11 cm stainless steel plate including latent heat)	1020	1056
PHOENICS (5 cm stainless steel plate without phase change)	173.2	170

Table 5.2 Grid Sensitivity Study for HEATRAN-1

No. of nodes	Time to reach melting point (s)	% difference
5	778	
10	858	9.3
20	870	1.4
40	879	1.0

5.6. SEQUENCE OF COMPUTATION

The sequential steps involved in the computation of melt-through time in HEATRAN-1 code are listed below.

1. Start
2. Input dimensions, initial & boundary conditions, melting temperature, latent heat of fusion and number of spatial nodes
3. Calculate Δz, Δt
4. Assign initial temperature to all nodes
5. Calculate $\kappa(T)$, $\rho(T)$, $C(T)$
6. Solve energy equation for all interior nodes by explicit method
7. Get nodal enthalpy
8. Apply inverse transformation to get temperatures
9. Apply boundary conditions
10. Get temperature at boundary nodes
11. Compare enthalpy at node between consecutive time steps
12. Locate phase change boundary if it crosses a node at that time step
13. Apply Voller-Cross algorithm for smoothening phase front
14. Store temperature values at all nodes

15. check for stainless steel melting or fuel boiling
16. If no, goto step 18
17. If yes, remove the melting/boiling portion and remesh the geometry
18. Increment time
19. Goto step 5 and repeat till last node crosses melting temperature
20. Write output to specified data files at the specified nodes
21. Write time vs phase change boundary location to file
22. Stop

5.7 RESULTS AND DISCUSSION FOR ULOFA

During a ULOFA, it is assumed that the core-melt reaches grid plate through open paths like control rod drive lines within a few seconds and starts heating it. In the first case, grid plate region alone is considered with insulated bottom and melting temperature of core-melt imposed on the top surface. In the second case, core-melt region with its decay heat content is modelled above the grid plate. In the third case adiabatic bottom boundary is relaxed and exchange of heat with the lower sodium plenum is modelled. The schematic of the computational domain for the different cases is illustrated in Fig. 5.11.

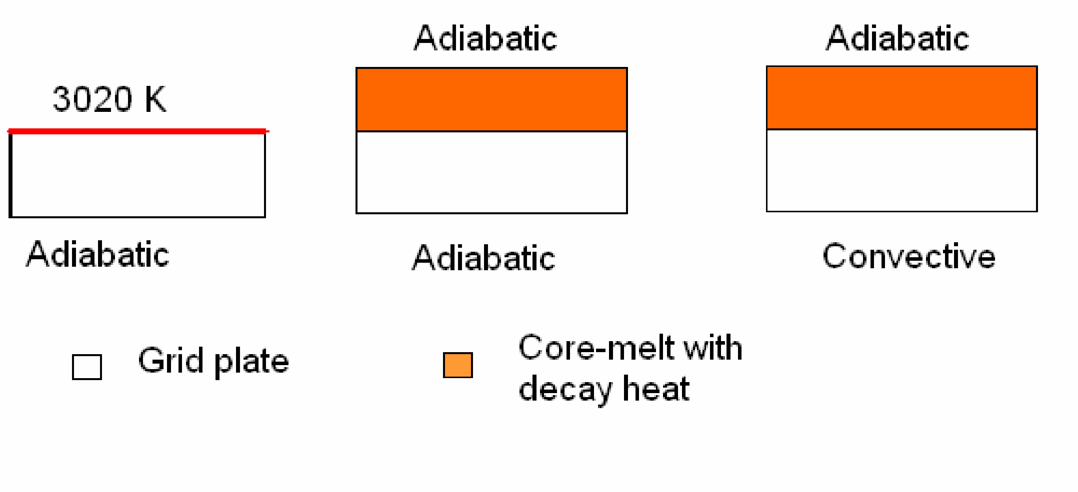

Fig. 5.11 Schematic of computational domain

5.7.1 Grid Plate Exposed to Core-melt at 3020 K

In the first case, constant temperature equal to the melting point of mixed oxide fuel is given as the top boundary condition. This condition is based on the conservative assumption that the decay heat in the core debris is sufficient to keep it in molten condition. But core-melt region is not explicitly modeled. It is assumed that there is no heat loss from the bottom of grid plate. This condition is imposed to get an estimate of the minimum time needed to melt the entire thickness of the plate. The axial temperature profile across the grid plate is shown in Fig. 5.12 at different instants of time up to the point when the last node touches the melting temperature of stainless steel. It is clear from this figure that when the grid plate is constantly exposed to molten core-melt attack, complete melt-through of grid plate will happen in about 300 s. This estimate can be taken as the minimum time of grid plate melt-through.

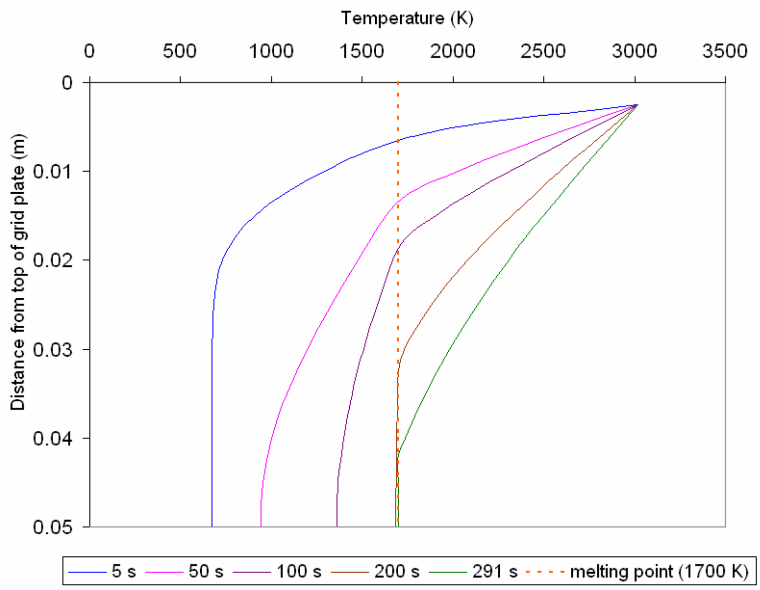

Fig. 5.12 Axial temperature profile across the grid plate at various instants

5.7.2 Adiabatic Grid Plate with Decay Heat Generating Core-melt

In the second case study, grid plate bottom is taken to be adiabatic. The radial extent of core-melt spreading on the grid plate is assumed to vary between 1 m to 3 m, the former being the radius of the active core region and the latter being the radius of the grid plate itself. The thickness of the core-melt varies accordingly, the mass of the core-melt being constant in all the cases. Melt arrival time on the grid plate is the time taken by the core-melt to get relocated to the grid plate from the core region after the accident. Deterministic calculations do not exist for this initial part of the accident and therefore this time estimate has been taken from information available in open literature and it is varied from 1s to 100s (Gluekler, 1982). Hence, the melt arrival time has been considered as a parameter. The decay heat of core-melt is a function of melt arrival time. Therefore, the melt-through analysis is repeated for different melt arrival time values.

Further, as already stated, it is essential to understand the reduction in melt-through time when molten steel mass is dynamically removed paving way for proper contact between sinking denser core-melt and stainless steel plate. Moreover, when the fuel temperature exceeds its boiling point, the fuel vapour could escape from the surface of the molten fuel leading to an increase in melt-through time. Hence, a detailed parametric study of all these phenomena is carried out using the HEATRAN-1 code and the consolidated results are presented in Table 5.3.

The results indicate that melt-through of grid plate can occur between 986 s and 1157 s for different times of arrival of core-melt and different settling radii assuming that melting steel portion remains intact. This is referred as 'Normal' in Table 5.3. A comparison is made between time estimates obtained with and without displacing the molten portion in grid plate and boiling portion in fuel. It is seen that for the plate thickness of 5 cm, the observed change in melt-through time is only about 15% of total time needed. For evenly spread core-melt on the grid plate, melt-through time is ~1000 s. It is to be noted that the decreasing thickness of grid plate due to melting is partly compensated by the decreasing thickness of fuel region due to boiling on top. Another reason is that when a melting stainless steel node gets displaced and a relatively cooler node comes in contact with the interface, the interface temperature decreases marginally. This reduces the flux across the interface and hence the heating rate.

Table 5.3 Grid plate melt-through time

Radius of fuel (m)	Melt arrival time (s)	Time to melt grid plate (s)		
		Normal (no material displace -ment)	Melting SS portion only displaced	Boiling fuel portion also displaced
1	1	986	791	844
	10	1011	815	862
	100	1097	897	927
2	1	990	799	861
	10	1014	823	879
	100	1101	909	948
3	1	1037	850	873
	10	1063	874	893
	100	1157	968	968

The predicted temperature history at a few important nodes is illustrated in Figure 5.13. The top of fuel initially at its melting point remains at the same temperature for a while absorbing the latent heat and then its temperature increases steadily till it reaches the boiling point. The temperature of the bottom of the fuel initially decreases because of the heat exchange with cooler grid plate at 673 K and then rises up due to the continued decay heat generation. The grid plate bottom temperature increases and at melting point, absorbs its latent heat and then rises sharply because of increased diffusivity of liquid stainless steel. Melt-through is said to have occurred when the temperature at grid plate bottom just crosses the melting point.

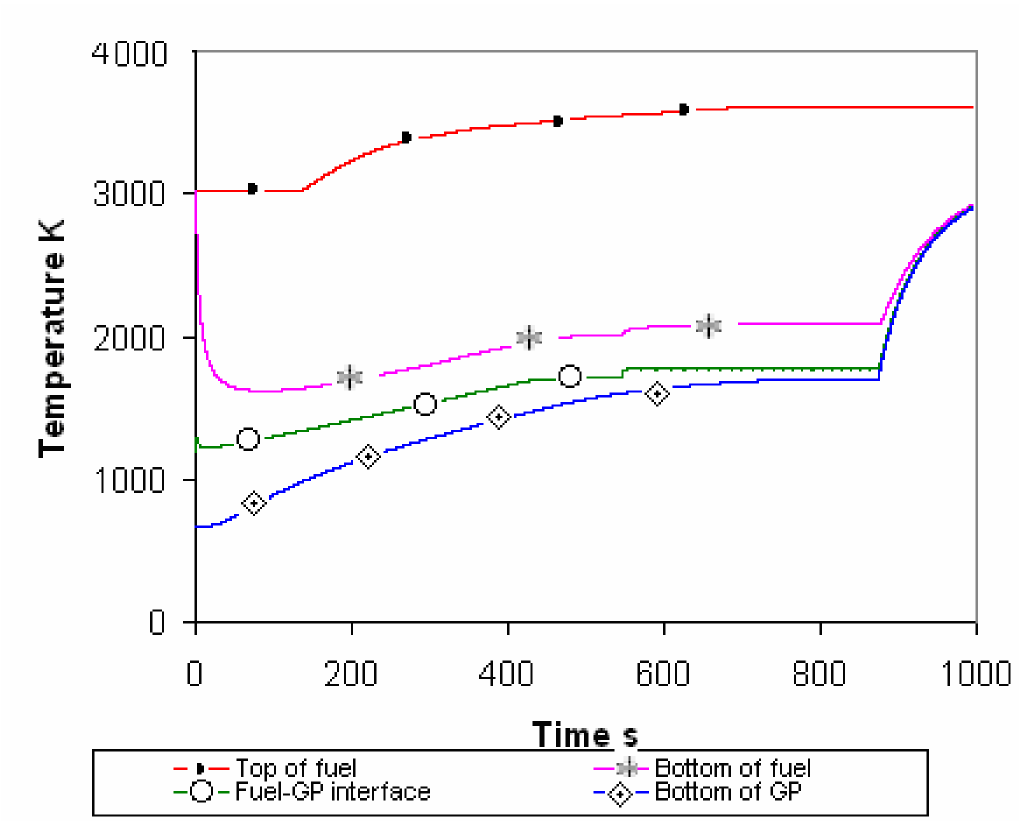

Fig. 5.13 Temperature at selective nodes

The temperature profile across the fuel (2m radius) and grid plate regions at various instants of time for adiabatic bottom of grid plate are shown in Fig 5.14. It is observed that upto 300s, no phase change is observed to occur in the grid plate and fuel regions. Then, boiling of fuel top portion results in reduced fuel thickness, as seen from the time curve at 430 s. Melting of grid plate region is complete at 950 s. The melt interface continuously migrates downwards but it is shown stationary in Fig 5.14 for the ease of plotting. The reduction in the line lengths in the fuel and grid plate regions arise because of boiling / molten material displacement respectively.

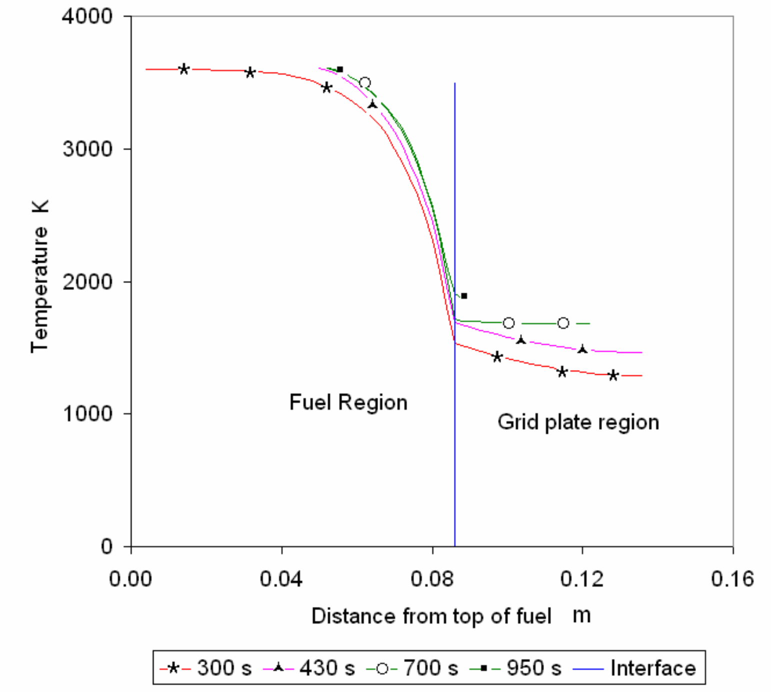

Fig. 5.14 Temperature profile across core-melt & grid plate

The position of melt front for two different radial extents of molten fuel is presented in Fig 5.15. When the extent of spreading on grid plate is large, the fuel thickness comes down and it takes a longer time to melt-through the grid plate. Onset of melting is observed in the grid plate only after a time lapse of about 400 s.

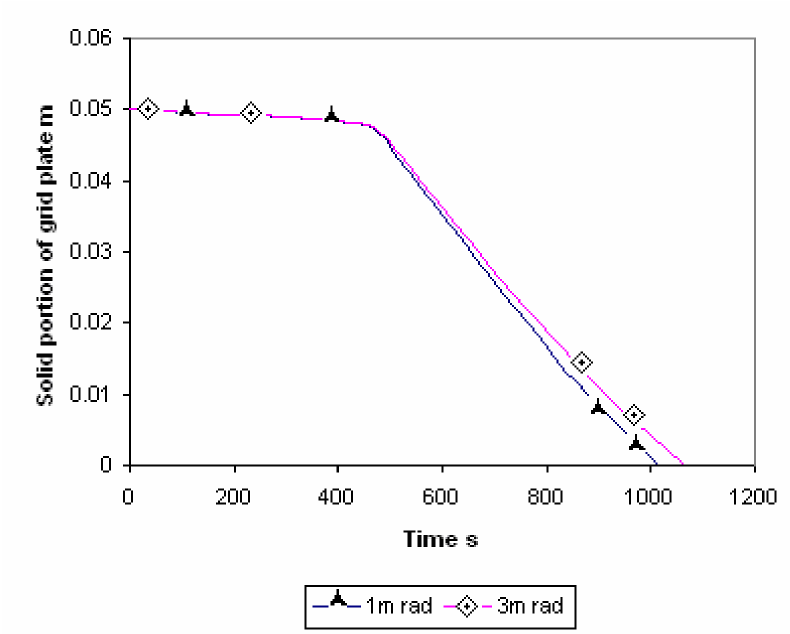

Fig. 5.15 Melt front position for different extents of melt spread

5.7.3 Grid Plate Exchanging Heat with Lower Plenum

In the next case, where heat exchange between grid plate and lower plenum is to be accounted, the transient natural convective heat transfer coefficient of sodium estimated using the PHOENICS code is prescribed as time varying boundary condition at grid plate bottom. Table 5.4 summarises the results of using constant and variable transient heat transfer coefficients *h*.

Table 5.4. Maximum temperature at grid plate bottom

Radius of fuel (m)	Melt arrival time (s)	Max. temperature at GP bottom (K)		
		Normal h=1000 W/m^2K	Nodes displaced h=1000 W/m^2K	Nodes displaced and transient h
1	1	1074	1029	1119
	10	1072	1026	1115
	100	1061	1010	1097
2	1	1065	1028	1118
	10	1062	1025	1115
	100	1059	1010	1098
3	1	1040	1028	1117
	10	1023	1025	1113
	100	995	1003	1089

When heat transfer coefficient is prescribed at grid plate bottom, melt-through does not occur. The time temperature history obtained at grid plate bottom for evenly spread core-melt on grid plate for different delay times of melt arrival is depicted in Fig. 5.16. It is observed that the maximum temperature at grid plate bottom is reached within a time period of 1000 s - 1500 s and then the grid plate bottom shows a decreasing trend due to reduction in decay heat.

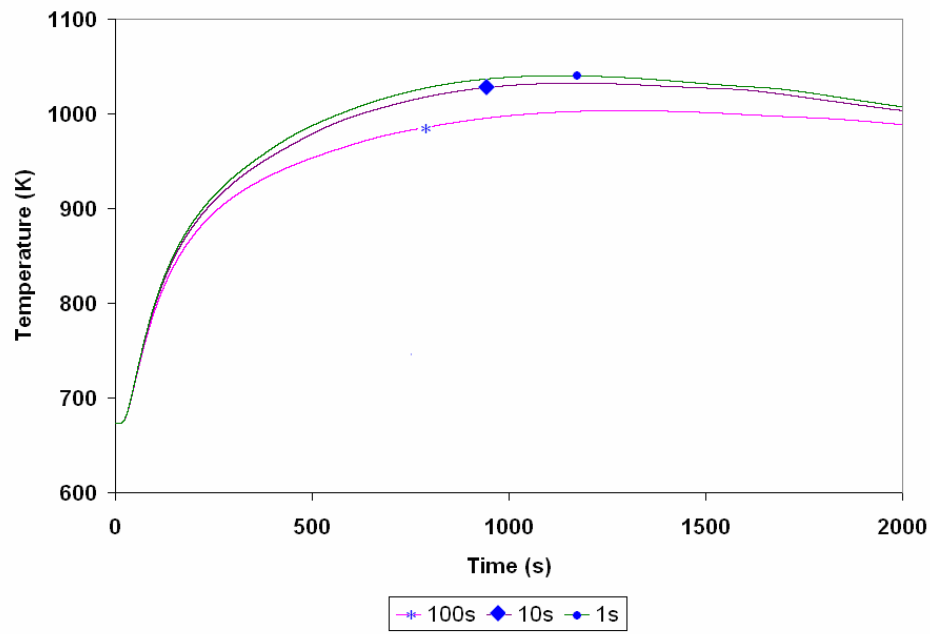

Fig. 5.16 Grid plate bottom temperature history for different melt arrival times

The maximum temperature reached at grid plate bottom when core-melt occupies 1 m radius on grid plate is 1120 K, which is about 575 K lower than the melting point of grid plate. Also, it is clear from Table 5.4 that the heat transfer coefficient calculated from general steady state correlations does not yield conservative results. It is prudent to use a transient heat transfer coefficient obtained from a conjugate heat transfer analysis as demonstrated here. Though the maximum temperature is less than the melting point of stainless steel and the boiling point of sodium, the temperature is high enough to cause failure of the plate by thermal creep at a later time. Therefore, the results indicate that the grid plate cannot serve as a permanent settling place for core-melt, emphasizing the need for an invessel core catcher.

5.8 CORE-MELT RELOCATION AFTER A PLOHS ACCIDENT

In case of PLOHS analysis, a commercial CFD code is used to analyse the sequential melting of all regions below the active core. Because of the implicit formulation in the CFD solver, large time steps could be accommodated to reduce the computational effort for the large length scale (~ 2m) and time scales (~16 hours) involved in this accident. But, dynamic rezoning of the computational domain is cumbersome in the code. Therefore, it is proposed to follow the philosophy adopted by Voronov (1994) for the BN 800 reactor where displacement is effected region wise.

As stated earlier in Chapter 3, PLOHS is a slowly progressing accident and its analysis is expected to yield the upper limit for molten core material or core-melt relocation time. A few possible cases of accident progression are analysed in the present study of PLOHS accident to estimate the core-melt relocation to the grid plate. Here too, axial heat conduction is considered. In the active core region nuclear fuel is assumed to be always at its boiling temperature because of the non availability of heat sink. Bottom of grid plate is assumed to be adiabatic in the first two cases. In the first case, the blanket region is assumed to remain intact until the uranium dioxide melting temperature of 3120 K is reached. Sodium boiling and steel melting would have happened much earlier than that, but still downward relocation of molten fuel is not envisaged to occur.

In the second case, a more logical reasoning is followed, postulating that with steel melting away, the blanket region cannot withhold the downward relocation of core-melt since stainless steel is the cladding material for the fuel pins encased in the subassembly. Moreover, with sodium evaporating in the upward direction and steel melting and flowing in the downward direction, about 2/3rd of the volume would have opened up, leaving enough gap and an open path for the high temperature core-melt to penetrate further downward. Therefore, the blanket region bottom temperature reaching the melting temperature of the stainless steel clad is set as the limiting time for the core-melt penetration through the blanket region. At this point blanket region is removed from the computational domain and the conduction analysis proceeds with the remaining four layers. The same criterion is then applied to subsequent regions and material displacement is effected to estimate the total core-melt relocation time. In the third case, grid plate exchanging heat to the lower cold sodium plenum is considered and a nominal value of heat transfer coefficient is prescribed at the bottom of grid plate. All other conditions are similar to case study – 2.

5.8.1 Case Study 1

With heat source imposed on top of the axial blanket region (3600 K), heat propagation along the vertically downward direction is analysed. It is found that the low conductivity of blanket region and high melting temperature greatly inhibit the downward heat propagation. Temperature contours at various instants of time along with its temperature scale is depicted in Fig. 5.17.

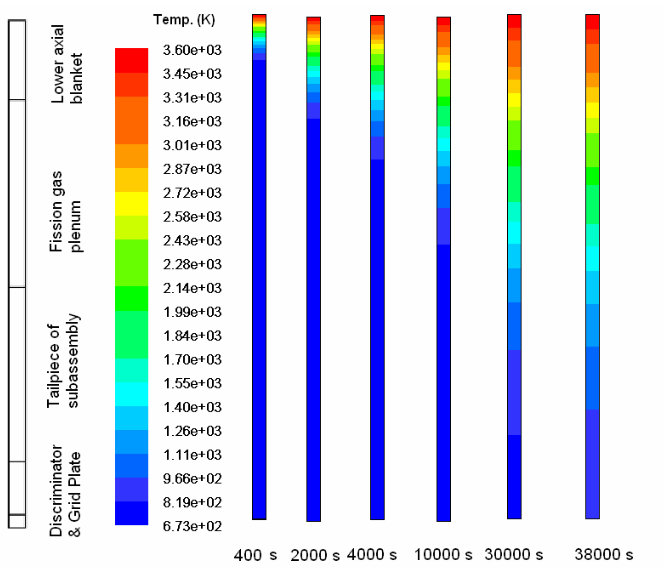

Fig. 5.17 Temperature field in five layers without displacement

For demarking the different regions, the interfaces are marked at its left side. Even after 16 hours of heating by core-melt on top, the maximum temperature at the bottom blanket region is only 3000 K and does not cross its melting point of 3120 K. The time evolution of temperature in various regions of interest is shown in Fig. 5.18.

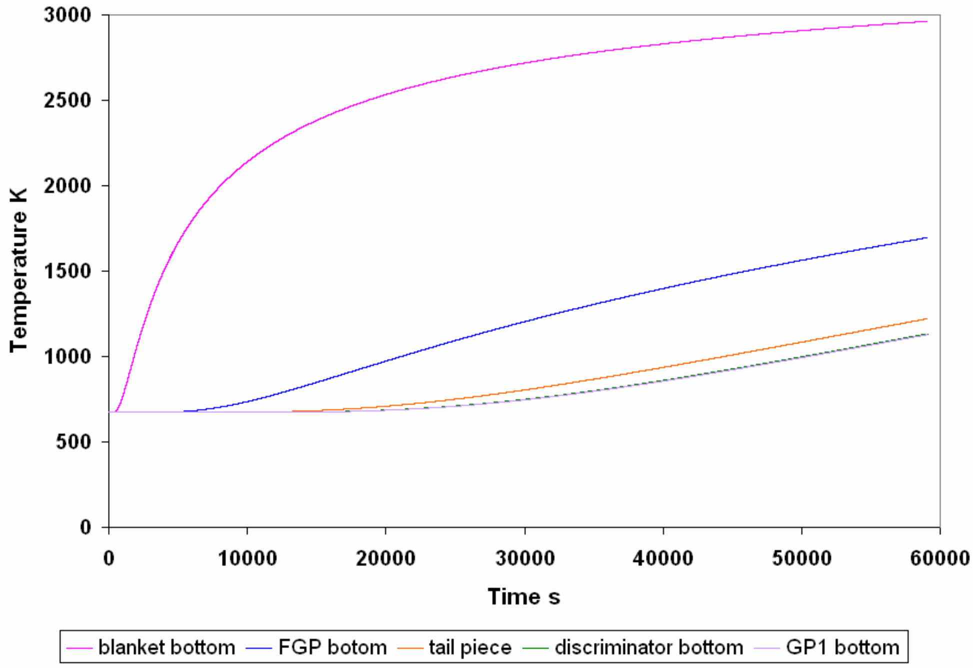

Fig. 5.18 Temperature evolution in the five regions

It is inferred that the grid plate bottom temperature exceeds the design safety limit temperature of 923 K in about 12.5 hours (45000s). After this point the load bearing ability of the grid plate comes down drastically with time due to thermal creep and it can give way, allowing the degraded core and other structures to fall into the lower sodium plenum. After 15.5 hours of heating, grid plate bottom temperature exceeds 1073 K after which creep rupture failure becomes inevitable. Hence this time is taken as core-melt relocation time to the core catcher in case of a PLOHS accident. In this case study, heat conduction analysis through the composite five layers is carried out without any change in the geometry, i.e., without displacement of any region throughout the analysis.

5.8.2 Case Study 2

In this case study, stainless steel melting point is assumed to be the threshold condition for any region to lose its integrity, giving way for downward relocation of the core-melt to the top of next region. As the temperature at the bottom of each layer reaches this threshold temperature, that region is removed from the computational domain. In this study, the removal of blanket, fission gas plenum, tail piece and discriminator takes place at 5238 s, 8428 s, 19038 s, 20492 s and 20536 s respectively. The quoted instants of time refer to the cumulative time counted from the beginning of computation. As each region is displaced, if the temperature at the bottom of the adjacent region has been influenced by the heat transfer so far, then the average temperature of that region is prescribed as the initial temperature of that region for the next phase of computation. But Core-melt temperature at its boiling point is maintained constant throughout the computation. Figure 5.19 depicts a pictorial representation of the different phases of computation along with the respective temperature field plotted at the instants when each region is removed. The analysis has indicated that it takes about 5.5 hours of time for the core-melt to reach the sodium inlet plenum by sequentially melting the underlying structures.

Apart from stainless steel melting event, an earlier event which is of significance is that of sodium boiling. A temporal plot of these two events versus the axial distance measured from the top of lower axial blanket region is illustrated in Fig. 5.20. The instants of time at which sodium boiling takes place are 2628 s, 4218 s, 8373 s, 9190 s and 9530 s for the five regions taken in order from blanket region to grid plate respectively.

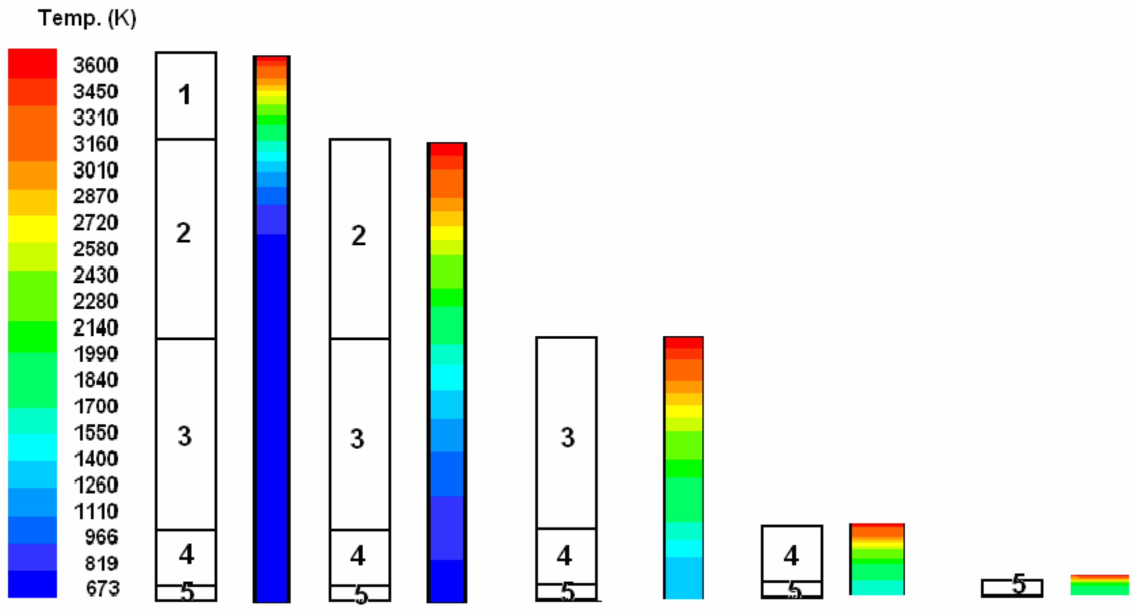

1 – Lower axial blanket 2 – Fission gas plenum 3 – Tail Piece

4 – Discriminator 5 – Grid plate top

Fig. 5.19 Temperature field at the instants of time when each layer is displaced

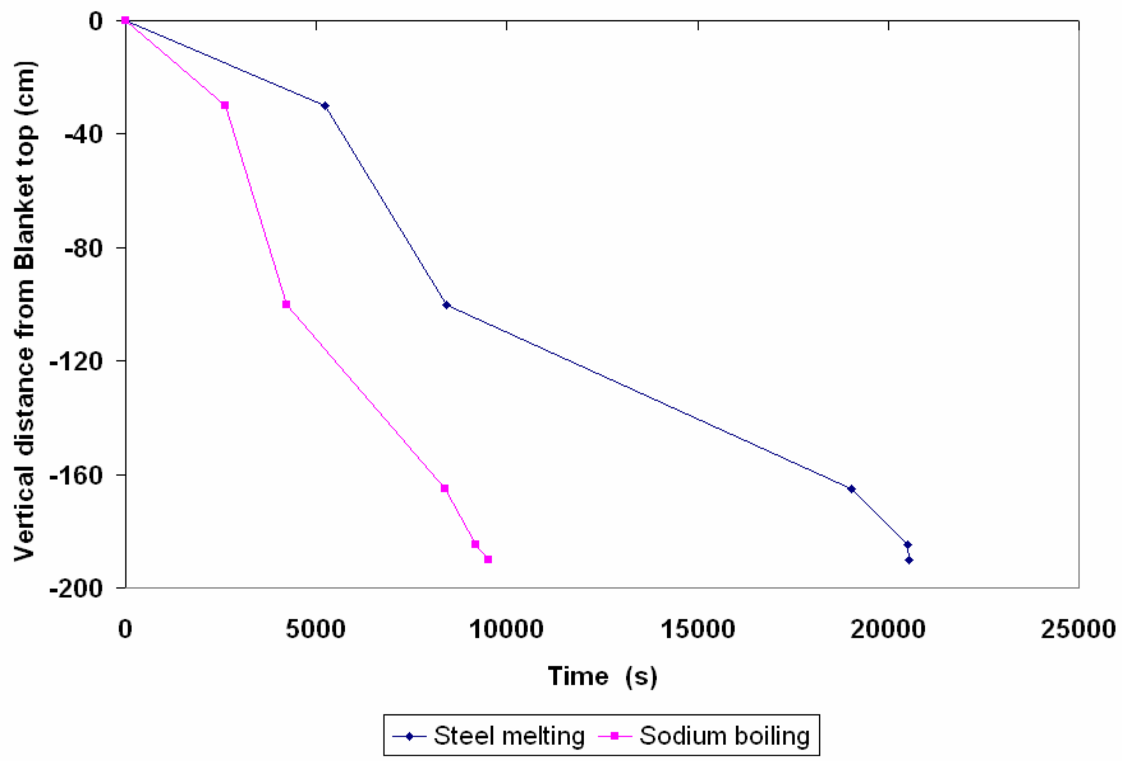

Fig. 5.20 Phase fronts along the vertical direction

This result indicates that the subassembly will go dry without sodium upto the foot in about 2.5 hours time, if there is no possibility of sodium rewetting. With sodium boiling taking place in the different regions, the effective thermophysical properties would no longer be the same, if sodium vapour occupies that place. But in the present study, sodium rewetting is envisaged to occur and hence sodium boiling does not alter the course of melt relocation.

5.8.3 Case Study 3

This case study is similar to case study 2 except that the bottom boundary condition is convective below the grid plate. Heat transfer coefficient of 1000 W/m^{2}K is prescribed below the grid plate. The predicted temperature field is given in Fig 5.21 and the phase front positions are given in Fig. 5.22.

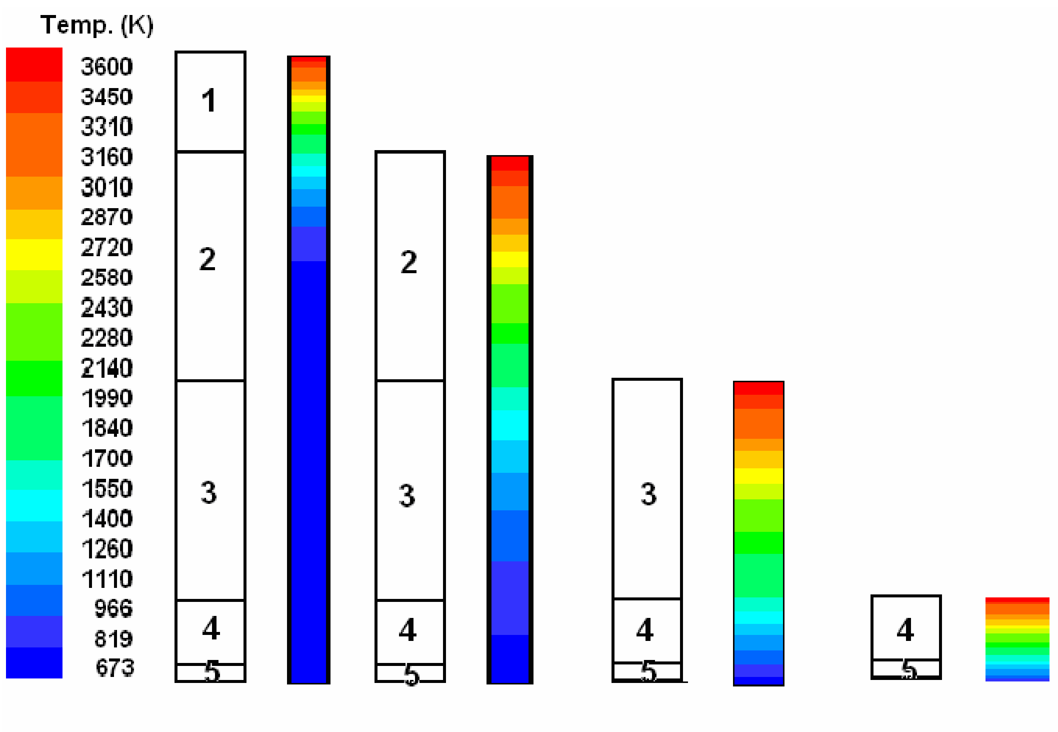

1 – Lower axial blanket **2 – Fission gas plenum** **3 – Tail Piece**

4 – Discriminator **5 – Grid plate top**

Fig. 5.21 Temperature field in various regions at instants of displacement (convective bottom)

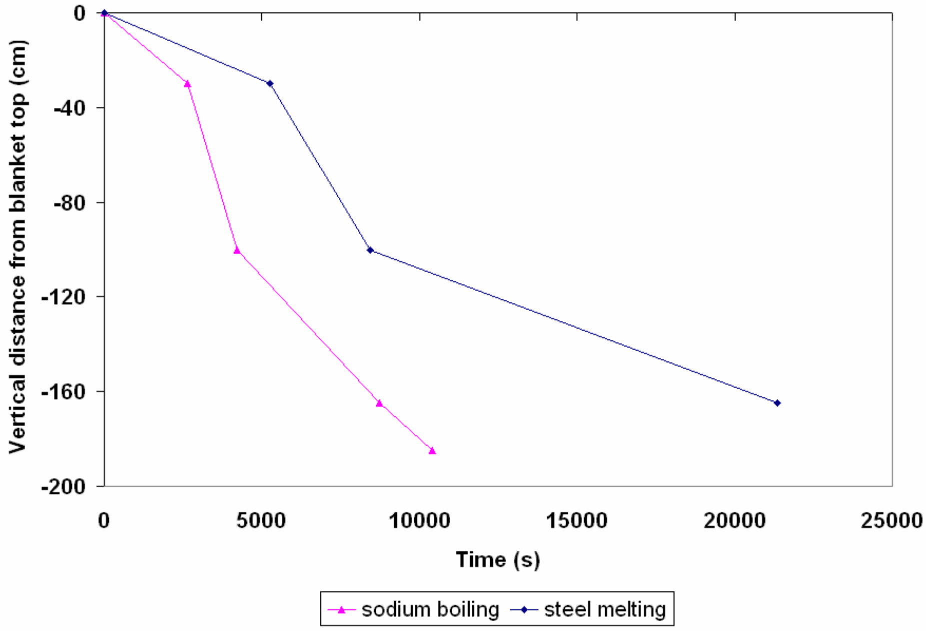

Fig. 5.22 Phase fronts along the vertical direction (convective bottom)

Displacement of top two regions namely blanket and fission gas plenum with melting of steel takes place at 5238 s and 8428 s respectively as in case 2. The influence of bottom boundary condition is felt only after this instant. The time at which tail piece crosses steel melting temperature is delayed and it occurs at 21348 s. Molten fuel is now displaced to the top of discriminator region. The maximum steady temperatures reached at the bottom of discriminator and the grid plate regions are 1486 K and 944 K respectively. They do not cross steel melting temperatures and hence are not displaced though a major portion of discriminator is molten. From Fig. 5.22 it is seen that sodium boiling front has crossed the discriminator whereas steel melting is not complete in the discriminator region.

5.8.4 Validation of PLOHS Model

The computational model for PLOHS is validated by comparing the predicted results against that predicted by the HEATRAN-1 code for a 5 cm stainless steel plate. The time required for the bottom of the plate to get heated to 1700 K from 673 K predicted by both the codes agreed with each other within 3%, thus validating the PLOHS model.

5.9 CLOSURE

Thermal analysis has been carried out both for ULOFA and PLOHS events with the objective of estimating core-melt relocation time to the core catcher. In the case of ULOFA where the core-melt can reach the grid plate within a few seconds, grid plate melt-through happens in 300s and 1000 s for constant molten fuel attack and for core-melt with time varying decay heat respectively. But PLOHS accident progression is much slower, where core-melt relocation is estimated to take a minimum of 5.5 hours. These time estimates are essential in estimating the initial thermal load on the core catcher in the case of accidents.

CHAPTER 6

MULTI LAYER CORE CATCHER

6.1 INTRODUCTION

For future design of FBRs, it is proposed to design a core catcher that can handle a whole core-melt to enhance the inherent safety of the reactor. One of the possible options to accomplish this objective is adopting a multi layer core catcher, consisting of a top sacrificial layer, a middle refractory ceramic layer (which can itself be single or multiple layers) and a base layer. It is proposed to house the composite core catcher inside a sheath of stainless steel / refractory metal so that during normal operating conditions, the components of the core catcher are not exposed to sodium which practically eliminates possible long term erosion and corrosion issues. This chapter explains the specific requirements from the core catcher and the choice of materials. It also discusses the results from the thermal analysis carried out for the proposed triple layer core catcher.

6.2 SELECTION OF MATERIALS

Some of the basic requirements for the core catcher materials are:

- The chosen materials should not be reactive with corium constituents, namely, fuel, blanket and clad materials.
- They should be compatible with coolant sodium at all temperatures
- They should not form a reactive mixture among themselves
- They should have sufficient high temperature strength and resistance to creep and corrosion.
- They should serve for the entire life of the reactor ~ 60 years.
- Ease of fabrication and cost effectiveness are the other factors

For sodium cooled FBR applications, stainless steel (SS316LN) is the favoured candidate for the base material of the core catcher plate because of its proven mechanical properties. The middle layer(s) should be of a refractory material of low thermal conductivity (to obtain large thermal gradient) and high melting point. Ceramics are often more resistant to oxidation, corrosion and wear than metals and can act as efficient thermal barriers (Cao et al., 2004). From reported literature, it is found that refractory materials, such as magnesia, alumina, and zirconia, which have low silica contents, are compatible with boiling sodium for at least four hours. (Borgstedt, 2008 and Mecham, 1976). Zirconia may not be a good candidate because of its corrosion in sodium at high temperatures. Thoria presents fabrication difficulties with implied escalation in cost. In the study carried out by Meacham et al. (1976), one magnesia specimen, containing 10.8% silica, was found compatible with 870°C sodium after a 100 hour exposure. Since cost, ease of fabrication and availability are also primary factors when considering large quantities of materials, magnesia should be considered as one of the desirable refractory material and further evaluation under specific conditions is necessary for its potential use in FBR core catcher.

Borgstedt (2008) and Mecham (1976) have studied extensively the influence of liquid sodium on mechanical properties of steels, refractory alloys and ceramics. A few of their findings relevant to the present application are summarized below:

- Mo, W and Re have extremely low solubility in sodium. Alloys based on these metals are highly compatible with sodium.
- Alumina, beryllia, magnesia, thoria and zirconia are also compatible with liquid sodium, depending on the purity of the ceramic materials.
- Increasing flow velocity and temperature of sodium increase corrosion rates in Inconel and Nimonic significantly.

The important candidate materials that can act as delay bed in the multi layer core catcher and their major drawbacks, as inferred from their study are indicated in Table 6.1. Thoria and magnesia are the delay bed materials which are considered in this study. Compatibility of thoria and magnesia with reactor fuel is proven since thoria is used as the blanket material in breeder reactors and magnesium based alloy has been used as clad in Magnox type reactors. High specific heat capacity and latent heat of magnesia allow high heat storage capacity enhancing its ability to act as delay bed. Moreover, the thermal expansion coefficient of magnesia matches well with that of stainless steel which serves as the base material of core catcher. Low thermal conductivity and higher melting point of thoria (higher than that of fuel), makes it an ideal insulating delay bed which is better than a sacrificial delay bed. Another important fact to be reckoned is the inability of these ceramics to withstand high thermal gradients, though they are suited for high temperature applications. Therefore, the delay bed needs to be split into an optimum number of layers of thin sheets with temperature gradients not exceeding their allowable limits.

The top most layer should have high melting point which would promote spreading of corium on the core catcher and a refractory metals like tungsten, hafnium or molybdenum could be considered. A few prospective materials for the top layer and their properties are listed in Table 6.2. Tungsten can act as an insulating layer with its melting point being higher than the core-melt. Molybdenum is a favoured material because of its low density and high specific heat compared to tungsten and also because of its good compatibility with fuel and sodium. Low density will reduce the weight of the core catcher which is advantageous from mechanical design considerations. Additional attractive advantage of hafnium is its ability to absorb neutrons, thus alleviating recriticality concerns. Its corrosion resistance is as good as stainless steel in sodium at 500°C (Holmes and Chang, 2005). Besides, it is easy to form and join hafnium because of its ductility and wear resistance. Another alternative for the top layer could be stainless steel, plasma sprayed with a protective coating of magnesia with a bond coating of Nickel or Inconel. The negative side of the multi layer core catcher is its manufacturing difficulties, particularly making large diameter sheets and bonding between the different layers.

Table 6.1 Delay bed materials and their characteristics

Material	Melting Point (°C)	Thermal Conductivity (W/m.K)	Density (kg/m^3)	Specific Heat Capacity (J/kg.K)	Latent Heat of Fusion (kJ/kg)	Remarks
Graphite	3600	25	1600	600	9750	Reacts with molten fuel forming UC_2.
Al_2O_3	2000	18	3850	1270	1936	Forms sodium aluminate.
SiO_2	1720	1.4	2500	1190	142	Forms sodium silicate.
$MgAl_2O_4$	2100	14.7	3580	1212	1328	Forms eutectic with FeO at 1400°C.
MgO	2852	6	3650	1445	1920	High purity devoid of alumina and silica should be ensured.
ThO_2	3300	4	10000	320	309	Difficulty in fabrication.

Cermets of the ceramic and metal to be joined could be used as the bonding agent to reduce the bonding problem. Metals like tungsten and molybdenum and ceramics like magnesia and thoria are amenable to form cermets and are already in use in various special applications (Backs and Holtbecker, 1982). But the right combination has to be researched and worked out for this application.

6.3 COMPOSITION OF MULTI LAYER CORE CATCHER

Having discussed about the favourable materials for the various layers of the core catcher, it is essential to define the composition of the multi layer core catcher to carry out heat transfer studies in order to predict temperature evolution in different layers of the core catcher following an accident when the volumetric heat generating core debris settles over the plate. The temperature gradient across the very thin top metallic layer will be very small. Hence in the present analysis, Molybdenum is chosen as the representative material for the top layer from the candidate materials listed in Table 6.2.

Table 6.2 Thermophysical properties of materials for top layer (at room temperature)

Material	Density (kg/m^3)	Sp. Heat (J/kg.K)	Conductivity (W/m.K)	Melting point (K)	Boiling Point (K)	Heat of Fusion (kJ/kg)
Molybdenum	10220	250	138	2893	4913	289
Hafnium	13310	144	23	2502	4876	135
Tungsten	19300	130	178	3673	5828	193
Niobium	8570	270	53	2740	5200	285
S.S	8000	500	21	1700	3173	267

Changing the material to tungsten or hafnium did not affect the results noticeably. The thickness of the base stainless steel structural layer is fixed at 2 cm. The main objective of the thermal analysis is to arrive at an optimum thickness of the delay bed so that the core catcher is able to cope up the heat load arising from a whole core accident. Analysis has been carried out with two different materials for the delay bed, viz, thoria and magnesia. The variation of thermal conductivity of magnesia with temperature as reported by Chawla et al. (1981) is included in this analysis. Other thermophysical quantities are assumed to be constant. The thickness of different layers chosen for heat transfer analysis and their role in the composite core catcher are explained in Table 6.3.

Table 6.3 A typical triple layer core catcher

Layer	Material	Thickness (cm)	Desirable Properties	Remarks
Top layer	Mo	0.5	• High melting point • High thermal conductivity	• Aids in radial distribution of heat load by promoting spreading • Withstands core-melt attack
Middle layer	ThO_2 MgO	2-5	• Refractory ceramics • Poor thermal conductivity	• Serves as delay beds • Allows Large Temperature gradient • Thickness varied as a parameter to limit the base temperature within safety limits
Base Layer	Stainless steel	2	• Good mechanical properties and strength at high temperatures • Low thermal conductivity	• Avoids sodium boiling below the plate

6.4 HEAT TRANSFER ANALYSIS

Thermal analysis is carried out on the core catcher plate for the bounding case of whole-core melt down accident. The heat source on the core catcher plate is decay heat contained in the core debris which is primarily a function of time. The time for molten material relocation to the core catcher plate is assumed to be the time taken for grid plate melt-through. From the results discussed in Chapter 5, the melt relocation time is computed to lie between 300 s and 1000 s depending on the initial conditions assumed for the core-melt on the grid plate. Therefore thermal analysis of multi layer core catcher is carried out for these two time limits. Another parameter which is a variable is the extent of spreading of core debris on the core catcher plate. The core debris after piercing through the grid plate interacts thermally with cold sodium in the lower plenum and gets quenched and fragmented before settling on the core catcher. There is also experimental evidence that the mechanism of self leveling due to sodium boiling within the debris bed is able to distribute the debris evenly on the core catcher plate within a few minutes (Rigoleur and Kayser, 1982). For the present study, the minimum radius for core debris spread is taken as 2m which is two third of core catcher radius and the maximum radius is the radius of the plate itself. The objective of the analysis is to optimize the thickness of the delay bed layer on the core catcher plate. Other input parameters and the boundary conditions are given in Table 6.4.

As stated above, for the triple layer core catcher as depicted in Fig. 6.1, 5 mm thick molybdenum forms the top most layer, followed by a layer of thoria whose thickness is to be optimized so that the maximum temperature on the base layer of 2 cm of stainless steel is within design safety limit. Conduction heat transfer analysis is carried out for this composite core catcher assembly. For modelling the core catcher with core-melt spread evenly on it and for the lumped core-melt occupying 2/3 rd radius of its radius, one dimensional geometry and axisymmetric two dimensional geometry are adopted respectively. Transient heat conduction equation along with decay heat as the source term in the core-melt region is solved to determine the temperature evolution.

Table 6.4 Input parameters for heat transfer analysis

Parameter	**Value**
Delay bed material	Thoria / Magnesia
Thickness of delay bed	2 cm – 5 cm (to be optimized)
Initial temperature of relocated fuel	3020 K
Initial temperature of core catcher	673 K
Heat transfer coefficient in sodium above fuel	1000 $W/m^2.K$
Heat transfer coefficient in sodium below core catcher	700 $W/m^2.K$

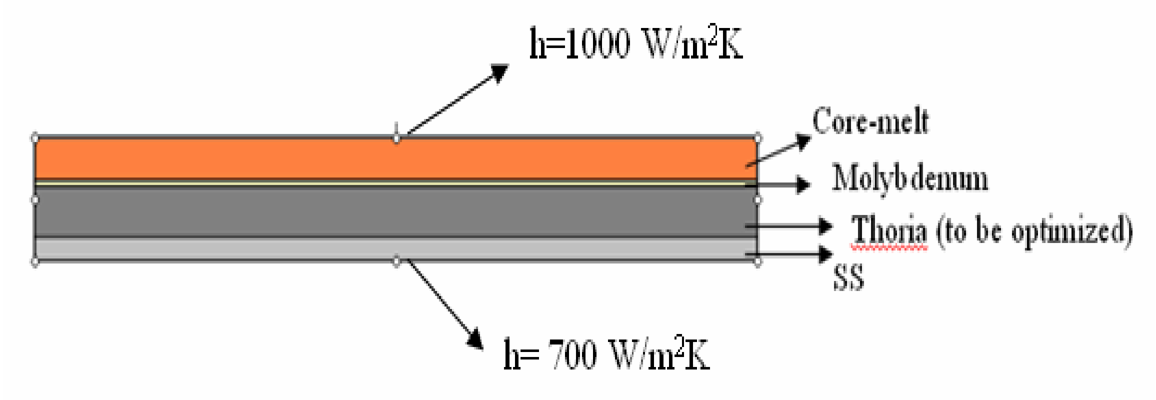

Fig. 6.1 Computational domain

6.5 RESULTS AND DISCUSSION

Detailed parametric studies have been carried out for the geometry shown in Fig. 6.1, by varying the thickness of the delay bed. Computations have been carried out till the temperature of bottom of the base SS layer shows a decreasing trend. Figure 6.2 illustrates the temperature evolution at the bottom of various layers with a 2 cm thick thoria delay bed for core-melt relocation time of 300 s. The temperature at the fuel top drops down with time because of the continuous heat removal by natural convection of sodium from that surface. It also indicates that decay heat is not able to sustain the initial prescribed temperature, which is the fuel melting temperature. At the same time because of the decay heat, fuel bottom interface temperature rises and it reaches the top surface temperature in about 50 s. Molybdenum layer follows the fuel bottom temperature closely

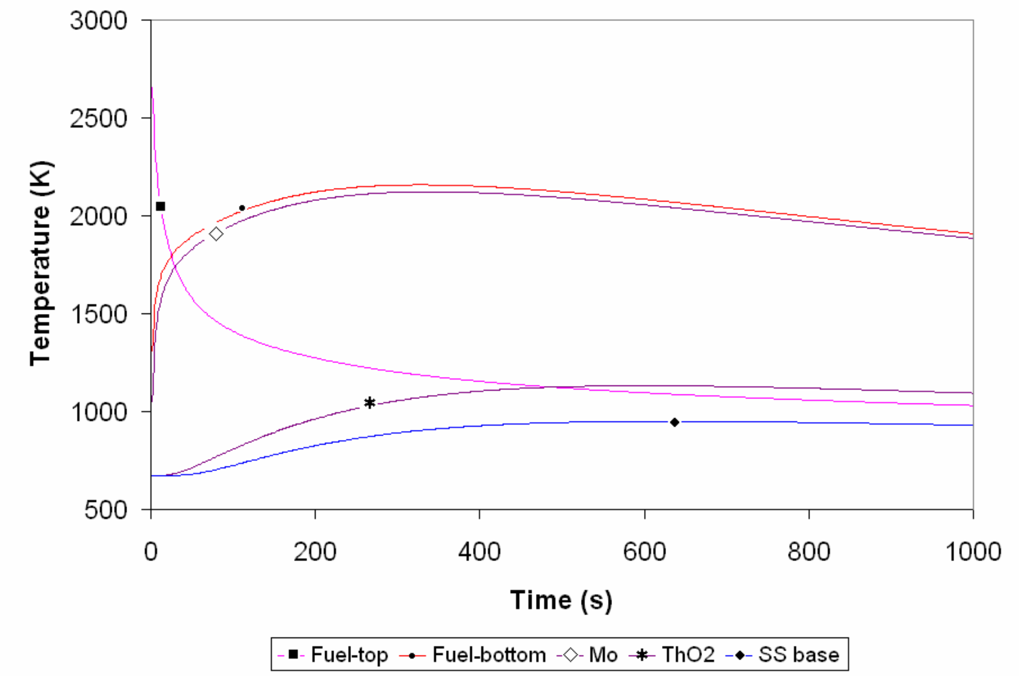

Fig. 6.2 Temperature history with 2 cm thick thoria delay bed

because of its high thermal conductivity. The maximum temperature drop is observed in the delay bed of thoria as anticipated. The lower most stainless surface of the composite core catcher sees the minimum temperature of all the layers with a temperature drop across its thickness being about 200 K.

It is seen that the temperature at core catcher bottom is 982 K which is above the design safety limit temperature of 923 K. Therefore computations were carried out for two more cases by increasing the thickness of thoria layer to 3 cm and 4 cm and the corresponding results are shown in Fig. 6.3 and Fig. 6.4 respectively. It is seen that in Fig. 6.3, thoria bed of three cm thickness reduces the base plate temperature to 888 K but the average temperature across the base layer of stainless steel is still above the design limit. In the next case with thoria bed of 4 cm, the average temperature of the base layer falls to 891 K which is 25 K less than the design limit temperature. This result shows that 4 cm thoria as delay bed is sufficient for a whole core accident, if the core-melt or core debris spreads uniformly on the entire surface of the plate.

A comparison of core catcher bottom temperatures for the conventional single layer 2 cm thick SS core catcher plate and the proposed triple layer core catcher with different thickness of thoria layer is given in Fig. 6.5. It is evident from this figure that the maximum temperature experienced by the stainless steel bottom layer decreases with increasing thickness of thoria bed and so is the rate of temperature increase.

Table 6.5 summarizes the temperatures at the top and bottom surfaces of the base layer and time to reach those temperatures for different thickness of thoria layers. If Magnesia is used as delay bed instead of thoria, it is seen that 5 cm thickness of the delay bed is necessary to restrict the base plate temperature within 923 K. The thickness of the core debris is taken to be 4 cm in all these cases, equivalent to debris spreading evenly on the entire core catcher surface and the melt relocation time is 300 s.

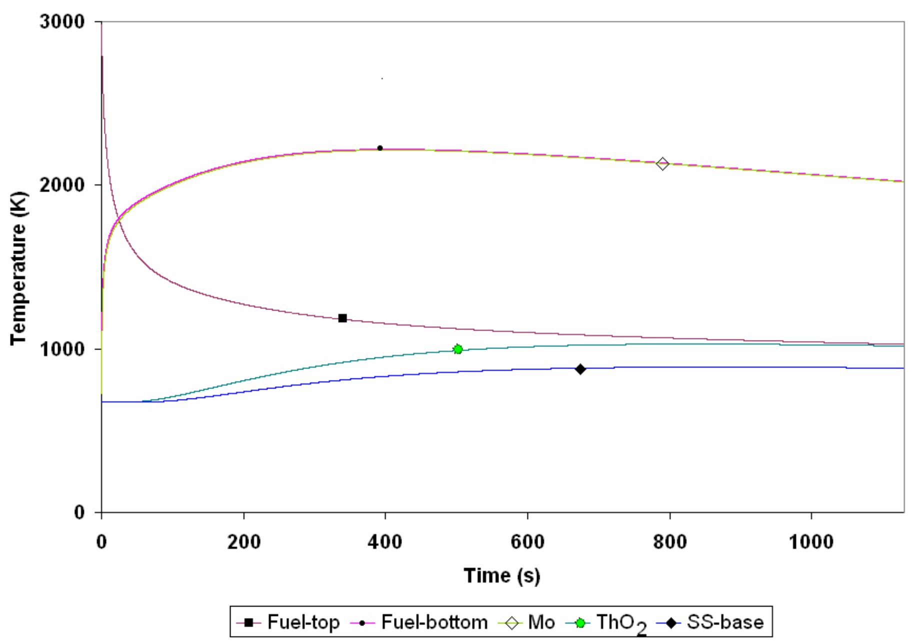

Fig. 6.3 Temperature history with 3 cm thick thoria delay bed

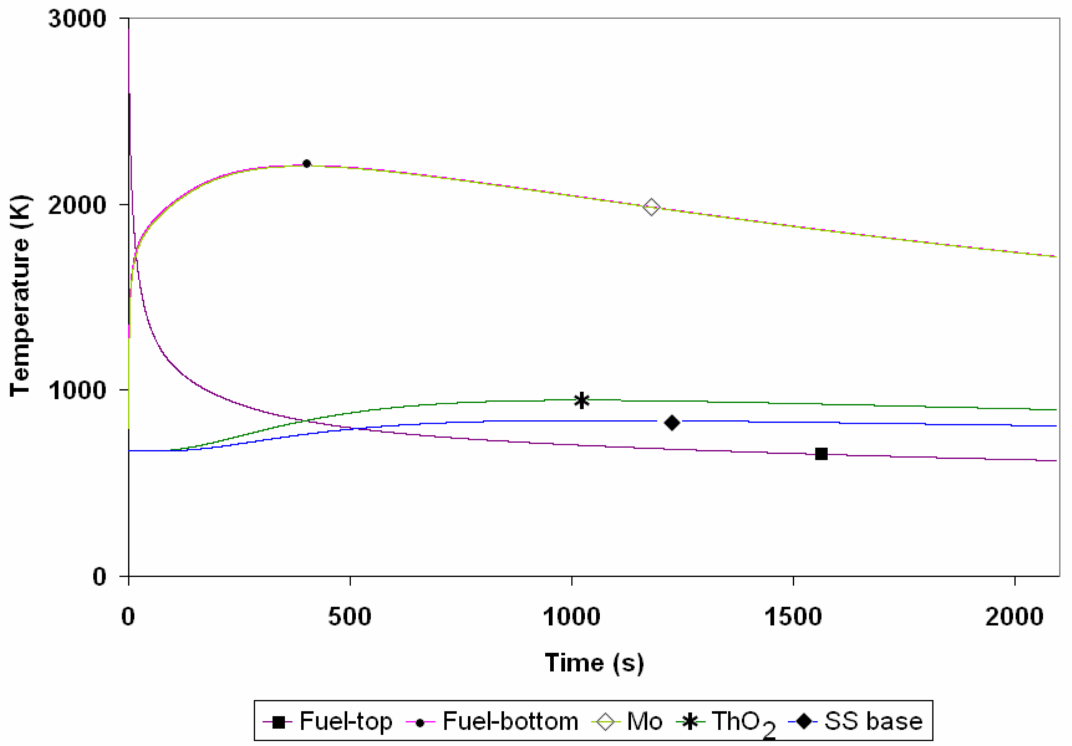

Fig. 6.4 Temperature history with 4 cm thick thoria delay bed

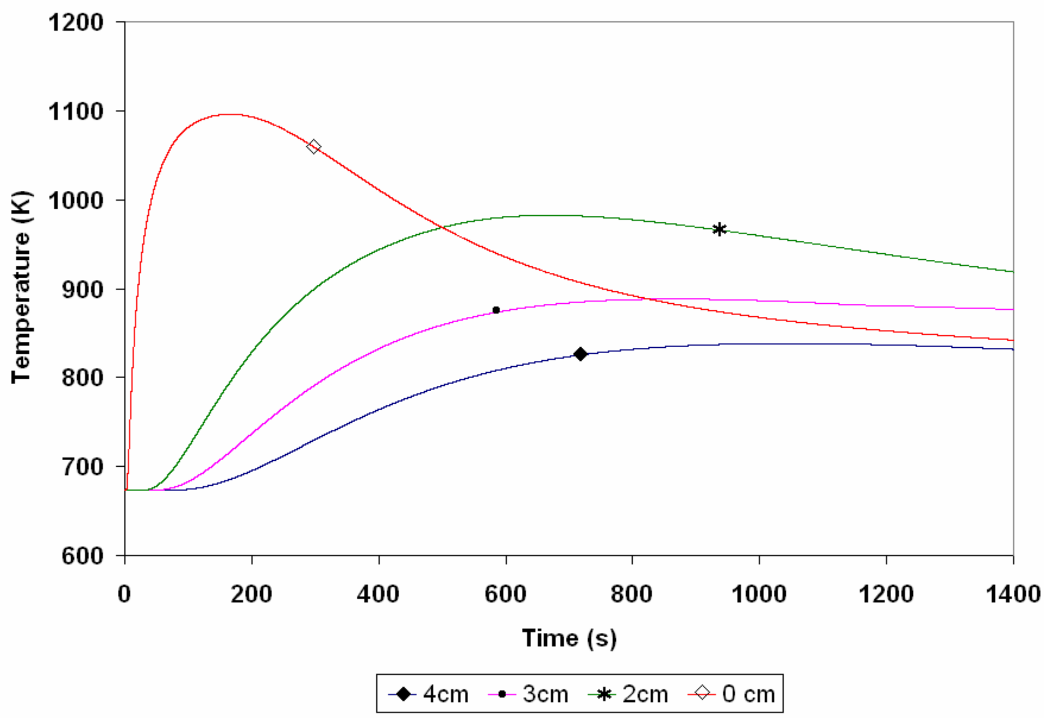

Fig. 6.5 Comparison of base layer temperature with various thickness of delay bed

Table 6.5 Temperatures on the base layer of core catcher
(evenly spread core debris)

Delay bed material	Thickness (cm)	Maximum temperature in base layer		Temperature at bottom of base layer	
		Temperature (K)	Time after debris arrival on core catcher (s)	Temperature (K)	Time after debris arrival on core catcher (s)
ThO_2	2	1185	640	982	669
	3	1025	838	888	865
	4	943	1017	838	1047
	5	880	1342	798	1371
MgO	4	1224	592	1005	668
	5	928	1430	827	1458

Temperature distribution across the thickness of the multi layer core catcher with 5 cm thick delay bed is depicted in Fig. 6.6 at various instants. The temperature in the core debris region is decreasing with time while that in the other regions are increasing with time, as expected. The maximum temperature at the base layer occurs in about 1400 s. Then the temperature show a decreasing trend as evidenced in the temperature contour with time stamp of 1600 s.

In the next study, the core debris is assumed to be partially lumped on core catcher, occupying 2/3rd of its radius. Consequently, core debris thickness on the core catcher increases. A two dimensional heat transfer study is performed in axi-symmetric cylindrical coordinate system. The core-melt relocation time to core catcher which defines the initial heat load is varied as a parameter. With increasing time for relocation, the volumetric heat source decreases drastically.

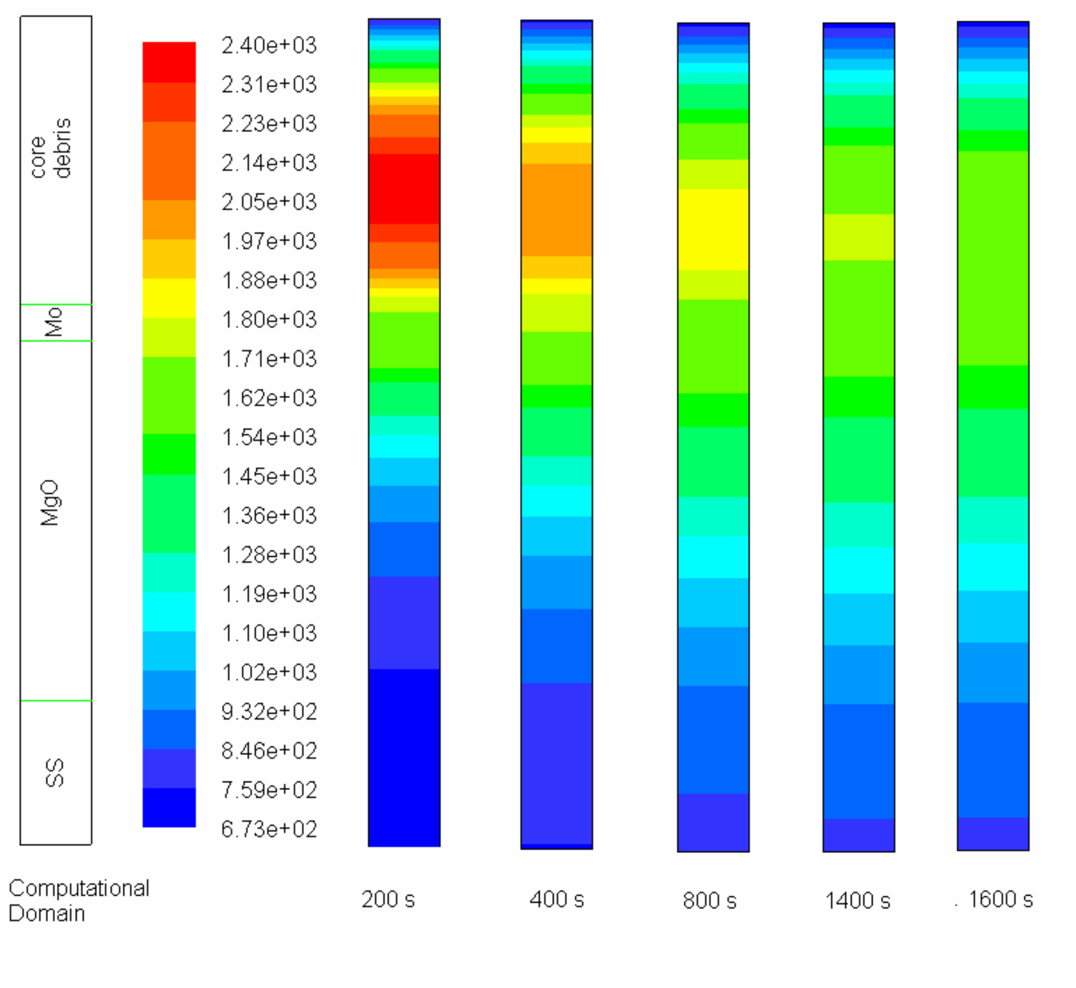

Fig. 6.6 Temperature (K) contours for magnesia bed along with their time stamps

For melt relocation time of 300 s and with thoria as delay bed, temperature history in the various layers of the core catcher is given in Fig. 6.7. The comparison of the stainless steel base of the core catcher between the thoria delay bed and magnesia delay bed is given in Fig. 6.8. As seen from the figure the maximum temperature experienced by the SS base layer with thoria as delay bed is 1000 K which is 100 K less than that with Magnesia delay bed.

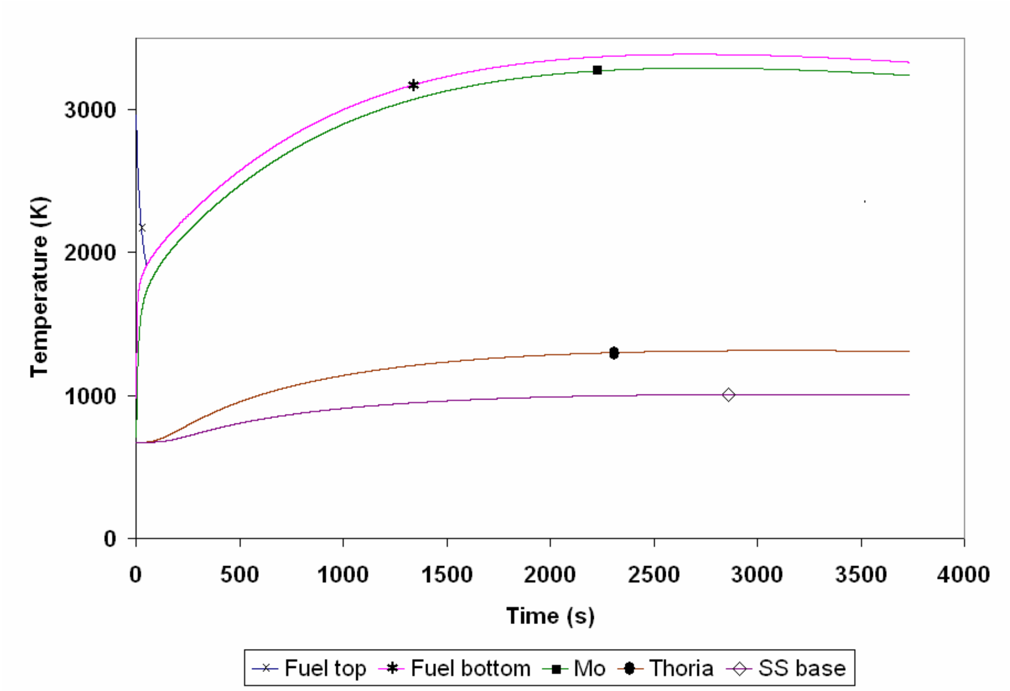

Fig. 6.7 Temperature history in different locations with thoria delay bed with lumped core-melt

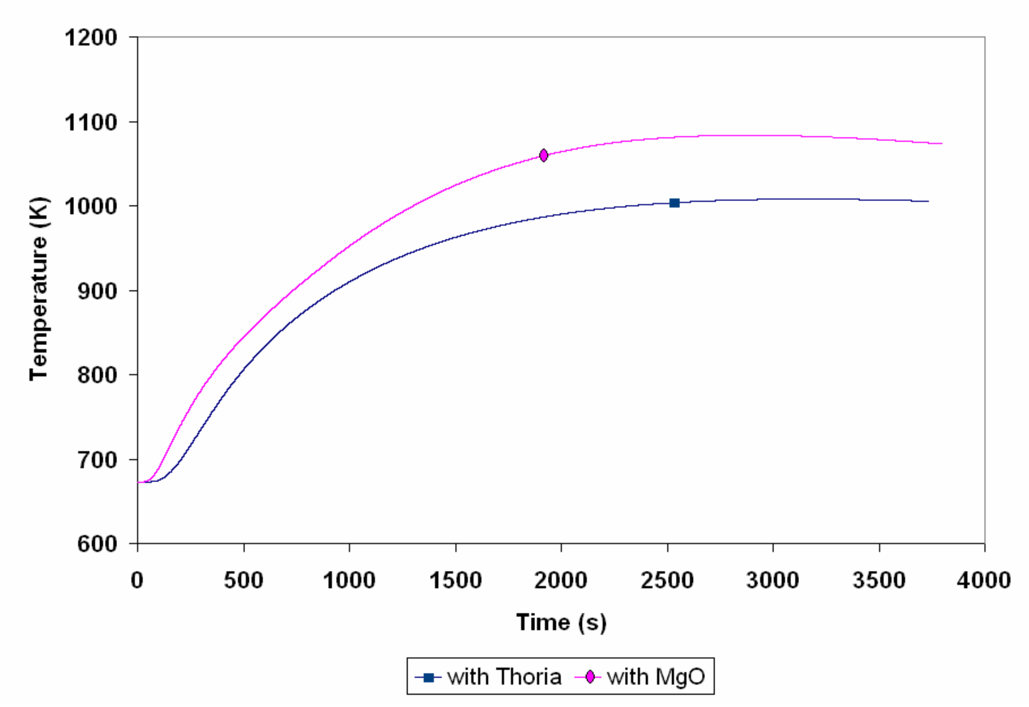

Fig. 6.8 Comparison of SS base temperature with thoria and magnesia delay beds with lumped core-melt

A plot of the temperature field and a few important isotherms are depicted in Fig. 6.9 at the instant of 3500s when the temperatures start showing a decreasing trend after attaining peak values. It is seen that 1700 K isotherm does not touch the bottom of SS base layer, proving that it is intact. Most of the core-melt is in molten condition (3020 K) with central portion even boiling. But the melting temperature of thoria is 3600 K and there is no trace of melting in thoria layer.

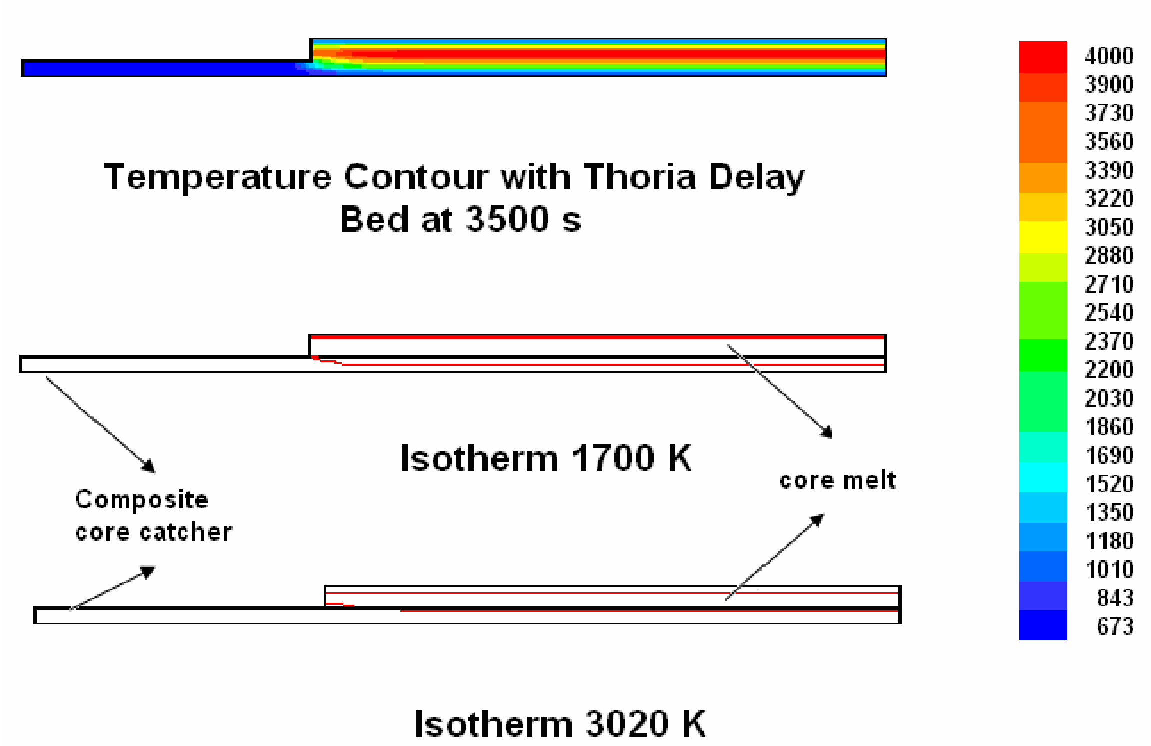

Fig. 6.9 Temperature contour & isotherms with thoria delay bed

The results of the parametric study are summarized in Table. 6.6. From Table 6.6 it is inferred that, beyond 1000 s, increase in melt relocation time to core catcher has negligible influence on the base temperatures. But lumping of core-melt i.e., increasing the fuel thickness, leads to increase in core catcher base temperature. In this case, 4 cm thoria delay bed is not sufficient to respect the design safety limit temperature of core catcher. But it is sufficient to prevent sodium boiling below the plate, which can prove detrimental to the plate. If sodium vapour is trapped below the plate preventing wetting of the bottom surface by liquid sodium lying below core catcher, it can lead to hot spots and damage the plate. Lumping of the core debris is only a transient phenomenon, as it will get leveled off within a few minutes, because of sodium boiling within the bed over the core catcher. Therefore, further increase in delay bed thickness is not warranted.

Table 6.6 Temperatures on the base layer of core catcher (lumped core debris on 2 m radius)

Material of delay bed	Melt relocation time (s)	Maximum temperature in base layer		Temperature at bottom of base layer	
		Temperature (K)	Time after debris arrival on core catcher (s)	Temperature (K)	Time after debris arrival on core catcher (s)
ThO_2	300	1315	3109	1008	3167
	1000	1248	3401	974	3448
	2000	1204	3531	950	3576
MgO	300	1404	2836	1084	2874
	1000	1315	3114	1036	3157
	2000	1257	3235	1004	3274

6.6 CLOSURE

The concept of multi layer core catcher consisting of a ceramic delay bed is highlighted and a triple layer core catcher is proposed for future FBRs. The thickness of the delay bed is optimized by heat conduction analysis for a whole core accident. Of the two materials considered for the delay bed, thermal performance of thoria is better than that of magnesia.

CHAPTER 7

CONCLUSIONS AND FUTURE SCOPE

7.1 FOREWORD

This research work has addressed a few important issues related to relocation of molten core materials in the downward direction following severe core melt down accidents by numerical analyses. Since the numerical simulations deal with accidents scenario, definition of input conditions is a difficult but vital task. This challenge is overcome indirectly by parameterizing the input conditions within certain physically realistic limits and assessing their influence on the output parameters. Grid independency tests and validation exercises have been performed for the computational models. The design of any safety device to mitigate the consequences of a core melt down considers the most conservative of the output values obtained. Major conclusions derived from the numerical analyses are summarized in this chapter.

7.2 CFD ANALYSIS IN SODIUM FILLED ENCLOSURES

Steady state natural convection heat transfer correlations are developed for liquid metal contained in a cylindrical cavity heated on the top surface and cooled along the curved side wall. The numerical analysis is carried out with a commercial CFD code and axisymmetric geometry is considered. The functional dependence of the Nusselt number on Boussinesq number is determined for isothermal and isoflux conditions on the top surface. It is seen that the power law dependence for the two cases are 1/5 and 1/10 respectively as listed below.

$$Nu = 0.8715\,(Bo)^{0.2029} \qquad for\ 2\times10^{6} < Bo < 2\times10^{11} \tag{7.1}$$

$$Nu = 2.9\,(Bo)^{0.096} \qquad for\ 4\times10^{4} < Bo < 2\times10^{9} \tag{7.2}$$

These correlations are valid for thin top plate approximation.

Conjugate natural convection and conduction heat transfer analysis has also been carried out for the same geometry, with a hot plate of finite thickness at top boundary. This enclosure represents the lower sodium plenum within the main vessel of a FBR bounded by the 5 cm thick grid plate on top, core support structure as the side wall and main vessel bottom as the base. Both steady and transient analyses have been carried out. In the initial unsteady state, the Nusselt number is found to be inversely proportional to square root of dimensionless time.

$$Nu = \left(\frac{t}{\tau}\right)^{-\frac{1}{2}} \tag{7.3}$$

For steady state, a correlation has been developed considering the temperature at the lower surface of the thick plate. This correlation is further useful in grid plate melting studies and the Nusselt number dependence on Boussinesq number is found out as follows

$$Nu = 0.4(Bo)^{0.2} \tag{7.4}$$

Comparison of this correlation with Eqn. (7.1) shows that there is a considerable decrease in heat transfer to the underlying liquid, in the case of thick plates and the reason attributed is the reduced convective velocity of sodium. Increasing the conductivity of the material of the plate is found to enhance the heat transfer.

In the steady state, conductivity ratio and height ratio are found to influence the heat transfer along with Boussinesq number, for thick plate configuration The following general correlation is derived accounting for their influence on Nusselt number for a downward facing hot thick plate heating a cylindrical enclosure containing liquid sodium

$$Nu = 0.15(Bo)^{0.07}(l^*)^{-0.6}(\kappa^*)^{0.27} \tag{7.5}$$

for $3.6\times10^{7} < Bo < 2\times10^{8}$; $0.27 < \kappa^* < 5.4$ and $6 < l^* < 60$

7.3 CORE-MELT RELOCATION STUDIES

In the next part of research, the lower and upper bounds of melt relocation time to core catcher have been estimated from ULOFA and PLOHS accidents. A computer code is developed in explicit enthalpy formulation to handle melting phenomenon along with transient heat conduction. An improved algorithm proposed by Voller and Cross (1981) is inbuilt in the code to track the melting front. The code uses finite difference method for discretising the energy equation.

The developed code HEATRAN-1 is used to analyse grid plate heating and melting sequence when decay heat generating nuclear fuel settles on it following a severe accident encompassing the whole core. The code is validated with Stefan's problem and benchmark data of BN 800 reactor. Thermal analysis including melting phenomenon predicts grid plate melt through time to 300 s when grid plate is exposed to constant temperature of 3020 K at its top surface. But when time varying decay heat is accounted within core-melt, melt through time is about 1150 s for evenly spread core-melt on the grid plate. Both these cases correspond to no heat transfer to the underlying sodium. To consider the effect of heavier fuel displacing the lighter molten stainless steel, a correlation developed by Moallemi and Viskanta (1985) for molten film thickness beneath a hot migrating source which buries itself in a melting substrate is utilized. The mesh is dynamically adapted to match the diminishing thickness of the grid plate. When molten material displacement model is adopted in the analysis, melt-through time decreases by about 15%-20% and it is about 1000 s for evenly spread core-melt. This analysis gives a conservative estimate of time for grid plate melt-through, assuming that heat transfer to underlying sodium is not possible.

When heat transfer to the lower sodium plenum is accounted for, by means of including heat transfer coefficient obtained from the CFD study using PHOENICS code as the boundary condition at the bottom side of the grid plate, grid plate melt through does not occur and it reaches a maximum temperature of 1120 K, which is about 580 K less than the melting point of grid plate material. But even in this case grid plate failure cannot be ruled out because the grid plate bottom temperature is in the creep regime. Therefore this analysis shows that grid plate cannot serve as a permanent hold up place for the core-melt expected from a whole core melt down accident. But it can substantially decrease the thermal load expected on the core catcher plate because the time delay involved in melting of grid plate decreases the decay heat content of core-melt.

The core-melt progression in the downward direction following a PLOHS accident has been analysed numerically by a heat conduction model incorporating porous body formulation with effective properties. The core-melt melts through lower axial blanket region, lower fission gas plenum, tail piece of subassembly, discriminator and grid plate top regions sequentially. A few possible cases are studied - the first one without displacement of molten region and the next one considering the displacement of different regions with the melting of the stainless steel which is the structural material. In both these cases the bottom of the grid plate is kept adiabatic. In the first case melting temperature of uranium dioxide is not reached at the bottom of lower axial blanket region even after 16 hours of heating by core-melt on its top. But the grid plate bottom crosses 1073 K after 15.5 hours which is taken as the time of its failure due to thermal creep. After the grid plate breaches, the subassemblies which are supported on the grid plate cannot remain in place and hence core-melt relocation to the sodium plenum and then to the core catcher follows immediately.

In the next case, clad melting point of 1700 K is fixed as the threshold for the core-melt penetration to the successive regions and the analysis is repeated. Each region is displaced when its bottom temperature touches 1700 K and core-melt is placed in contact with the next layer, thus quickening the melt relocation process. In this case, molten material relocation time is estimated to be about 5.5 hours, assuming sodium rewetting of the subassemblies at all times.

In the third case study with convection to sodium below grid plate, though melting of steel propagates through the first four regions, it is seen that grid plate bottom temperature reaches a steady temperature of 944 K only. Considering the results from all the case studies, it is concluded that the minimum time required for core-melt relocation to the core catcher is 5.5 hours following a PLOHS accident with conservative inputs. As per this time estimate, for a whole core accident, the heat load on the core catcher is about 14 MW which is about one third of the thermal load due to an ULOFA where the relocation time is taken to be 300 s.

7.4 MULTI LAYER CORE CATCHER

Finally, the concept of multi layer core catcher is put forth, after considering the available options, to qualify the core catcher for a whole core accident. The adequacy of the same has been established purely from thermal considerations. Core-melt relocation times obtained from ULOFA analysis are given as input for defining the initial decay heat load on the core catcher. The relative merits and demerits of a few candidate materials for the different layers of core catcher are highlighted. The proposed multi layer core catcher consists of a top sacrificial layer, a middle refractory ceramic layer (which can itself be single / multiple layers) and a base structural layer. For the thermal analysis, molybdenum is taken as the top layer material, magnesia and thoria are considered as the middle layer acting as the delay bed. The base layer is stainless steel (SS 316LN) which supports the entire core catcher assembly.

Thermal analysis predicts that a delay bed of thoria, 4 cm in thickness or of magnesia 5 cm in thickness, can cater to the need of restricting the core catcher base temperature below design safety limit of 923 K, when the whole core debris spreads evenly on the entire core catcher. Even for a conservative case of the debris occupying two thirds radius of core catcher, with 4 cm thickness of either thoria or magnesia delay bed, the base SS layer temperature does not exceed sodium boiling point which rules out downward sodium boiling. The multi layer core catcher concept proposed above has to be subjected to rigorous feasibility study, considering the metallurgical and manufacturing aspects and validated with experiments before being put into use. The concept of adding a delay bed layer in the internal core catcher is new to FBRs. The present numerical analysis has indicated that thoria is better than magnesia based upon its ability to produce large thermal gradients.

7.5 FUTURE SCOPE

- The code HEATRAN-1 can be improved further to solve energy equation in implicit formulation so that large time steps can be accommodated when dealing with long drawn transients such as a PLOHS accident.
- Combined thermal hydraulic study of upper and lower sodium plena of reactor main vessel during accidental conditions can be carried out.
- Evaluation of new core catcher concepts such as refractory material coated core catcher and multi tray concepts can be evaluated before finalizing the core catcher for future reactors.

APPENDIX - 1

PAHR Comic Strip by Kayser (Muller and Gunther, 1982)

This cartoon portrays the different possible (but not exhaustive) configurations of core debris on the core catcher. The composition of core debris, the size distribution, density stratification of the debris due to travel through sodium column and several other factors influence the settling aspects of the debris on the core catcher. Initially, the debris may form a heap which may later get levelled due to sodium boiling within the bed. If the decay heat is high enough leading to sodium dryout, re-melting can happen within the debris, fusing the debris into lumps. This picture is shown to signify the plethora of initial conditions that can be defined for the settling aspects of core debris. The same can be true for any physical processes / phenomena that are postulated for an accident progression.

REFERENCES

Ahmed E.K.S., Podowski M.Z., Lahey R.T., 1990. An experimental and theoretical investigation of melt propagation in a rubble bed with application in severe accident analyis. Proc. NURETH IV, WA DC. 111-118.

Akins R.G., Lin Y.S., 1986. Transient behaviour of natural convection inside a vertical cylinder. Chem. Eng. Commun., Vol. 43(1), 69-83.

Akopov F.A., Akopyan A.A., Barykin B.M., Borodina T.I., Val'yano G.E., Virnik V.A. M., Mineev N., Chernyshov G.P., 1998. Behaviour of plasma-sprayed zirconium dioxide ceramic under the thermochemical effect of components of the reactor core-melt. Atomic Energy, Vol. 85(2), 540-543.

Akopov F.A., Borovkova L.B., Vlasov A.S., Vorob'ev A., 2003. Titanate composites for core catcher donor material in a nuclear reactor. Glass and Ceramics, Vol. 60, 9-10.

Backs H., Holtbecker H., 1982. The European PAHR in-pile programme objectives and general layout. Proc. LMFBR Safety Topical Meeting, Lyon, France, 317-325.

Baliga B.R., 1997. Control volume finite element methods for fluid flow and heat transfer. Advances in heat transfer, (Ed) Minkowycz W.J., Sparrow E.M., Vol. 1, 97-135.

Bejan A., 2004. Convection heat transfer, John-Wiley & Sons, New Jersey.

Borgstedt H.U., 2008. Materials issues for generation IV systems status, open questions and challenges. (Ed) Véronique Ghetta, Dominique Gorse, Dominique Mazière and Vassilis Pontikis. NATO Science for Peace and Security Series B: Physics and Biophysics, DOI: 10.1007/978-1-4020-8422-5.

Bowers C.H., Tentner A.N., Wider H.U., 1979. Analysis of TREAT tests L7 and L8 with SAS3D. LMFBR safety experiments specialists workshop, Los Alamos, 242-256.

Brackbill J.U., Saltzman J.S., 1982. Adaptive zoning for singular problems in two dimensions. J. Comp. Phys, Vol. 46, 342-368.

Caldwell J., Ching Cheun Chan, 1998. Numerical solutions of the Stefan problem by the enthalpy method and the heat balance integral method. Numer. Heat Transfer, Part B, Vol. 33, 99-117.

Caldwell J., Chiu C.K., 1994. Numerical solution of two phase Stefan problems by the heat balance integral method. Adv. in Comp. Methods in Heat Transfer, Computational Mechanics Publications, 225-234.

Caldwell J., Kwan Y.Y., 2003. On the perturbation method for Stefan problem with time-dependent boundary conditions. Int. J. Heat Mass Transfer, Vol. 46, 1497–1501.

Cao, H.Q., Vassen, R. Stoever D., 2004. Ceramic materials for thermal barrier coatings. J. European Ceramic Society, Vol. 12(1), 1-12.

Carslaw H.S., Jaegar J.C., 2005. Conduction of heat in solids, Oxford Science Publishers, UK.

Chawla T.C., Graff D.L., Borg R.C., Bordner G.L., Weber D.P., Miller D., 1981. Thermophysical properties of mixed oxide fuel and stainless steel type 316 for use in transition phase analysis. Nucl. Eng. Des., Vol. 67(1), 57-74.

Chen WZ, Zhao YS, Sun FR, Chen ZY, Gong M, 2008. Analysis of ΔT driven contact melting of phase change material around a horizontal cylinder. Energy Convers. Manage., Vol. 49(5), 1002-1007.

Chetal S.C., Balasubramaniyan V., Chellapandi P., Mohanakrishnan P., Puthiya vinayagam P., Pillai C.P., Raghupathy S., Shanmugham T.K., Sivathanu Pillai C., 2006. The design of the Prototype Fast Breeder Reactor. Nucl. Eng. Des., Vol. 236, 852–860.

Chida K., 2000. Surface temperature of a flat plate of finite thickness under conjugate laminar forced convection heat transfer condition. Int. J. Heat Mass Transfer, Vol. 43, 639-642.

Clifton J.V., Chapman A.J., 1969. Natural convection on a finite size horizontal plate. Int. J. Heat Mass Transfer, Vol. 12, 1573-1584.

Condie K.G., 2004. Design and evaluation of an enhanced in-vessel core catcher. Proc. ICAPP '04, Pittsburgh, PA, USA, Paper-4122.

Croft D.R., 1977. Heat transfer calculations using finite difference equations. Applied Science Publications, London.

Dosanjh S.S., 1988. Analysis of the late core-melt progression phase of severe accidents using MELPROG code. Proc. NURETH IV, WA DC.

Dufour, 2007. Post accident heat removal analysis for SPX and EFR. CEA-IGCAR Tech. seminar on LMFR safety aspects related to severe accidents, Kalpakkam.

Endo, 1986. Analysis of core melt down for PLOHS accident in a FBR. BNES Conference on Science and Technology of Fast Reactors, Guernsey, Vol. 2, 77-83.

Farmer M.T., Sienicki J.J., Spencer B.W., 1990. The Meltspread-1 computer code for the analysis of transient spreading in containments. Report No: CONF901101-30.

Friedland A.J., Tilbrook R.W., 1974. Ex-vessel core catcher design requirements and preliminary concepts evaluations. Report No: FRT-1561 Rev-1.

Fujii T., Honda H., Morioka T., 1973. A theoretical study of natural convection heat transfer from downward-facing horizontal surfaces with uniform heat flux. Int. J. Heat Mass Transfer, Vol.16, 611-627.

Garner P.L., Abramson P.B., 1979. Fuel and coolant motions following pin failure: EPIC models. LMFBR safety experiments specialists workshop, Los Alamos, 141-152.

Gazit D., 1988. Natural heat transfer in a mercury bath and the effect of introduced partitions. Int. J. Heat Mass Transfer, Vol. 31(1), 177-182.

Gluekler E.L., Hunsbedt A., Lam S.T., Shahin A.F., 1982. Analysis of in-vessel core debris retention in large LMFBRs. Proc. LMFBR Safety Topical Meeting, Lyon, France, 409-417.

Grotzbach G., Worner M., 1999. Direct numerical and large eddy simulations in nuclear applications. Int. J. Heat Fluid Flow, Vol. 20, 222-240.

Groulx. D., Lacroix. M., 2003. Effects of convection and inertia on close contact melting. Int. J. Therm. Sci., Vol. 42, 1073-1080.

Gupta R.S., Kumar D., 1981. Variable time step methods for one-dimensional Stefan problem with mixed boundary condition. Int. J. Heat Mass Transfer, Vol. 24, 251-259.

Gusarov V.V., 2001. Sacrificial materials for safety systems of nuclear power stations: a new class of functional materials. Therm. Eng., Vol. 9, 721-723.

Heim D., 2005. Two solution methods of heat transfer with phase change within whole building dynamic simulation. 9^{th} Int. IBPSA Conf., Montreal, 397-402.

Henkes R.A.W.M., Van Der Vlugt F.F., Hoogendoorrn C.J., 1991. Natural convection flow in a square cavity calculated with low Reynolds number turbulence models. Int. J. Heat Mass Transfer, Vol. 34(2), 377-388.

Henry H., Argyropoulosz S.A., 1996. Mathematical modelling of solidification and melting: a review. Modelling Simul. Mater. Sci. Engg., Vol. 4, 371-396.

Honnor M.E., Davies A.J., 2004. Nonlinear transient field problems with phase change using the boundary element method. Engineering Analysis with Boundary Elements, Vol. 28, 561-570.

Jabbar A.N.K., 2001. Natural convective heat transfer coefficient – a review - surfaces in two and three dimensional enclosures. Energy Convers. Manage., Vol. 42, 505-517.

Kanga K.H., Rae-Joon Park, Sang-Baik Kima, Suhb K.Y., Cheungc F.B., Rempe J.L., 2007. Simulant melt experiments on performance of the in-vessel core catcher. Nucl. Eng. Des., Vol. 237, 1803-1813.

Kek V., Muller U., 1993. Low Prandtl number convection in layers heated from below. Int. J. Heat Mass Transfer, Vol. 36(11), 2795-2804.

Kwang A., KimD.H., Kim B.S., 2004. Numerical investigation on the heat transfer characteristics of a liquid metal pool subjected to a partial solidification process. Prog. Nucl. Energy, Vol. 44(4), 277-304.

Lewis R.W., Morgan K., Zienkiewicz O.C., 1981. Numerical methods in heat transfer, Vol. 1, John Wiley and sons, UK.

Makinde O.D., Aziz A., 2011. Mixed convection from a convectively heated vertical plate to a fluid with internal heat generation. ASME J. Heat Transfer, Vol. 133, 122501, 1-6.

Mamun A.A., Chowdhury Z.R., Azim M.A., Maleque M.A., 2008. Conjugate heat transfer for a vertical flat plate with heat generation effect. Nonlinear Analysis Modelling Control, Vol. 13(2), 213-223.

Meacham S,A., 1976. The compatibility of refractory materials with boiling sodium. Report No: CONF-760508.

Moallemi M. K., Viskanta R., 1985. Melting around a migrating heat source. J. Heat Transfer, Vol. 107(2), 451-458.

Mohamad, A.A., Viskanta, R., 1993. Modelling of turbulent buoyant flow and heat transfer in liquid metals. Int. J. Heat Mass Transfer, Vol. 36(11), 2815-2826.

Mostofa M.M., Sarkar M.A.R., Huq A.M.A., Islam M.A., 2003. Study of natural convective heat transfer in a rectangular enclosure from one cooled side wall. Proc. Int. Conf. Mech. Eng., ICME-03-TH-11, Bangladesh, 1-4.

Muller U., Gunther C., 1982. Post accident debris cooling: Proceedings of the fifth post accident heat removal information exchange meeting, NRC, Karlsruhe.

Naaktgeboren, 2007. The zero phase Stefan problem. Int. J. Heat Mass Transfer, Vol. 50, 4614-4622.

Naterer G.F., 2000. Predictive entropy based correction of phase change computations with fluid flow - Part 1: Second law formulation. Numer. Heat Transfer, Part B, Vol. 37, 393-414.

Naterer G.F., 2000. Predictive entropy based correction of phase change computations with fluid flow - Part 2: Application Problems. *ibid.*

Nithiyarasu P., 2000. An adaptive finite element procedure for solidification problems. Heat Mass transfer, Vol. 36, 223 – 229.

Niwa H., 1994. Future research needs on material interaction and re-location in LMFR safety. IWGFR-89, IAEA-IWGFR - Technical Committee Meeting on Material Coolant Interactions and Material Movement and Relocation in LMFR, O-arai, Ibaraki, Japan.

Ozisik M.N., 1977. Basic heat transfer, McGraw Hill, NY.

Ozisik M.N., 1994. Finite difference methods in heat transfer, CRC Press, USA.

Patankar, S.V., 2004. Numerical heat transfer and fluid flow, Hemisphere Publishers, India.

PHOENICS user's manual. 2005. CHAM Co., UK.

Poulikakos D., Wei Zheng Cao, 1989. Solidification of a binary alloy from a cold wire or pipe: Modelling of the mixed phase region. Numer. Heat Transfer, Part A, Vol. 15, 197-219.

Poulikakos, 1994. Conduction heat transfer, Prentice Hall, NJ.

Revathy K., Nema V., Vinod V., Padmakumar G., Anand Babu C., Rajan K.K., Kalyanasundaram P., 2011. Transient Analysis in a natural circulation sodium loop for decay heat removal in LMFBR. Proc. 10th ISHMT-ASME Heat and Mass Transfer Conference, Chennai, India. Paper ID: ISHMT-IND-12-067, 1-7.

Rigoleur C.L., Kayser G., 1982. The internal corecatcher in Superphenix I. Proc. Int. Topical Meeting on FRS, Lyon, France, 285-296.

Rigoleur C.L., Tenchine D., 1982. Sodium natural convection heat transfer around internal core-catcher in Super Phenix 1. Proc. LMFBR Safety Topical Meeting, Lyon, France, 53-62.

Roychowdhury D.G, 1998. Sizing of core catcher. IGCAR internal report: PFBR/31150/DN/1021.

Roychowdhury D.G., Joseph Winston S., 2003. Design of corecatcher. IGCAR internal report: PFBR/31230/DN/1003.

Sajish S.D., Srinivasan R., Chellapandi P., Chetal S.C., 2009. Structural integrity assessment of DHX under CDA pressure loading. SmiRT -20, Espoo, Finland, 92-93.

Sathiyasheela T., Srinivasan G.S., Mohanakrishnan P., 2008. Analysis of ULOF, UTOP events and CDA energy release. IGCAR internal report: PFBR/01117/DN/1021.

Sati B.C., Srinivasan R., Selvaraj P., Chellapandi P., 2010. Assessment of creep-fatigue damage at main vessel triple point of PFBR after CDA. Trans. Indian Inst. Met., Vol. 63(2-3), 657-660.

Sato I., Yoshiharu T., Kensuke K.Y., Kenji K., Jun-Ichi T., Ryodai N., Shigenobu K., Shoji K., Kazuya K., Vassiliev Y., Vurim A., Vladimir Z., Alexander K., 2011. Safety strategy of JSFR eliminating severe recriticality events and establishing in-vessel retention in the core disruptive accident. J. Nucl. Sci. Technol., Vol. 48(4), 556-566.

Seetharamu K.N., Paragasam R., Ghulam A Quadir, Zainal Z.A., Sathya Prasad B., Sundararajan T., 2001, Finite element modelling of solidification phenomena. Sadhana, Vol. 26, 103-120.

Shaarawi M.E., Negm A.A.A., 1999. Conjugate natural convection heat transfer in an open ended vertical concentric annulus. Num. Heat Transfer, Part A, Vol. 36, 639-655.

Shamsundar N., Sparrow E.M., 1975. Analysis of multidimensional conduction phase change via the enthalpy method. J. Heat Transfer, Vol. 97(3), 333-340.

Sharma A.K., Velusamy K., Balaji C., 2008. Conjugate transient natural convection in a cylindrical enclosure with internal volumetric heat generation. Annals Nucl. Energy, Vol. 35(8), 1502–1514.

Sharma A.K., Velusamy K., Balaji C., 2009. Turbulent natural convection of sodium in a cylindrical enclosure with multiple internal heat sources: A conjugate heat transfer study. Int. J. Heat Mass Transfer, Vol. 52, 2858–2870.

Sheriff N., Davies N.W., 1979. Liquid metal natural convection from plane surfaces, a review including recent sodium measurements. Int. J. Heat Fluid Flow, Vol. 1(4), 149-154.

Shyy W., 1994. Computational modelling for fluid flow and interfacial transport, Elsevier Publications, Amsterdam.

Silva W.D., 1994. A front tracking Boundary Element method (BEM) formulation for solidification and melting problems. Advanced Computational Methods in Heat Transfer, (Ed) Wrobel L.C., Brebbia C.A., Computational Mechanics Publications, Southampton.

Sridharan M.S., 2002. Total decay heat estimates in PFBR. IGCAR internal report: PFBR/01115/DN/1118.

Srinivasan G.S., Mohanakrishnan P., 2008. ULOF and CDA analysis of PFBR with Reactivity Worths based on ABBN – 93 Cross section Set. IGCAR internal report: RPD/SAS/177.

Szabo L., Richard P., Bergamaschiand Y., Seiter J., 1995. Multi crucible core catcher concept - design considerations and basic results. Nucl. Eng. Des., Vol.157, 417-435.

Tenchine D., 2010. Some thermal hydraulic challenges in sodium cooled fast reactors. Nucl. Eng. Des., Vol. 240, 1195–1217.

Thakur H., Singh K.M., Sahoo P.K., 2009. Meshless local Petrov-Galerkin method for non linear heat conduction problems, Numer. Heat Transfer, Part B, Vol. 56, 393-410.

Trevino C., Becerra G., Mendez F., 1997. The classical problem of convective heat transfer in laminar flow over a thin finite thickness plate with uniform temperature at the lower surface. Int. J. Heat Mass Transfer, Vol. 40(15), 3577-3580.

Uddin R., 1999. One dimensional phase change with periodic boundary conditions. Numer. Heat Transfer, Part A, Vol. 35, 361-372.

Uotani M., 1987. Natural convection heat transfer in thermally stratified liquid metal. J. Nucl. Sci. Technol., Vol. 24(6), 442-451.

Velusamy K., 2008. Interim report of the task force to investigate the phenomena and impliciations of CDA: present capabilities and future needs. IGCAR internal report: CFBR/01100/TF/1006.

Velusamy K., Chellapandi P., Chetal S.C., Raj B., 2010. Overview of pool hydraulic design of Indian Prototype Fast Breeder Reactor. Sadhana, Vol. 35(2), 97-128.

Velusamy K., Sundararajan T., Seetharamu K.N., 2001. Interaction effects between surface radiation and turbulent natural convection in square and rectangular enclosures. ASME J. Heat Transfer, Vol. 123(6), 1062-1070.

Venkateshan S.P., 2004. First course in heat transfer, ANE Books, New Delhi.

Viskanta R., Kim D.M., Gau C., 1986. Three dimensional natural convection heat transfer of a liquid metal in a cavity. Int. J. Heat Mass Transfer, Vol. 29(3), 475-485.

Vlasichev G.N., Csynin G.B., Kuzavkov N. G., 1994. Computational investigation of the movement of a melted mass to the bottom of the vessel during an off-design accident in a fast reactor. Atomic Energy, Vol. 77(3) 666-671.

Voller V., Cross M., 1981. An explicit numerical method to track a moving phase front. Int. J. Heat Mass Transfer, Vol. 26, 147-150.

Voller V.R., 1997. An overview of numerical methods for solving phase change problem. Advances in heat transfer, Vol. 1, (Ed). Minkowycz W.J., Sparrow E.M, Taylor and Francis Publications, 341-375.

Voronov S.A., Kiryushin A.I., Kuzavkov N.G., 1994. Evaluation of downmotion time interval of molten materials to core catcher during CDA postulated in LMFR. IWGFR-89, IAEA-IWGFR - Technical Committee Meeting on Material Coolant Interactions and Material Movement and Relocation in LMFR, O-arai, Ibaraki, Japan, 545-551.

Vynnycky M., Kimura S., 1996. Conjugate free convection due to a heated vertical plate. Int. J. Heat Mass Transfer, Vol. 39(5), 1067-1080.

Waltar A.E., Reynolds A.B., 1980. Fast Breeder Reactors. Pergamon Press, New York.

Wenxian L., Armfield S.W., 2005. Scaling analysis and direct simulation of unsteady natural convection cooling of fluid with $Pr < 1$ in a vertical cylinder. Phys. Rev. E, Vol. 72, 016306, 1-12.

Wilcox D.C., 1994. Turbulence modelling for CFD, DCW Industries, California.

Wolff F., Beckermann C., Viskanta R., 1988. Natural convection of liquid metals in vertical cavities. Exp. Thermal Fluid Sci., Vol. 1(1), 83-91.

Yadav V., Kant K., 2008. Experimental validation of analytical solution for vertical flat plate of finite thickness under natural convective cooling. ASME J. Heat Transfer, Vol. 130(3), 032503, 1-11.

Yigit F., 2008. Sinusoidal perturbation solution for solidification of pure materials on a planar mold of finite thickness. Int. J. Thermal Sciences, Vol. 47, 25-34.

Zabaras N., Mukherjee S., 1987. An analysis of solidification problems by the boundary element method. Int. J. Numer. Methods Eng., Vol. 24, 1879-1900.

Zhifeng D., Zhong Q.C., Wang Q., 1988. BEM for predicting the motion of solid-liquid phase change interface. Proc. Int. Symp. Heat Mass Transfer, China, B53343.

LIST OF PUBLICATIONS BASED ON THIS THESIS

[1] **A.Jasmin Sudha**, K.Velusamy, 2013. Numerical analysis of natural convection in sodium plenum below the grid plate of a fast reactor during a severe accident. Annals Nucl. Energy, Vol. 54, 120-128.

[2] **A.Jasmin Sudha,** K.Velusamy, 2013. Numerical analysis of grid plate melting following a severe accident in a fast breeder reactor. Sadhana, Academy Proceedings in Engineering Sciences (Springer), Special issue on Multi-phase Flow and Phase Change Phenomena, Vol. 38(6), 1241-1257.

[3] **A.Jasmin Sudha**, K.Velusamy, P.Chellapandi, 2014. Conceptual multi layer core catcher for future FBRs. Annals Nucl. Energy, Vol. 65, 253-261.

[4] **A. Jasmin Sudha,** K.Velusamy, Assessment of post accident molten material relocation time to the core catcher in a FBR. (*communicated to Annals of Nuclear Energy*).

Conference Proceedings

[1] **A.Jasmin Sudha,** K.Velusamy, 2010. An enthalpy method to predict core-melt propagation during severe accident in a fast reactor, Proc. ASME-ISHMT Conf. on Heat and Mass Transfer, IIT-Mumbai, 296-302.

[2] **A.Jasmin Sudha**, K.Velusamy, 2011. CFD analysis of natural convection in liquid sodium transiently heated from above in a large cylindrical enclosure, Proc. National Conf. in Emerging Research and Advances in Mechanical Sciences, Chennai, 255-261.

[3] **A.Jasmin Sudha,** K.Velusamy, 2011. Computational model for core-melt penetration in grid plate following a severe accident in a fast breeder reactor**,** Proc. ASME-ISHMT Conf. on Heat and Mass Transfer, Chennai, 93-100.

[4] **A.Jasmin Sudha**, K.Velusamy, 2013. Computational model for molten material relocation after a protected loss of heat sink accident in a FBR**,** ASME-ISHMT Conf. on Heat and Mass Transfer, IIT-Kharagpur, Paper ID: HMTC1300085, 1-7.